ANGULAR CORRELATION MEASUREMENTS ON THE REACTION $^{7}Li(d,n\alpha)^{4}He$

by

JOHN COWAN PHILP HEGGIE
B.Sc., University of Auckland, 1964
M.Sc., University of Auckland, 1966

A THESIS SUBMITTED IN PARTIAL FULFILMENT OF
THE REQUIREMENTS FOR THE DEGREE OF
DOCTOR OF PHILOSOPHY

in the Department
of
Physics

We accept this thesis as conforming to the
required standard

THE UNIVERSITY OF BRITISH COLUMBIA
June, 1972

In presenting this thesis in partial fulfilment of the requirements for an advanced degree at the University of British Columbia, I agree that the Library shall make it freely available for reference and study. I further agree that permission for extensive copying of this thesis for scholarly purposes may be granted by the Head of my Department or by his representatives. It is understood that copying or publication of this thesis for financial gain shall not be allowed without my written permission.

Department of PHYSICS

The University of British Columbia
Vancouver 8, Canada

Date 4/8/72

ABSTRACT

An experimental investigation of the sequential process $^{7}Li(d,\alpha)\ ^{5}He \rightarrow \alpha + n$ was carried out at an energy of $\sim$1.0 MeV. Neutron-alpha particle coincidences were measured with the neutron energy being obtained from time of flight measurements. The results are presented in the form of neutron-alpha particle angular correlations.

The lifetime of ^{5}He lends support to the argument that the two stages of the reaction, the formation of ^{5}He and its subsequent decay can be treated separately. Three possible reaction mechanisms have been considered for the first stage. It is expected that direct processes such as two and three particle transfer contribute very little to the yield at such a low bombarding energy. Certainly, calculations of the two-particle transfer amplitude using the formulism of DWBA are unable to fit the results.

The most important reaction mechanism is shown to be compound nucleus formation through ^{9}Be. In particular, in the neighbourhood of 1.0 MeV deuteron bombarding energy, the reaction proceeds largely by compound nucleus formation through the 17.28 MeV and 17.48 MeV levels of ^{9}Be. The results suggest a spin and parity assignment of $5/2^{+}$ for the 17.48 MeV level and agree with a previous assignment of $5/2^{-}$ for the 17.28 MeV level.

TABLE OF CONTENTS

LIST OF TABLES

LIST OF FIGURES

ACKNOWLEDGEMENTS

To Dr. Peter Martin, my friend and supervisor, I express my sincere gratitude for his continued interest, support and encouragement. I also wish to thank Dr. George Griffiths and Dr. Eric Vogt for many fruitful discussions.

From among my friends at the Van de Graaff my special thanks goes to Mr. Peter Bosman for assisting in the running of the accelerator and to Mr. Cy Sedger for his willingness to help in overcoming the technical problems encountered in my work.

To my friends at the Cecil my thanks goes for helping to make my stay in Canada so memorable.

I wish to thank the National Research Council of Canada for awarding me a Studentship for three years.

CHAPTER 1

INTRODUCTION

§1.1 General Introduction

The fundamental problem of nuclear physics is to understand the forces acting between the nuclear particles. Unlike atomic physics, where the interactions between the electrons and the nuclear core are known to be predominantly Coulomb in origin, the interaction between two nuclear particles cannot yet be exactly described. Rather, one proposes a form for the interaction, the validity of the model being tested by a comparison of theoretical predictions with experimentally known properties of nuclei. Accordingly early research followed the obvious course with intensive studies being undertaken of the simplest nuclear systems in which only two nucleons interact.

Unfortunately, little information on the details of the nuclear potential can be obtained from nucleon-nucleon low energy scattering experiments. In particular, at energies of less than 10 MeV, the scattering of the neutron-proton system is completely determined by just two quantities, the "scattering length", a, and the effective range, r_o(Bl 52, Pr 62). In general, any potential function contains at least two constants which can be adjusted to give the experimental values of a and r_o. Consequently, such low energy scattering experiments cannot determine the shape of the potential. This is not to imply that such experiments are of little value. An examination of the energy levels of mirror nuclei suggests that the n-n, n-p

and p-p nuclear forces are the same when the levels have the same angular momentum and spin-isospin symmetry. After corrections for all electromagnetic effects, a comparison of the singlet-spin scattering lengths for n-p and p-p scattering indicates that the nucleon-nucleon interaction is charge independent to within 2.1% (He 69). Conceivably, more accurate estimates of the respective scattering lengths could decrease this discrepancy.

The extension to more complicated reactions in which many nucleons are involved can be made if one considers that nucleons have a tendency to cluster into alpha particles or other larger clusters. Evidence that such is the case is afforded by the success of the cluster model (Ph 64, Ph 60) and of the nuclear shell model in predicting ground state spin and parity assignments. A separate treatment of the internal interactions and the interactions existing between the two particles can then often be made. An example of such an approach is illustrated by the Distorted Wave Born Approximation of direct reactions.

§1.2 Sequential Reactions

Another important class of reactions arises when three or more particles occur in the final state. Now the situation is considerably more complicated because of the multiplicity of possible correlations existing between pairs of the final state particles. As an example, consider the case of three particles in the final state. Firstly, the

reaction can proceed instantaneously as represented by

$$a + A \rightarrow b + c + d. \qquad (1)$$

If such is the case the energy spectra of any one of the final state particles is determined by the conservation laws and by the available phase space. On the other hand, any or indeed all of the "sequential" processes

$$a + A \rightarrow X^{*} \rightarrow b + B^{*} \rightarrow b + c + d. \qquad (2)$$

$$a + A \rightarrow X^{*} \rightarrow c + C^{*} \rightarrow c + b + d. \qquad (3)$$

$$a + A \rightarrow X^{*} \rightarrow d + D^{*} \rightarrow d + b + c. \qquad (4)$$

may take place. The compound nucleus state, X^{*}, is introduced to account for the possibility that the first stage of the reaction might proceed via compound nucleus formation. Often, however, the reaction may proceed via a direct mechanism in which case it should be written

$$a + A \rightarrow b + B^{*} \rightarrow b + c + d. \qquad (5)$$

When a sequential process takes place, the energy spectrum of the first emitted particle will exhibit definite structure, due to the "final state" interaction existing between the other two particles. Clearly, interference effects between the different final state interactions, (2) to (5), will further complicate the energy spectra observed in a particular experiment and the relative contributions of these processes will depend upon the structure of the nuclei involved. A study of sequential reactions can hence be used as a useful probe in determining details of nuclear structure.

When the lifetime of the intermediate state, B^{*} say, is comparable to the transit time of a particle across the

nucleus ($\sim 10^{-22}$ sec.), the reaction is no longer sequential and instantaneous breakup occurs. On the other hand, the intermediate state may be of sufficient duration that its decay products are not influenced by the first emitted particle. The formation and decay of the intermediate state can then be treated independently. One can then usefully investigate not only the shape of the "resonance" but also the angular dependence of its decay products. The dependence on the direction of the first emitted particle, as revealed by angular correlation measurements, yields important information not only on the spin and parity of the intermediate state, but also on its polarisation. The polarisation will in turn indicate what the reaction mechanism is, whether it be direct or compound nuclear in nature.

In the intermediate lifetime case, the interaction between two of the final state particles may be modified by the presence of the third particle. Rescattering, where one of the secondary decay products has sufficient energy to catch up to and interact with the first emitted particle, is one such example. The kinematical conditions under which rescattering can be expected are discussed by Aitchison and Kascer (Ai 66) and Valkovic et al (Va 68). The contribution of such a process should be large only when two particles rescatter into one of their resonant states.

§1.3 Review of Previous Work

The theory of final state interactions is now largely

understood due to the efforts of Watson (Wa 52), Migdal (Mi 55) and Phillips, Griffy and Biedenharn (Ph 60a). In the Watson-Migdal theory a sequential reaction such as (2) is considered as proceeding backwards in time: the particle c bombards d and produces a metastable nucleus B^*

$$c + d \rightarrow B^* \tag{6a}$$

which serves as the target particle for the next step of the reaction

$$b + B^* \rightarrow X^* \rightarrow a + A. \tag{6b}$$

The probability of the whole reaction (6a), (6b) proceeding should then be proportional to the formation cross section of B^* by reaction (6a). This is expected to be true whenever the nucleus B^* is produced in a narrow resonant state by strong short range interactions. Detailed balancing then gives the cross section for the sequential reaction (2) as proportional to the cross section for reaction (6a) viz.

$$\sigma \propto \sin^2 (\delta + \phi)/P \tag{7}$$

where δ is the scattering phase shift for c + d, ϕ the usual hard sphere phase shift and P the barrier penetration factor.

In the theory of Phillips et al (PGB theory) the three body decay is considered as a well separated time sequence of two body decays. Thus it is supposed that the decay of X^* (see equation (2)) first occurs to all states of B^* that are energetically allowed by the emission of the observed particle b. Subsequently, the localised system B^* decays into c + d, with the restriction that c and d be localised for a time slightly longer than is required for particle b to escape from

the interaction volume. Under these conditions the cross section for observing b with a discrete energy is proportional to the number of ways in which B^* may be left localised in space at the appropriate energy of excitation, E_B. Appropriately enough, the calculated quantity is called the "generalised density of states function" and one approximate form of this function is given by

$$\rho(E_B) \propto \frac{d}{dE_B} (\delta_1 + \phi_1). \qquad (8)$$

which in the limit of a single isolated resonant state reduces to the Watson-Migdal form.

Of particular interest are three particle final state interactions in which at least two of the particles are nucleons. These reactions allow the determination of the singlet spin scattering length, a^s, of the two nucleon systems. One reason for this interest is the possibility of determining the parameters describing the n-n interaction by observing this interaction as a final state interaction.

An example of how this technique can be applied is illustrated by the reactions d(p,n)2p and d(n,p)2n. Niiler et al (Ni 69) carried out measurements using the former reaction with incident proton energies in the range of 6.5 to 13.0 Mev. They detected the two final state protons in coincidence and found, depending on the detector configuration, that the yield was dominated by either direct knockout of a target nucleon or by sequential decay through the singlet state of the n-p system. By applying the PGB theory they were able to fit their results

with $a^s_{np} = -23.9 \pm 0.8$ fm, a value in excellent agreement with that obtained from free n-p scattering ($a^s_{np} = -23.71 \pm 0.01$, He 69). Such excellent agreement instills some confidence in one's ability to extract the n-n scattering length from the mirror reaction d(n,p)2n. Zeitnitz et al (Ze 70) using an incident neutron beam of 18.5 MeV and a double time of flight technique obtained a value for the singlet scattering length of $a^s_{nn} = -16.4\ ^{+2.6}_{-2.9}$ fm, in this instance using the Watson-Migdal approach. This result is in agreement with that of Grassler and Honecker (Gr 69) and Slobodrian et al (Sl 68).

For similar reasons the triad of reactions ^{3}He(^{3}He,α)pp, T(^{3}He,α)pn and T(T,α)nn have been the subject of intensive study. Now, however, the energy spectrum of a final state particles shows considerable structure, largely owing to sequential decay through the mass five system, and the influence of the nucleon-nucleon final state interaction is in some cases not clearly established. For example, the ^{3}He(^{3}He,α)pp reaction has been studied using coincidence techniques over a wide range of bombarding energies and information on the p-p scattering length has been obtained with varying degrees of success. At an energy of 1.5 MeV, Blackmore and Warren (Bl 68) have observed both the ^{5}Li ground state and p-p final state interactions. No definite value was extracted for the singlet scattering length , a^s_{pp}, because of uncertainties in estimating the contribution from the ^{5}Li* first excited state. At higher energies in the range 3.0 to 18.0 MeV, Bacher and Tombrello (Ba 65) found the yield to be dominated by sequential decay through the ^{5}Li ground state with little or no

evidence of the singlet p-p interaction. At even higher energies in the neighbourhood of 50 MeV, Slobdrian et al (Sl 67) clearly observed the p-p interaction and using the PGB theory were able to assign a value of $a^s_{pp} = -7.7$ fm to the p-p singlet scattering length. In all instances the contribution to the spectra from the ^{5}Li ground state was well described by either the PGB or Watson-Migdal formulism.

Beveridge and Johnson (Be 71) measured α-p coincidences and employed particle identification techniques in an experimental measurement of the reaction T(^{3}He,α)pn. At a bombarding energy of 1.5 MeV they found the reaction to be dominated by sequential decay through the ^{5}He ground state with some contribution from simultaneous breakup and the singlet n-p interaction. They found that both the Watson-Migdal and PGB theories gave equally good fits to the experimental spectra and obtained a best fit with a value of $a^s_{np} = -21\ ^{+3}_{-4}$ fm for the n-p singlet scattering length. The large errors result from their inability to determine precisely the contribution to the yield from sequential decay through the first excited states of ^{5}Li and ^{5}He. Their analysis suggests that the T(T,α)nn experiment would lead to a determination of a^s_{nn} with similar large errors and they conclude that the n-n singlet scattering length would be better obtained from the d(n,p)nn reaction discussed above or the d(π^-,γ)nn reaction.

There are several other reactions in which sequential decay through the mass five system are important. One such example is the ^{6}Li(^{3}He,pα)α reaction. Young et al (Yo 65) measured the α-α coincidence yield at a bombarding energy of

2.7 MeV. While they were unable to obtain any quantitative results they were able to observe sequential decay through the ground state of ^{5}Li and the 16.62 and 16.92 MeV states of ^{8}Be. A more serious attempt to obtain an insight into the reaction mechanism for the formation and decay of ^{5}Li in this reaction has been made by Reimann et al (Re 67, Re 68). The experiment was performed at bombarding energies of 1.0, 1.25 and 1.5 MeV with sufficient energy being released in the breakup to allow all three final state particles to be detected in coincidence. In this manner background effects were largely eliminated. Their results showed the existence of an asymmetry of the decay products about the ^{5}Li recoil direction. In addition, the total cross section for the formation of ^{5}Li was of the order of a few hundred millibarns. Such a large cross section is suggestive of a direct mechanism, involving for example one or two particle transfer. By invoking a semiclassical argument in which the ^{5}Li nucleus retained some memory of its formation they were able to explain the gross energy dependence of this asymmetry. In particular, they showed that the origin of the asymmetry depended on the short lifetime of the ^{5}Li state and the memory retained by the "extra core" proton, during this short time, of its localisation at the time of the ^{5}Li formation. As a result of this work it was felt that a study of the reaction ^{7}Li(d,α)nα, in which ^{5}He is produced as an intermediate state, would provide a further test of this model. This was the initial reason for undertaking the work described in this thesis.

Studies of the reaction ^{7}Li(d,α)αn have been reported

in the literature on several occasions. These experiments can be broadly classified into three groups. The first group consists of those experiments in which only one of the final state particles was observed. Consequently, considerable ambiguity existed in interpreting the spectra. Within this category falls the work of Weber (We 58), Paul and Kohler (Pa 63) and Manalis and Henkel (Ma 64). Their measurements, performed at a variety of bombarding energies in the range 1.175 MeV to 2.0 MeV did establish that the reaction was dominated by sequential decay through the ground state of ^{5}He. By using known n-α phase shifts they were able to fit the gross features of the alpha particle spectrum.

The second group of experiments includes those in which a coincidence measurement was performed but the momentum of only one of the final state particles was recorded. One such experiment was performed by Riviere (Ri 56, Ri 57). At an incident bombarding energy of 0.9 MeV he recorded α-α coincidences and obtained the angular correlation for the decay of ^{5}He in its rest frame in the form $1 + k\sin^2\theta$ with $k \sim 7$. In addition, he established that the angular distribution of the first emitted alpha particles, corresponding to the formation of ^{5}He, was isotropic to within 10%. Also he imposed an upper limit of 10% on the contribution to the yield from simultaneous breakup and sequential decay through ^{8}Be. His conclusions disagree with those of French and Treacy (Fr 51) who performed a similar measurement at an energy of 0.93 MeV. They found the angular correlation of the ^{5}He decay products to be given by $1 + 1.2\sin^2\theta$. At a somewhat lower energy, E_d = 0.15 to 0.2 MeV, Fessenden and Maxson (Fe 64) obtained the α-α angular

correlation in the form $1 + k\sin^2\theta$ with $k = 2.4\ ^{+1.5}_{-1.0}$ which suggests that compound nucleus formation through a $5/2^-$ state of ^{9}Be is largely responsible for the yield. In addition, they claim to have observed the ^{5}He first excited state although there was considerable ambiguity regarding the correct identification of the alpha particle groups. Farley and White (Fa 57) performed the experiment at 0.16 MeV but rather than detect α-α coincidences they measured γ-n coincidences. However, they did not measure the neutron energy by time of flight techniques. After correction for neutron detector efficiency they obtained the angular correlation as $1 + 0.7\sin^2\theta$. This result is at odds with the measurement of Fessenden and Maxson and points to the need for performing "complete" experiments such as those discussed below.

In the third category, which is by far the most important, fall those experiments in which the momenta of at least two of the final state particles are recorded. The first such measurement on the ^{7}Li(d,α)nα reaction was reported by Jones *et al* (Jo 65) at an incident energy of 2.0 MeV. By recording the results in a two dimensional array using a dual parameter multichannel analyzer, they were able to observe clearly sequential decay through the ^{5}He ground state and the 16.62 MeV excited state of ^{8}Be. Some evidence for sequential decay through the ^{5}He first excited state and the broad 11.4 MeV level of ^{8}Be was also observed. In addition, the contribution from simultaneous breakup was shown to be small by observing the coincidence yield in a region in which it was kinematically

impossible for the ^{5}He ground state to appear.

Similiar conclusions were obtained by Assimakopoulos et al (As 65, As 66) in an experiment at 0.38 MeV. They detected α-α coincidences using solid state detectors. They found the reaction to be dominated by sequential decay through the ^{5}He ground state and first excited state. Contributions from instantaneous breakup and sequential decay through the 11.4 MeV state of ^{8}Be were shown to be not more than a few percent. The only experimental measurement in which there has been any substantial evidence for the existence of this latter state was performed by Hofmann and Domke (Ho 69). They claim to have observed this state and have assigned a width of 2.8 MeV to it, a value considerably less than that found in the literature ($\Gamma \sim 7$ MeV, La 66).

Milone and Potenza (Mi 66) carried out α-α coincidence measurements at an incident energy of 0.8 MeV. They found the reaction yield to be dominated by sequential decay through the ^{5}He ground state and that the angular distribution of the alpha particles while symmetric about 90^{o} was not isotropic. In addition the α-α angular correlation was found to be symmetric about the ^{5}He system centre of mass recoil direction and could be expressed in the form $1 + k\sin^{2}\theta$ with $k = 3.0 \pm 0.3$. This suggests that the level of spin $5/2^{-}$ at an excitation energy of 17.28 MeV in ^{9}Be is largely responsible for the yield.

More recently, a thorough study of this reaction has been reported by Valkovic et al (Va 67). Their work considered deuteron beams with energies of 2.0 to 4.0 MeV. Both α-α and

α-n coincidences were simultaneously recorded with the neutron energy being determined by time of flight. Their work clearly showed that the reaction proceeds by sequential decay through the ^{5}He ground state, the 2.9 MeV, 16.62 MeV and when energetically allowed the 16.92 MeV excited states of ^{8}Be. They found it difficult to establish the existence of either the ^{8}Be* (4+) state (at 11.4 MeV) or the ^{5}He first excited state.

In summary, then, the literature establishes quite clearly that, over a large range of bombarding energies, the reaction ^{7}Li(d,α)αn proceeds sequentially through states of ^{5}He and ^{8}Be, with the ^{5}He ground state being particularly prominent. Also at E_d = 0.8 MeV, it seems the reaction mechanism responsible for the formation of ^{5}He is compound nucleus formation through a $5/2^-$ level at an excitation energy of 17.28 MeV in ^{9}Be. At other energies the reaction mechanism is less clear, a conclusion partially accounted for by ambiguities in interpreting the results of incomplete experiments.

In this thesis, an experimentally complete measurement of this reaction at 1.0 MeV bombarding energy will be discussed in which both α-α and α-n coincidences are recorded. In particular, angular correlation measurements are made with a view to determining the reaction mechanism for the formation of the ^{5}He ground state. The situation at 1.0 MeV is particularly interesting since this corresponds to an excitation energy in ^{9}Be of 17.46 MeV, in the region of which a level of positive parity but unknown spin has been reported (La 66). The existence of this level has been noted by Bagett and Bame (Ba 52) and

Baskkin (Ba 54) in studies of the reaction $^{7}Li(d,p)^{8}Li$. Moreover, the elastic scattering of deuterons by ^{7}Li shows an anamolous rise at about 1.0 MeV which is consistent with the existence of a positive parity resonance in ^{9}Be (Fo 64). Thus one would anticipate that the reaction mechanism for the formation of ^{5}He at 1.0 MeV would be dominated by compound nucleus formation through the 17.28 and 17.48 MeV states of ^{9}Be. Angular correlation measurements at this energy might well lead to a spin assignment for the latter level in ^{9}Be.

CHAPTER 2

KINEMATICS OF THE REACTION ^{7}Li (d, α) n α.

§ 2.1 Three Particle Final State Kinematics

When three particles are produced in the final state, this state is completely determined by specifying the laboratory momenta of the three particles. These nine degrees of freedom, however, are readily reduced to five by imposing energy and momentum conservation. For instance, an experiment on three body decay would completely determine the final state by measuring the momentum of one particle, while specifying the direction of emission of the second. In actual practice it is customary to measure the momenta of two particles and use this overdetermination of the final state for the elimination of background effects.

When the directions of two of the final state particles are determined their respective energies are kinematically restricted to a contour which expresses one energy as a function of the other. Such a contour, on an energy-energy plot, is elliptical and varies with the choice of detector positions. For a given reaction, the energy-energy contours are readily calculated from a knowledge of the conservation laws.

The position of an event on the appropriate contour is determined by the particular distribution of the available energy among the three particles. In the case of simultaneous decay, all points on the contour are accessible with the density of events along the contour being determined solely by phase space considerations (Br 65). In direct contrast with this, a sequential

process, which can be regarded as a time separated sequence of two body events and thus determines the energy distribution uniquely, appears as a point on the contour. Sequential processes going through short lived intermediate states then appear as line segments on the contour, owing to the natural width of these states. In any experimental measurement these segments are broadened by the finite solid angles of the detectors used, since they allow an uncertainty in the angle of emission of the observed particles.

§ 2.2 Kinematics of the Reaction $^{7}Li\ (d,\alpha)n\alpha$.

At an incident deuteron energy of 1.0 MeV, the final state of two alpha particles and a neutron can be achieved through any of the following channels (Q - values from Maples et al, Ma 66):

$d + {}^{7}Li \longrightarrow$

- $\alpha + \alpha + n + 15.122$ MeV
- $\alpha + {}^{5}He(0,\ 3/2^{-}) + 14.165$ MeV
  - $\longrightarrow n + \alpha + 0.957$ MeV
- $\alpha + {}^{5}He^{*}(2.6,\ 1/2^{-}) + 11.6$ MeV
  - $\longrightarrow n + \alpha + 3.5$ MeV
- $n + {}^{8}Be(0,0^{+}) + 15.027$ MeV
  - $\longrightarrow \alpha + \alpha + 0.095$ MeV
- $n + {}^{8}Be^{*}(2.89,\ 2^{+}) + 12.13$ MeV
  - $\longrightarrow \alpha + \alpha + 2.99$ MeV
- $n + {}^{8}Be^{*}(11.4,\ 4^{+}) + 3.6$ MeV
  - $\longrightarrow \alpha + \alpha + 11.5$ MeV

The number in parentheses is the excitation energy of the

intermediate state and the $J\pi$ assignment for that state respectively.

While all of the above channels are possible energetically, sequential decay through the $^{8}Be^{*}(2.89)$ state and ^{5}He ground state are expected to be the dominant ones. The main concern of this thesis is to determine the reaction mechanism for the formation of the ^{5}He ground state by measuring $\alpha-\alpha$ and and α-n angular correlations. It is appropriate, then, to assign the label "α_1" to the alpha particle associated with the formation of ^{5}He, and the label "α_2" to the alpha particle resulting from the decay of ^{5}He. Once the position of the α_1 detector has been selected, a recoil direction is defined for the ^{5}He system and the latter's decay products are confined by momentum and energy conservation to a cone about this recoil direction. Kinematic calculations have been performed for four possible angles of emission of α_1, namely $\alpha_1 = 60^{\circ}$, 65°, 100° and 120° on the assumption that all particles are detected in a plane coplanar with the beam. The results of these calculations are shown in Fig. 2.1 to Fig. 2.4 respectively. Since the characteristic features are similar in all four cases it is necessary to discuss only one, say $\alpha_1 = 60^{\circ}$.

Fig. 2.1 is divided into two sections. The upper part gives the energy of neutron groups associated with various intermediate states as a function of neutron angle on the assumption that an n-α coincidence measurement is performed, whilst the lower portion is a similar diagram for an $\alpha-\alpha$ measurement. Neutron and alpha particle energies resulting

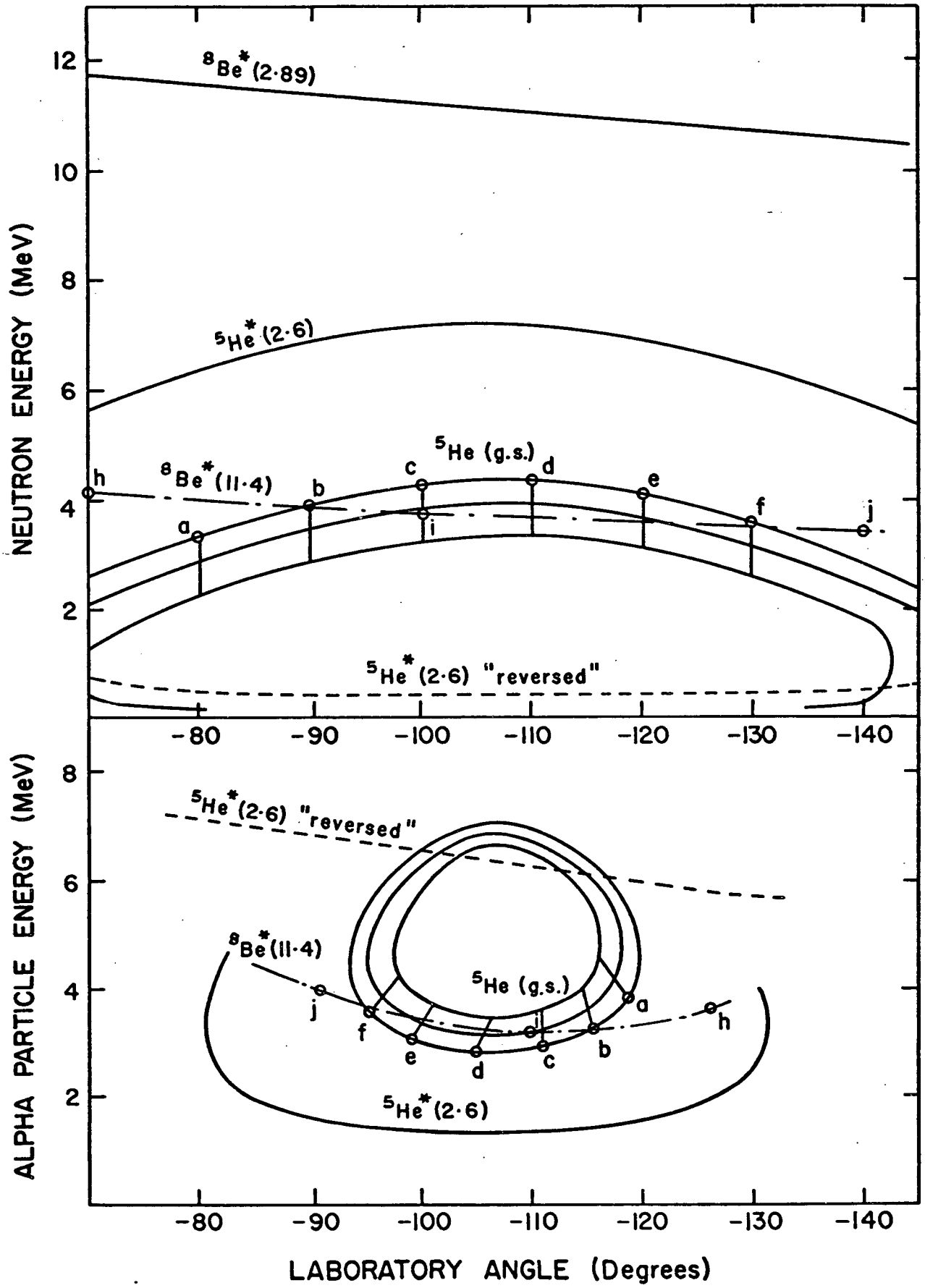

Fig. 2. 1. Kinematic Phase Diagram for α_1 at 60° and a bombarding energy of 1.0 MeV. Lower case letters indicate corresponding points on neutron and α-particle curves.

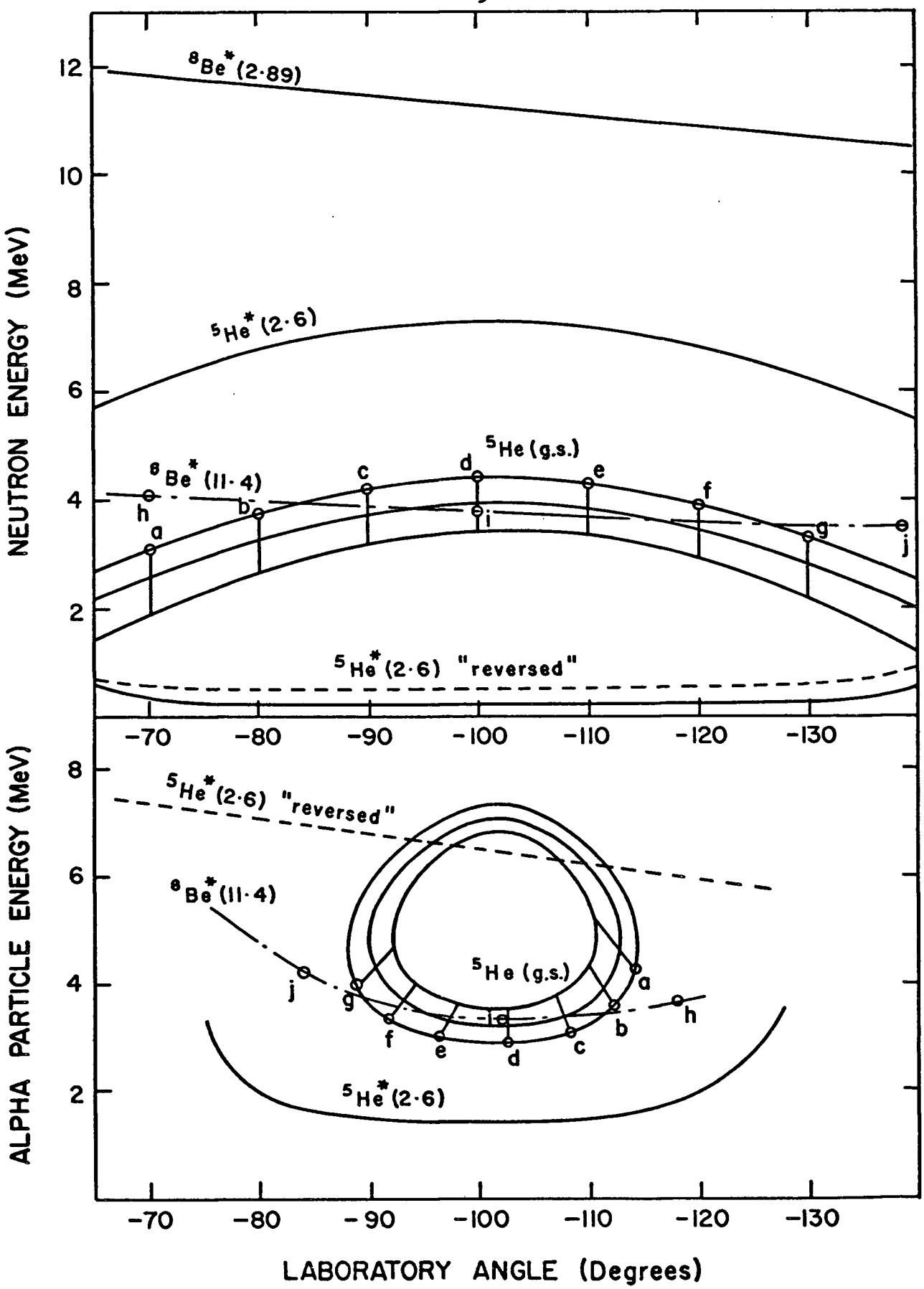

Fig. 2.2 Kinematic Phase Diagram for α_1 at 65° and a bombarding energy of 1.0 MeV. Lower case letters indicate corresponding points on neutron and alpha particle curves.

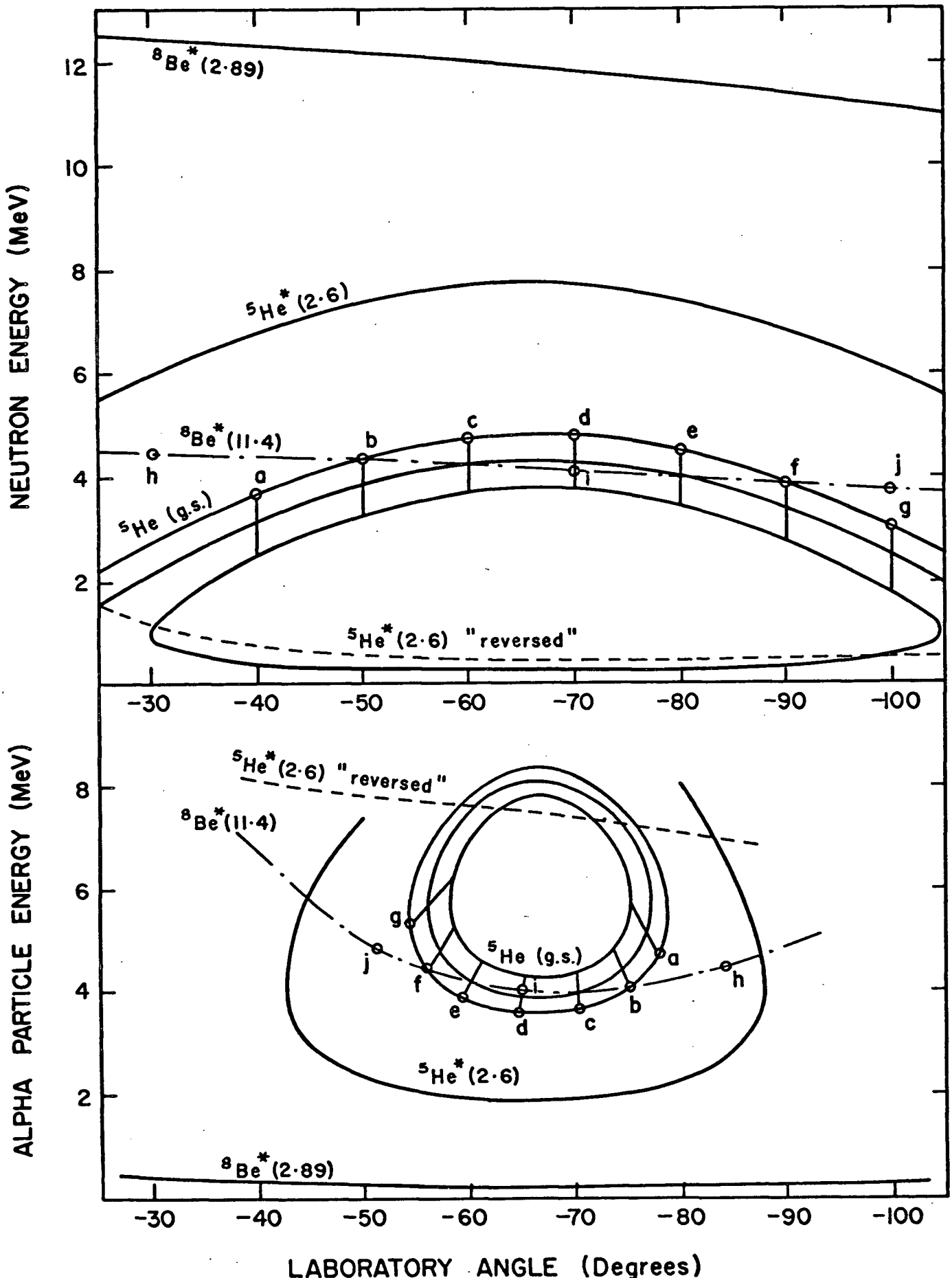

Fig 2.3 Kinematic phase diagram for α_1 at 100° and a bombarding energy of 1.0 MeV. Lower case letters indicate corresponding points on neutron and alpha particle curves.

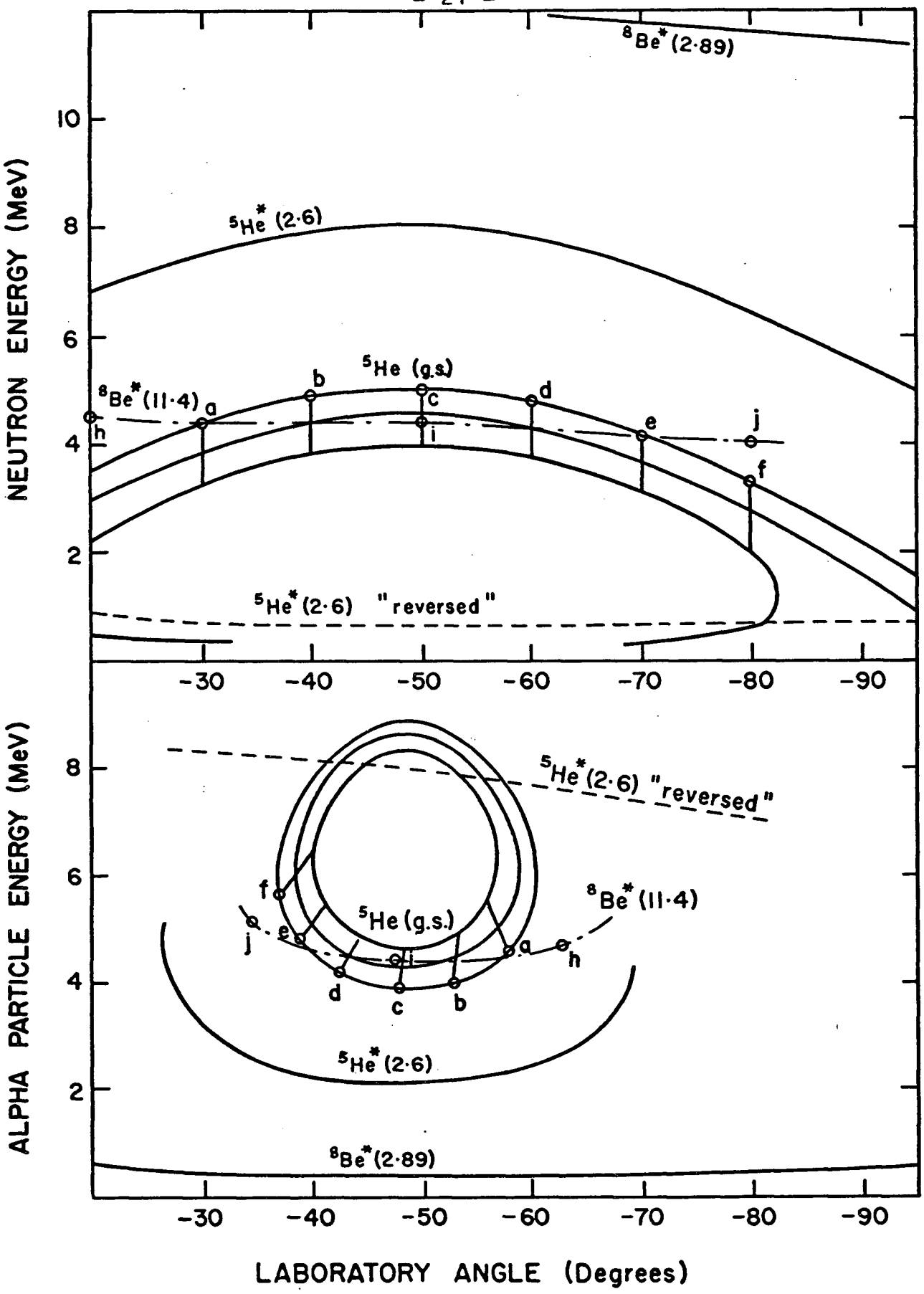

Fig 2.4 Kinematic Phase Diagram for α_1 at 120° and a bombarding energy of 1.0 MeV. Lower case letters indicate corresponding points on the neutron and α-particle curves.

from the decay of the ^{5}He ground state are shown as bands, representative of the width of this state ($\Gamma \sim 0.6$ MeV). Corresponding points on the neutron and alpha particle curves are labelled by lower case letters running from "a" to "f". It is immediately apparent that it is more appropriate to perform an n-α angular correlation measurement rather than an α-α coincidence measurement because of the larger angular spread over which measurements can be made. This fact is somewhat counterbalanced by the experimental difficulty associated with the variation of neutron detector efficiency as a function of energy. For the moment this point will not be discussed further.

Unlike the ^{5}He ground state, contributions from the broad first excited state of ^{5}He ($\Gamma \sim 4$ MeV) can arise in two distinct ways. On the one hand, the first emitted alpha particle can be detected by the α_1 detector with the subsequent decay of the ^{5}He* state being determined by the α_2 or neutron detectors in an analogous fashion to that described above for the decay of the ground state. The mean neutron and alpha particle energies resulting are shown labelled by "^{5}He*(2.6)" in Fig 2.1. The other alternative kinematic situation arises when the alpha particle resulting from the decay of the ^{5}He* state is detected by the α_1 detector whilst the first emitted alpha particle is detected by the α_2 detector. Under these circumstances the two curves labelled by "^{5}He* (2.6) reversed" are obtained. In all cases, the mean neutron energy resulting from the decay of ^{5}He* state is well separated from the group resulting from the decay of the ground state. The large width of the excited state does

imply that some interference will arise from contributions proceeding through the lower extremity of this state. These interference effects, however, should be small.

The energies of the final state particles resulting from the formation and decay of the $^{8}Be^{*}$ (2.89) and $^{8}Be^{*}$ (11.4) states are also shown. (The ground state has not been drawn because the neutron removes 13.5 MeV leaving the two alpha particles to share something like 2.0 MeV. Thus they are not going to appear in a region of interest.) The neutron group resulting from the $^{8}Be^{*}$ (2.89) state is of the order of 10 to 12 MeV and is well separated from the neutron group associated with the ^{5}He ground state decay. However, the same cannot be said of the neutrons from the $^{8}Be^{*}$(11.4) state. In fact, this state gives rise to neutron and alpha groups of almost the same energy as those of interest. Fortunately, the large width of this state ($\Gamma \sim 7$ MeV) implies that for given detector settings, the energy distribution of the detected particles will be very broad. In fact, it may well be inappropriate to regard this reaction as a sequential process. In any event, previous experimenters have shown this state to be at best only weakly excited.

An examination of Figs 2.1 to 2.4 does show that sufficient energy is liberated by the breakup to enable the simultaneous detection of all three final state particles. Such an experimental arrangement is naturally very desirable, since random background coincidences, largely attributable to the high count rate in the neutron detector, would be almost entirely

eliminated without loss of overall efficiency. Examples of appropriate detector positions are shown by pairs of lower case letters in Figs 2.1 to 2.4.

Considerable care must be excercised in order to avoid the creation of geometrical asymmetries. For example, it would seem most appropriate in this experiment to record α_1-n coincidences in a two dimensional multichannel analyser using the α_2 signal to generate an external gate pulse. Under these circumstances, the α_2 detector must be chosen to subtend a sufficiently large solid angle at the target so as to accept all the ^{5}He breakup alpha particles associated with neutrons incident on the neutron detector. Further problems arise when the α_2 and neutron detectors are placed close to the recoil direction. Now the α_2 detector and its mounting cause attenuation of the neutrons incident on the neutron detector. Unfortunately, the amount of attenuation is not readily calculable and consequently the need for performing both double and triple coincidence experiments becomes apparent.

In an experiment such as the one discussed here it is often convenient to record the data in the form of a two dimensional energy-energy array using a multichannel analyser. In the case of n-α coincidence measurements, however, the measured quantities are effectively the neutron time of flight (to be specific, the difference in arrival time between the neutron and alpha particle pulses) and the alpha particle energy. It is appropriate, then, to perform kinematic calculations giving the locations of the various intermediate states in the alpha particle

energy versus neutron time of flight plane. Typical examples of these calculations are shown in Fig 2.5 and Fig 2.6 for $\alpha_1 = 65^\circ$ and 100° respectively. By choosing the neutron and alpha particle flight paths to be 1.00 metre and 0.08 metres respectively, a situation closely resembling the experimental one is realised (see Chapter 4). The solid curves are calculated kinematical contours along which all processes leading to a three body final state of two alpha particles and a neutron must lie. Contributions from sequential decay through the various intermediate states should then appear as enhancements on a smoothly varying background attributable to simultaneous breakup. The predicted locations of these enhancements are shown in Fig 2.5 and Fig 2.6.

Fig 2.7 is a similiar diagram showing the predicted location of the intermediate state enhancements if α-α coincidence measurements are recorded. The two contours correspond to the α_1 detector being at 100° and the α_2 detector at -65° and -75° respectively.

The situation is a little more complicated than in the case of n-α coincidence measurements because enhancements from both the ^{5}He ground and first excited states can appear in four different locations. Nevertheless, two of the ground state groups can be isolated provided simultaneous breakup and sequential decay through the ^{8}Be* (11.4) state are relatively unimportant. The usefulness of doing α-α coincidence measurements, however, is seriously limited by the small angular range ($\sim 20^\circ$) over which the α_2 detector can be moved. It seems more convenient,

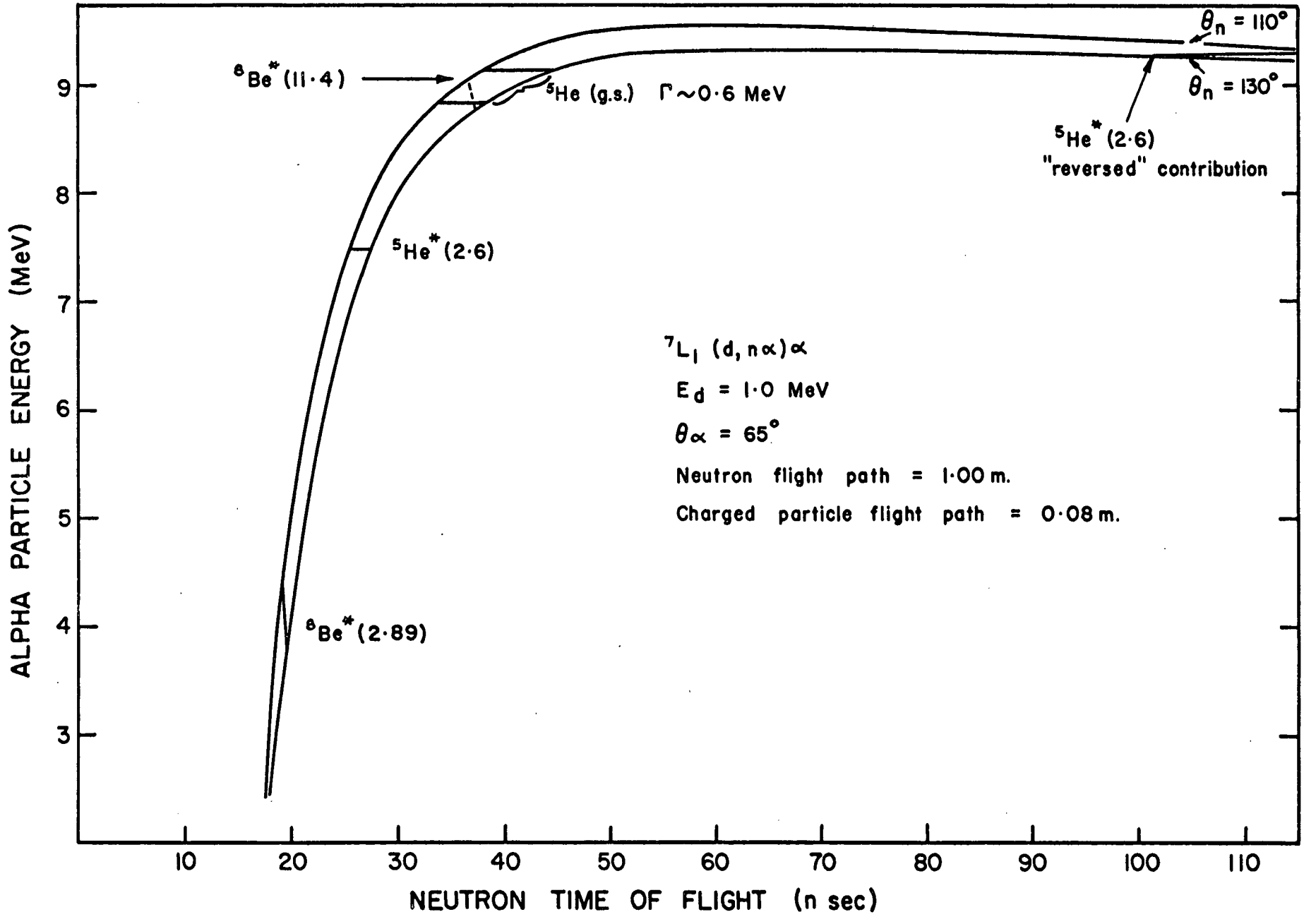

Fig 2.5 Neutron-alpha particle contours showing location of possible final state interactions.

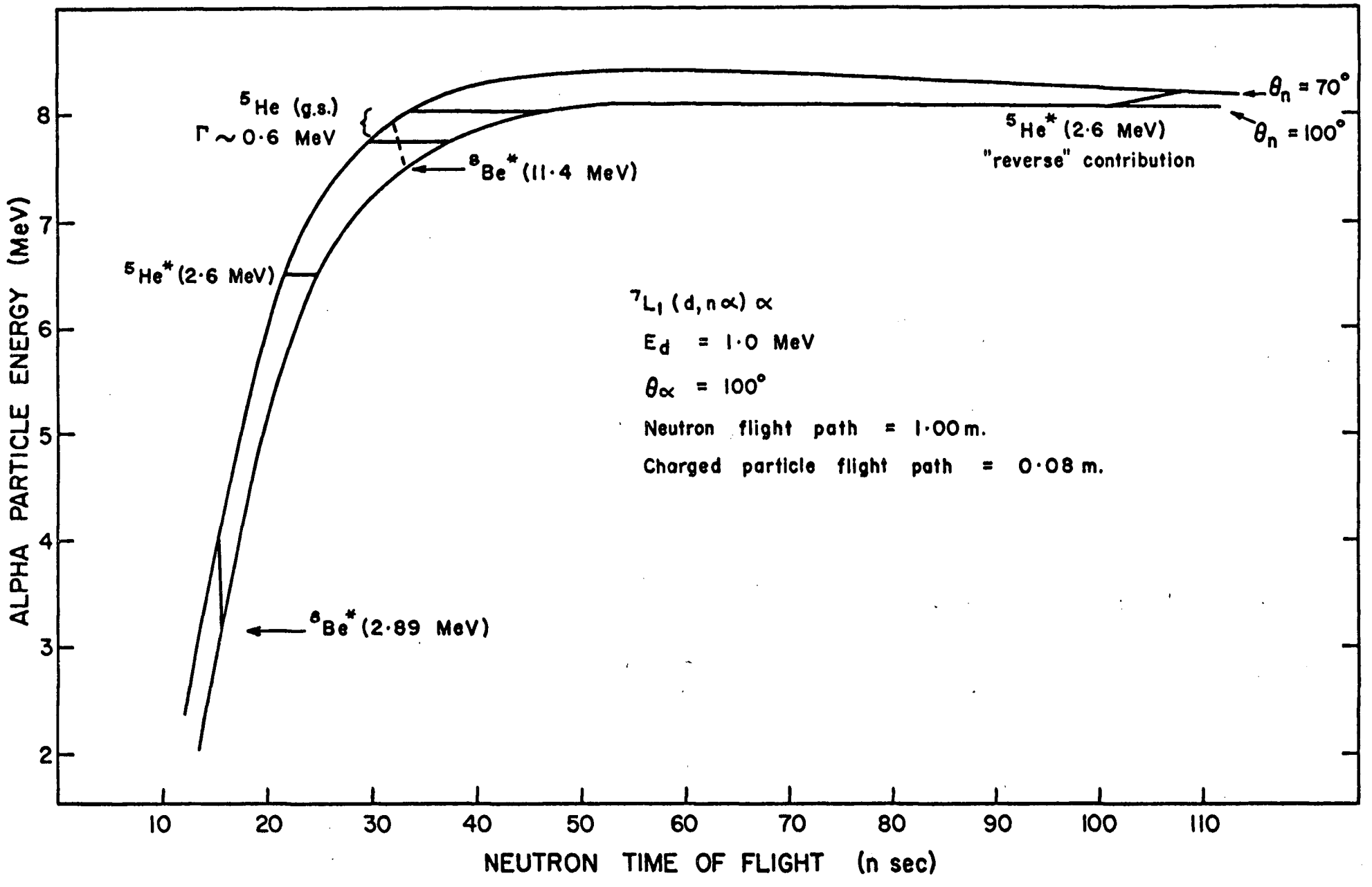

Fig 2.6 Neutron-alpha particle contours showing location of possible final state interactions.

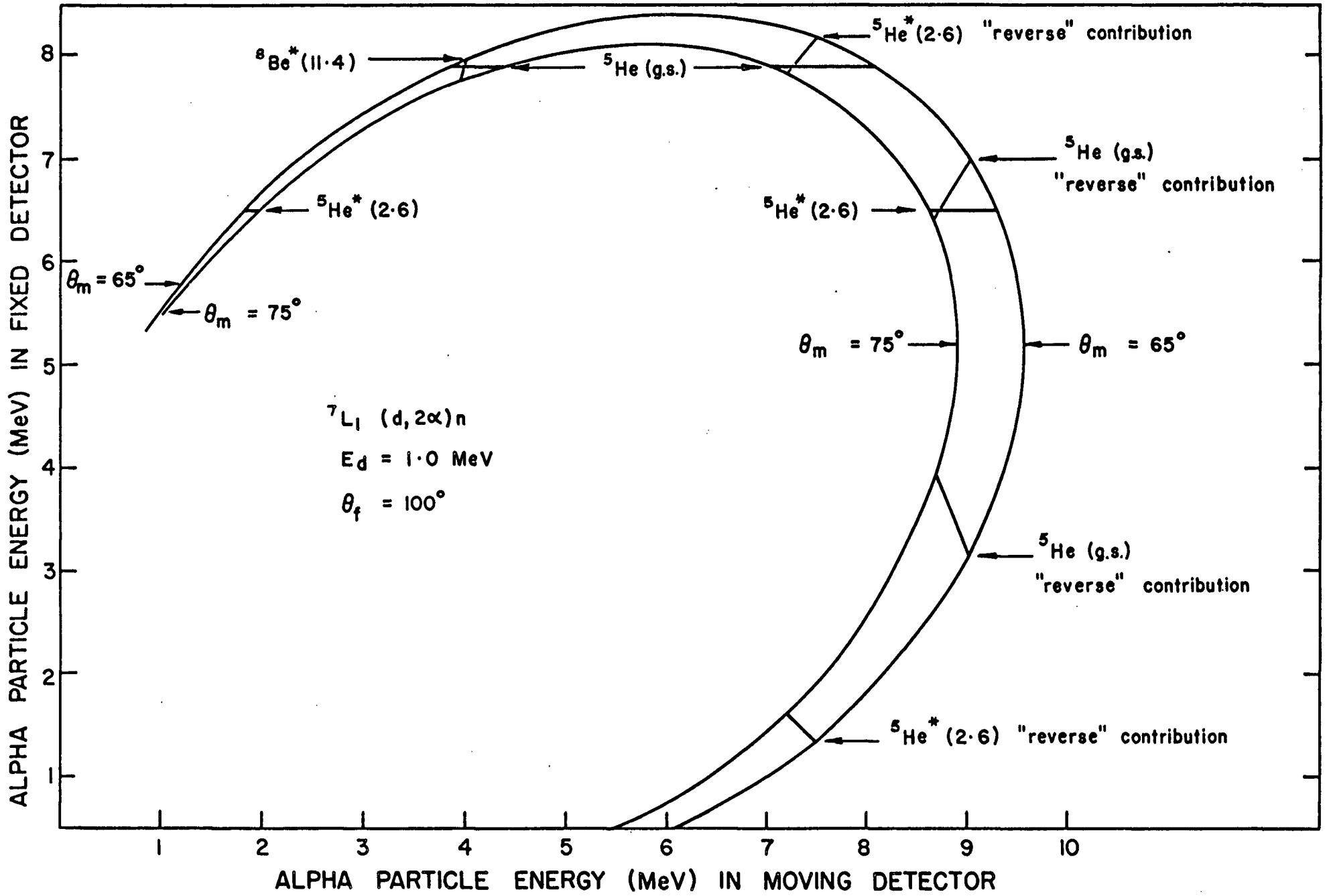

Fig 2.7 Alpha-Alpha contour plots showing location of possible final state interactions.

then, to measure α-n coincidences and when possible to employ triple coincidence techniques.

CHAPTER 3

EXPERIMENTAL TECHNIQUE

§3.1 Introduction

A 0.3μA beam of 1.0 MeV deuterons obtained from the UBC 3 MeV Van de Graaff was allowed to bombard a target of enriched ^{7}LiF evaporated onto a thin film of carbon. Charged particle reaction products were detected using silicon surface barrier detectors whilst neutrons emanating from the target were detected with a liquid scintillator coupled to a suitable photomultiplier tube. Both α-α and α-n coincidence spectra resulting from the reaction

$$d + {}^{7}Li \rightarrow \alpha_1 + {}^{5}He \quad (\rightarrow \alpha_2 + n)$$

were obtained and accumulated using a two parameter multi channel analyser as energy-energy and energy-time of flight contours respectively.

For a particular angular correlation (fixed α_1 angle), relative normalisation of the coincidence yield was achieved by setting a single channel analyser window on the high energy end of the spectrum of particles detected by the α_1 detector. Absolute normalisation was accomplished by comparing the counts in this window with the elastically scattered deuterons from ^{19}F monitored by an additionalfixed detector placed at an angle of 120^{o} in the laboratory frame of reference.

The technical aspects of these measurements are now discussed in this chapter.

§3.2 Scattering Chamber

A brass chamber, nominally 12" in diameter and 9½" deep was used to mount the target and solid state detectors. The chamber was equipped with its own 100 L sec $^{-1}$, liquid nitrogen baffled oil diffusion pump. Two detector holders, one mounted on the top and the other on the bottom of the chamber, could be externally positioned at any angle in the reaction plane. Beam definition was achieved using two 1.6 mm diameter tantalum collimators spaced some 18.3 cm apart. The choice of tantalum, which is difficult to machine, for the collimator material was dictated by the need to keep the background γ-ray level as low as possible. Slit scattering was reduced by employing a 2 mm diameter skimmer some 12 mm behind the second collimator. With the distance between the skimmer and target being some 8.6 cm a beam spot of $\sim$8 mm^2 on the target was illuminated. Measurement of beam current was carried out using a Faraday cup equipped with an electron suppression ring. A long side arm making an angle of 120.0 ± 0.5° with the forward beam direction was attached to the chamber. At its outer extremity a detector holder was placed for mounting the monitor detector. Additional lucite ports were available for viewing the target.

The target holder assembly consisted of a flat aluminum strip 12½" x 1½" x ¼" attached to a 3/8" stainless steel rod. The latter rod passed through the chamber bottom, a rotating seal providing the vacuum seal and also facilitating the external adjustment of target angle. The aluminum strip was guided by a locating strip in the chamber lid (suitably domed) and could

be moved vertically over a range of several inches. Seven equally spaced $\frac{1}{2}$" diameter holes were drilled through the strip and were counterbored to a depth of 1/8" using a 1" diameter bit. Brass collars with inside and outside diameters of $\frac{1}{2}$" and 1" respectively (the target holders proper) were then mounted in the body of the aluminum strip using small screws. The geometry of the holder was carefully chosen so that the vertical symmetry axis of the chamber was located in the plane of the target.

Preliminary alignment of the collimator system was performed using the beam from a gas laser, placed some distance away from the chamber. The chamber position was adjusted until the beam passed through the collimators and illuminated the tip of a removable pointed spindle attached to the target holder rod. The zero positions for the external angular scales for the two movable solid state detectors were fixed by rotating each detector in turn until the detector collimator was illuminated by the laser beam. Simultaneously, the height of each detector was adjusted to ensure that it was in the horizontal plane containing the beam. Further checks on the detector geometry were carried out by measuring the elastic scattering of 1.0 MeV protons from a thin self supporting film of ^{12}C. The detector fixed at 120° was used as the monitor whilst each of the two movable detectors was placed first at 45° and then -45°. A comparison of the yield in the two cases indicated that the external angular settings were accurate to better than $\frac{1}{2}$°.

§3.3 Target Preparation

The targets used in this experiment consisted of a thin layer of ^{7}LiF evaporated onto a self supporting film of carbon. The preparation of the carbon foils was carried out in a manner similar to that described by Dearnaley (De 60). Clean glass microscope slides were positioned some 7 cm above two pointed $\frac{1}{4}$" diameter carbon rods held in contact by tension springs. When a current of $\sim$100 A passed through the rods the contact point reached a sufficiently high temperature that an arc was produced in which the carbon evaporated. With the evaporation being carried out in a vacuum $\sim 10^{-6}$ Torr. a total elapsed time of 30 sec, achieved with several short evaporations, resulted in carbon foils of thicknesses between 15 and 30 $\mu gm\ cm^{-2}$ being deposited on the glass slides. The carbon deposit was cut into pieces of appropriate size, floated off in water and finally picked up on brass target holders. After drying for several hours the foils had considerable durability and were ready to accept the final evaporation of ^{7}LiF.

A sample of LiF isotopically enriched to 99.9% ^{7}Li was obtained from AECL at Chalk River. The salt was evaporated under vacuum using a carbon rod hollowed out on one side to form a boat. A current of $\sim$110 A, passed through the boat was sufficient to cause the LiF to become molten. Several target holders were placed on a stand some 15 cm above the carbon boat and exposed to the evaporating LiF for 30 sec to 1 minute. Targets of varying thickness were produced in this manner, but the exact thickness of each target was determined experimentally

by noting the shift in energy of 1.0 MeV deuterons scattered from the carbon backing in the two cases when a) the carbon is facing the deuteron beam and b) the LiF is facing the deuteron beam. Those targets whose LiF deposits were 10-16 keV thick for 1.0 MeV deuterons were used in this experiment.

§3.4 Normalisation of the Reaction Cross Section

In any experimental determination of a reaction cross section, an accurate knowledge of both beam intensity and areal target density must be known. The beam intensity can be determined by monitoring the total charge per unit time using a Faraday cage equipped with an electron suppression ring. If the targets are metallic, or are thick, then it is feasible to measure the target density by simply weighing the target. Often, however, as in the present case, the target is not self supporting and any weighing procedure has to involve the target holder whose mass is orders of magnitude greater than the target mass. Under these circumstances, the cross section normalisation is likely to be subject to large systematic errors.

In the experiment discussed in this thesis, such large systematic errors were avoided by using a surface barrier detector, fixed at a laboratory angle of 120^{o}, to monitor the deuterons elastically scattered from ^{19}F in the target whilst the yield from the reaction was being simultaneously measured. On the assumption that there is a one to one ratio of fluorine to lithium atoms in the target, the ratio of the two yields is equal to the ratio of the respective cross sections (apart from

solid angle factors). For deuterons incident on ^{19}F, the Coulomb barrier is close to 3.0 MeV. Thus, at an energy of 1.0 MeV, the elastic scattering should be predominantly Coulomb in nature, the differential cross section being given by

$$\frac{d\sigma}{d\Omega} = \left(\frac{e^2zZ}{2E}\right)^2 \frac{1}{\sin^4\theta} \frac{\left\{\cos\theta + \left[1-\left(\frac{m}{M}\right)^2\sin^2\theta\right]^{\frac{1}{2}}\right\}^2}{\left[1-\left(\frac{m}{M}\right)^2\sin^2\theta\right]^{\frac{1}{2}}}$$

where m,z and E are the mass, atomic number and laboratory energy of the deuteron, M and Z are the mass and atomic number of ^{19}F, and θ is the laboratory angle at which the scattered deuteron is observed. This formula yields a value of 184 mb.sr^{-2} for the differential cross section at a laboratory angle of 120°.

§3.5 Charged Particle Detectors

The charged particle detectors used in this experiment were silicon surface barrier semiconductor diodes obtained from Oak Ridge Technical Enterprises Corporation (ORTEC). These diodes consist of an extremely thin p-type layer on the sensitive face of a high purity, n-type silicon wafer. Electrical contact is made to the p-type surface through a thin gold film ($\sim 40\mu$gm.cm^{-2}) evaporated onto the surface, and through a 40μgm.cm^{-2} thick aluminum contact to the n-type silicon on the back surface. The sensitive volume of the detector is obtained by applying a reverse bias to the diode, the depletion depth varying as the square root of the applied bias.

Table 3.1 lists the details of detector geometry as used in this experiment. In order to decrease the large flux of

Table 3.1

Detector Geometry

Detector Use	Mean Collimator Diameter (mm)	Target-Collimator Distance (cm)	Solid Angle (msr)
α_1	1.75±0.01	3.81±0.05	1.65±0.05
α_1*	3.28±0.01	7.62±0.05	1.45±0.02
Ruth.	4.80±0.01	67.3±0.2	$(4.03\pm0.06)10^{-2}$
Ruth.*	7.21±0.02	67.8±0.2	$(8.87\pm0.07)10^{-2}$
α_2	~12.7	~5.08	Subtends 14° at target.
α_2**	4.93±0.02	7.23±0.05	3.64±0.06

*Detector geometry used for α_1 at 60°.

**Geometry for α_1 detector when α_1-α_2 coincidences were recorded on a dual parameter analyser.

Table 3.2

Properties of NE 218

1	Pulse Height	70% of anthracene
2	Decay constant, main comp.	3.9 nsec.
3	Density	$0.879 gm.cm^{-3}$
4	Pure hydrocarbon	
5	Ratio of H:C	1.379

elastically scattered deuterons incident on the sensitive surface of the detectors, nickel foils of thickness 40μin.* were placed between the target and the detectors (except the Rutherford detector). The resolution of the detectors was measured using the 5.477 MeV alpha particles from a thin ^{241}Am source and found to be typically less than 25 keV.

§3.6 Neutron Detector

A scintillation detector consisting of a right circular cylinder of NE 218** with a diameter of 5 in. and a length of 3 in. viewed by a Phillips XP 1040 photomultiplier was used to detect the neutrons. The choice of scintillator was dictated by the need for fast timing and pulse shape discrimination qualities. In this respect NE 218, whose physical properties are given in Table 3.2, supersedes NE 213. Because of a mismatch of diameters (the photocathode effective diameter was ~4 in.) the optical coupling between the tube and scintillator was achieved using a lucite light pipe cut in the shape of a 1 in. thick frustrum of base diameter 5 in. and smaller diamer 4 in.. Dow Corning 20-057 clear viscous silicone fluid was used to make the necessary optical joints. The three constituent parts of the detector were then bound together with black adhesive tape, surrounded with a mu-metal magnetic shield and mounted under spring tension in an aluminum can. The room background flux

---

* Obtained from Chromium Corporation of America, Waterbury, Connecticut.

** Obtained from Nuclear Enterprises Ltd., Scintillator Division, 550 Berry St., Winnipeg 21, Manitoba.

of γ-rays incident on the scintillator was reduced by mounting the front portion of the can in a hollow cylindrical lead collimator of thickness 3 in. and length 6 in.. Additional lead shielding was placed around the remainder of the can. The entire assembly, consisting of detector and shielding was placed on a table which could be positioned in the horizontal plane at any angle with respect to the beam direction to better than 1^{o}. With a flight path of 1.00 metre, the neutron detector subtended a solid angle of $(1.25 \pm 0.02)\ 10^{-2}$ sr. at the target.

A high voltage of -2150 v, for biasing the photocathode of the XP-1040, was provided by a Model RE-5001 AW1, Regulated Power Supply obtained from North East Scientific Corp., Acton, Massachusetts, USA. The phototube was operated in combination with an ORTEC 268 Timing Discriminator and Preamplifier (TDPA), this latter unit serving the dual purpose of providing a linear signal (derived from the 10th dynode and amplified) together with a walk-free timing signal (derived from the anode). Power for the preamplifier was provided by an ORTEC 403 A Time Pick Off Control Unit (TPOC) which also provided for external adjustment of the discriminator level.

A difficulty always encountered in the detection of neutrons is the energy dependence of the detector efficiency. This variation must be accounted for before angular correlations or cross sections can be calculated. In the present instance, both experimental measurements, using the $d(d,n)^{3}He$ reaction, and theoretical calculations of the detector efficiency were performed, a discussion of these results being deferred to

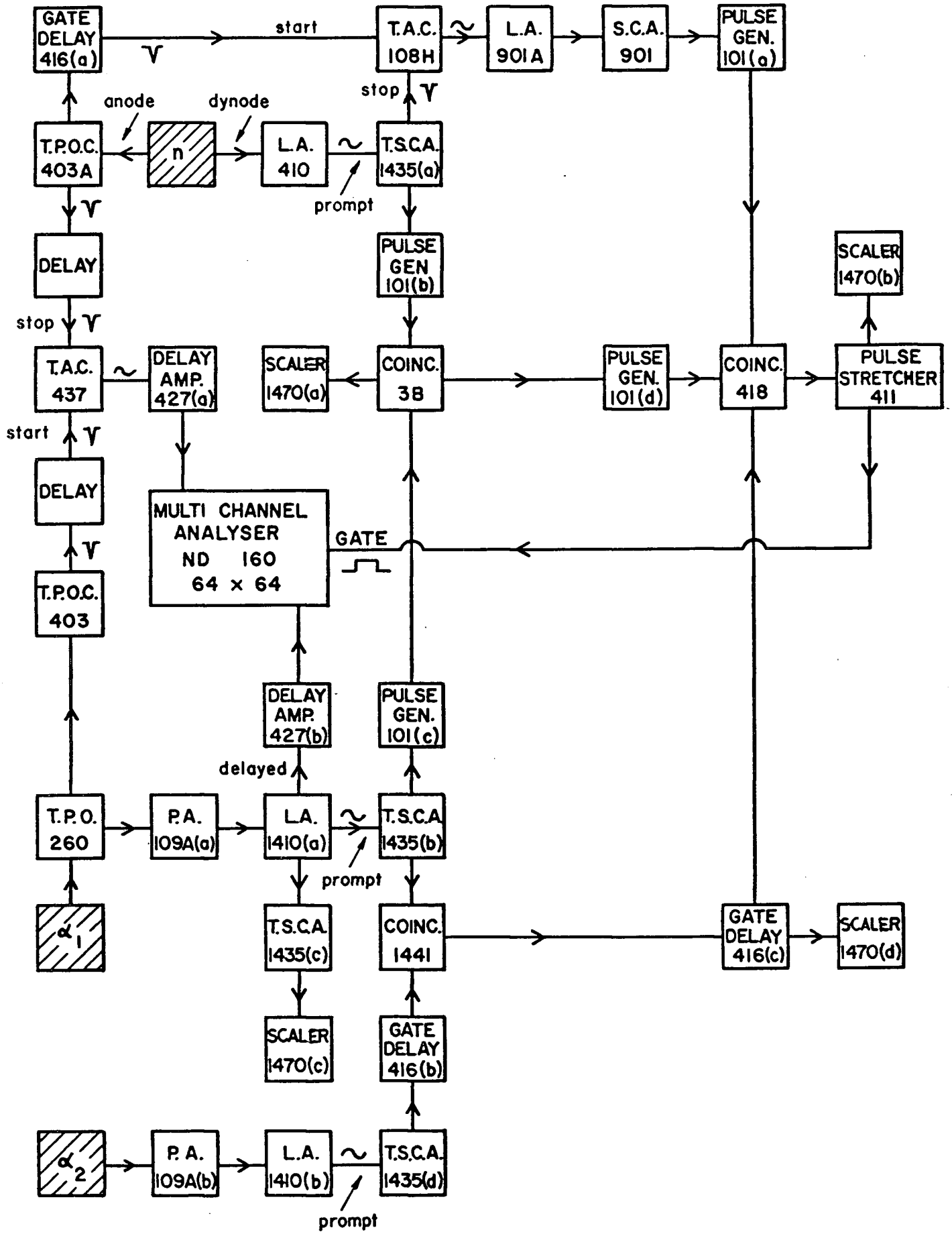

Fig 3.1 Block diagram of electronics.

Table 3.3

Electronics used in Experiment

Number	Device	Manufacturer
109A	Low Noise Preamplifier	
115	Preamplifier Power Supply	
210	Detector Control Unit	
260	Time Pickoff	
268	Timing Discriminator and Preamp.	
403	Time Pickoff Control Unit	
410	Multi Mode Amplifier	Oak Ridge Technical
411	Pulse Stretcher	Enterprises Corp.,
416	Gate and Delay Generator	Oak Ridge, Tenn.
418	Universal Coincidence	
427	Delay Amplifier	
437	Time to Amplitude Converter	
1410	Linear Amplifier	Canberra Industries,
1435	Timing Single Channel Analyser	Meriden,Connecticut.
1441	Fast Coincidence	
1470	Scaler	
3B	Coincidence	Lecroy Research Systems
108H	Time to Amplitude Converter	Corp.,Irvington, N.Y.
901	Single Channel Analyser	Cosmic Radiation Labs
901A	Linear Amplifier	Inc., Bellport, N.Y.
101	Pulse Generator	Datapulse Inc.,
		Inglewood, California.
ND 120	512 Channel Analyser	Nuclear Data Inc.,
ND 160	Dual Parameter Analyser	Palatine, Illinois.

Appendix 1.

§3.7 Electronics

Several different experimental configurations were employed during the course of the experiment but the electronics block diagram illustrated in Fig.3.1 was appropriate whenever the neutron time of flight and energy of α_1 were recorded simultaneously using a multichannel analyser. Other configurations, such as α_1-α_2 coincident events, could easily be recorded with only minor alterations to the electronics being necessary. Details of the commercial units employed are given in Table 3.3.

The start pulse for the time of flight measurement was derived from the α_1 signal by sensing the charge collection current from the detector to a charge sensitive preamplifier using a Time Pick Off Unit (TPO). The output of the TPO was regenerated as a fast negative pulse by the TPOC module, suitably delayed and presented to the start input of the Time to Amplitude Converter (TAC) operated on the 100nsec range. On the neutron side, the TDPA (not shown in Fig.3.1 but discussed in previous section) generated a fast negative signal at the input to a TPOC unit which in turn enabled the stop input of the time of flight TAC. The delayed output of the TAC was presented to one analogue input of the ND 160 dual parameter analyser, the other input being provided by a suitably shaped, amplified and delayed pulse from the α_1 linear amplifier.

An additional fast positive pulse from the neutron TPOC unit triggered a Gate and Delay Generator which in turn enabled

the start input of a second TAC (time range 200nsec). The stop input of this TAC was triggered whenever the linear pulse height from the neutron detector, after amplification and shaping (double delay line), satisfied the window requirements of a Timing Single Channel Analyser (TSCA) operated in zero cross over mode. (It is the lower level discriminator of this TSCA which determines the bias level and hence the efficiency of the neutron detector. The procedure for setting this level is outlined in Appendix 1). Since neutrons and γ-rays interacted with the scintillator in different ways and therefore produced different pulse shapes at the linear amplifier output, two different amplitudes of converter outputs were obtained. A single channel analyser, with a suitably adjusted window, used in conjunction with the TAC determined whether or not a scintillator event was caused by a neutron. A positive conclusion resulted in a signal being sent, after regeneration by a pulser, to one input of a Universal Coincidence Unit ($\tau \sim 0.5 \mu$sec).

Two separate coincidence units, operated with resolving times of 50 and 100nsec respectively, served to produce logic signals whenever simultaneous events occurred in α_1 and α_2 or in α_1 and the neutron detector. A timing signal was generated by the TSCA associated with each detector and presented to the input of the appropriate coincidence box, correct time relationships between the pulses being achieved by using pulse or gate and delay generators. The logic pulses from the two coincidence units were delayed and fed to the Universal Coincidence which could be operated in single, double or triple coincidence mode

by a front panel switch. A suitable gate pulse for enabling the dual parameter analyser was obtained by lengthening the coincidence unit output pulse with a pulse stretcher.

Three scalers were used to record the α_1-n, α_1-α_2 and triple coincidence yields respectively whilst a fourth scaler served to monitor those particles incident on the α_1 detector whose pulse height fell within a narrow energy window. For a given α_1 angle, the count rate in this scaler represents a relative normalisation for the angular correlation measurement. An absolute normalisation was obtained by comparing this count rate with that in the Rutherford detector.

Particle pulses from the Rutherford detector (not shown in Fig.3.1) were amplified in conventional fashion and stored in an ND 120 multichannel analyser. Also not shown in Fig.3.1 are ORTEC115 Power Supplies, for use with the charge sensitive preamplifiers, and an ORTEC 210 Detector Control Unit. The entire system of counting and data accumulation equipment was started and stopped remotely.

The energy calibration of the charged particle spectra was achieved using a thin ^{241}Am alpha particle source and a pulse generator. Relative time of flight calibration was performed by inserting known delays of up to 60nsec in the stop side of the fast timing electronics. By noting the position of the neutron group resulting from the reaction ^{7}Li(d,n)^{8}Be*(2.89), the absolute time of flight scale was established.

CHAPTER 4

EXPERIMENTAL RESULTS

§4.1 Single Particle Spectra

Initial experimental work involved checking out the various aspects of the electronics and the accumulation of single particle spectra. Fig 4.1 illustrates a typical spectrum obtained with the Rutherford detector. Three peaks corresponding to elastically scattered deuterons from ^{7}Li, ^{12}C and ^{19}F are clearly evident with a smaller peak attributable to deuterons elastically scattered from an ^{16}O contaminant in the target. Scattering tests with a ^{12}C foil showed no traces of ^{19}F leading one to conclude that the counts in the ^{19}F peak all result from scattering from ^{19}F in combination with ^{7}Li.

Since the Q-value of the reaction $^{7}Li(d,\alpha)n\alpha$ is large (15.123 MeV) , alpha particle spectra resulting from this reaction are largely independent of scattering angle at an incident energy of 1.0 MeV. A representative spectum, obtained with a detector at a laboratory angle of 100^{o} is shown in Fig. 4.2. The energy scale has not been corrected for the energy loss of the particles in a nickel foil ($\sim 40\mu$in) placed in front of the detector. One alpha particle group, associated with the formation of the ^{5}He ground state is clearly evident at the higher end of the spectrum while proton groups arising from the reactions $^{12}C(d,p)^{13}C$ and $^{19}F(d,p)^{20}F^{*}$ are also prominent. The broad continuum of events extending from zero energy to 7.0 MeV are alpha particles resulting from the decay of the ^{5}He ground state.

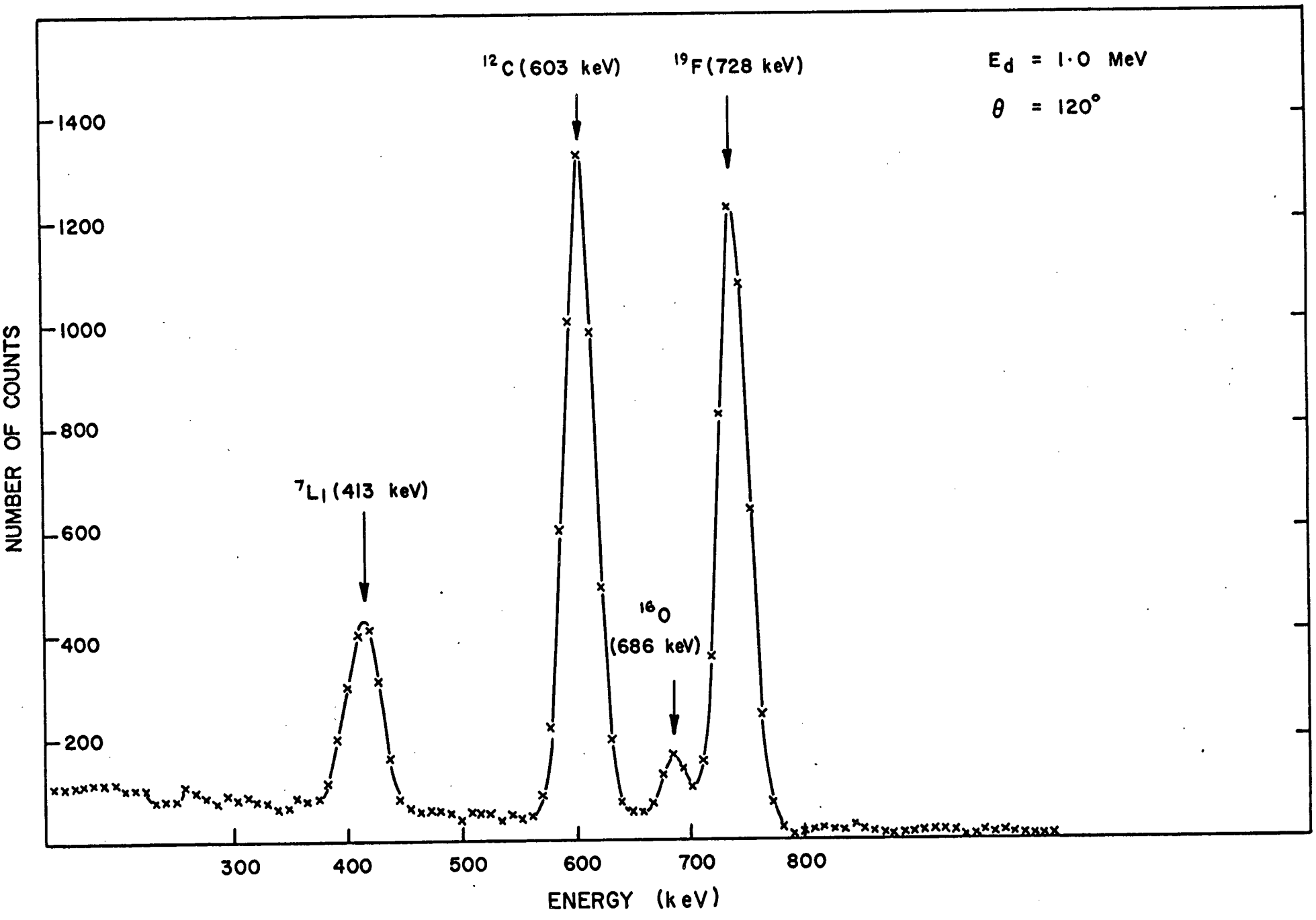

Fig 4.1 Elastic scattering of deuterons from ^{7}LiF evaporated onto a thin carbon foil.

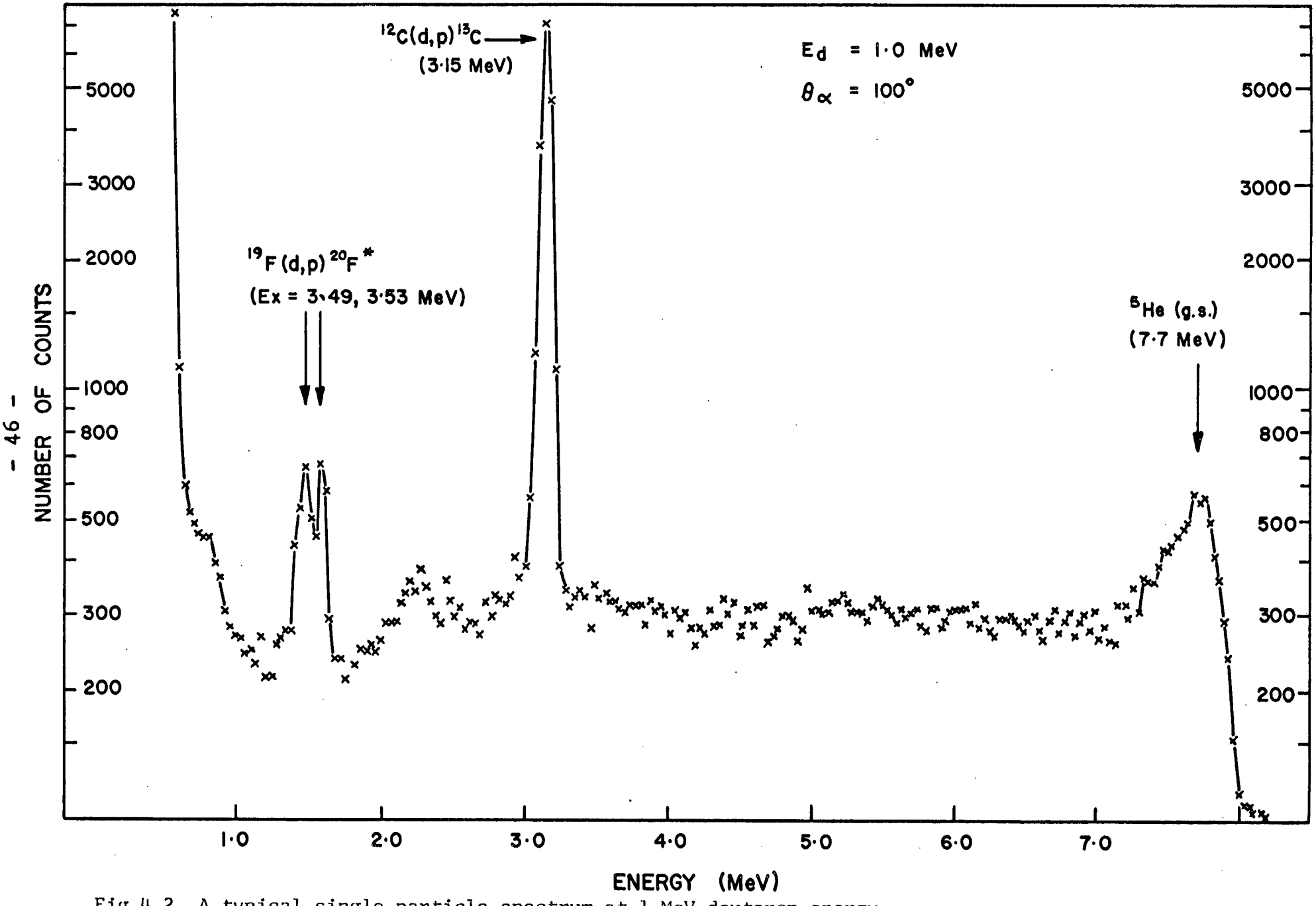

Fig 4.2 A typical single particle spectrum at 1 MeV deuteron energy.

Since events above about 4.0 MeV are due to the interaction of deuterons with ^{7}Li, a single channel analyser set on this region with a window of about 1.0 MeV serves as a convenient relative normalisation for each angular correlation.

The operation of the pulse shape discrimination circuitry is best illustrated by reference to Fig. 4.3. This figure shows the time spectrum obtained with a TAC when an ^{241}Am - Be neutron source is used to irradiate the neutron detector. This spectrum was obtained with the lower level discriminator set at 0.39 MeV and at a count rate of $\sim 10^{4}$ cps. The separation between the neutron and γ-ray peaks is clearly evident, allowing neutron events to be selected, using a single channel analyser, as indicated by the arrows in Fig. 4.3. A comparison of the n - α coincidence yield when gated and not gated by the pulse shape discrimination electronics indicated that as many as 20% of the events were random coincidences between γ-rays and alpha particles. The usefulness of employing pulse shape discrimination is thus apparent.

§ 4.2 Excitation Function

A crude excitation function, obtained by integrating the counts under the alpha particle peak resulting from the formation of ^{5}He, is illustrated in Fig. 4.4 (upper points). The alpha particle detector was located at a laboratory angle of 100^{o} for these measurements. The relative normalisation was obtained by noting the yield of deuterons scattered from ^{19}F in the Rutherford detector. At a machine energy in the neighbourhood

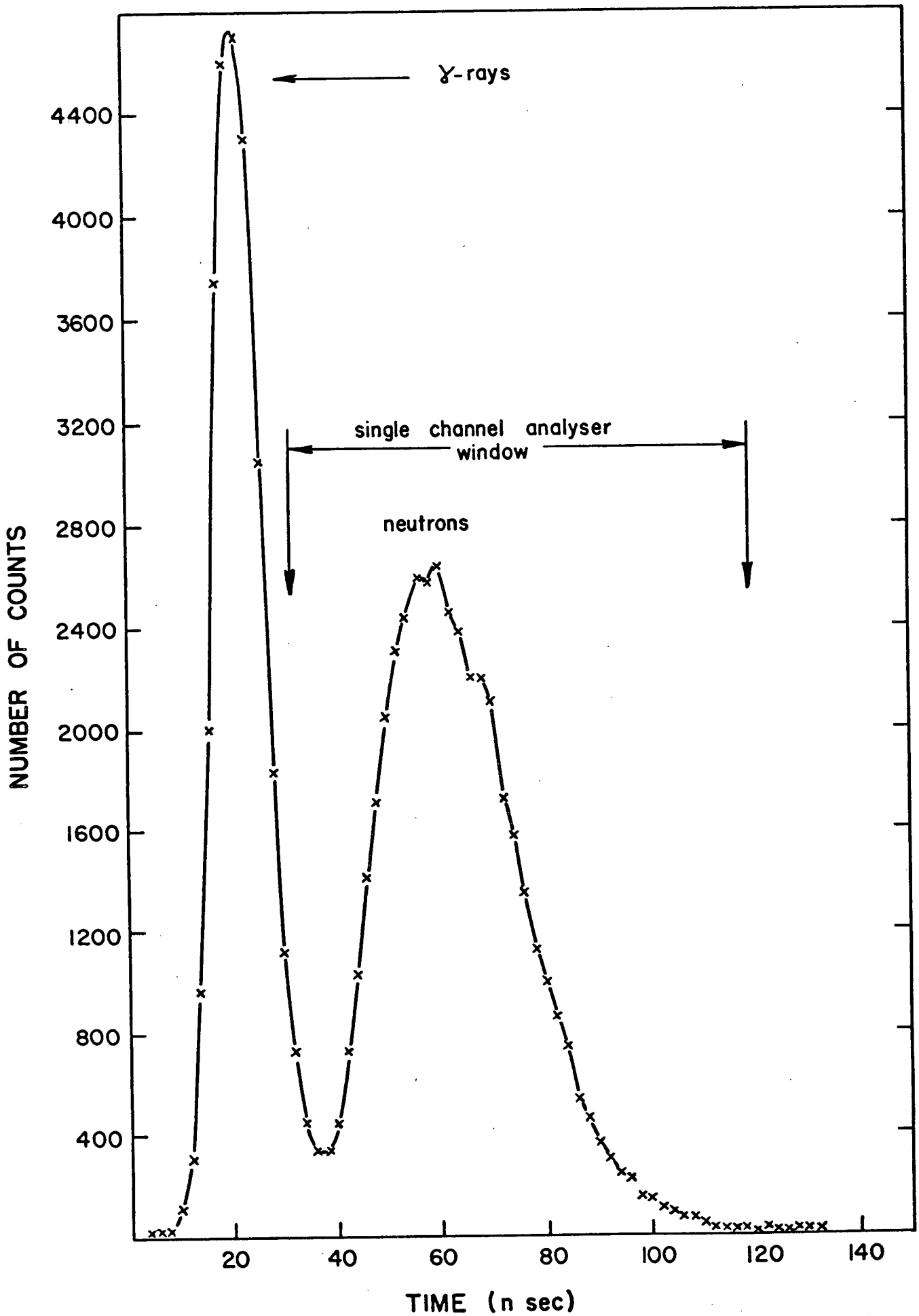

Fig 4.3 Output of Time to Amplitude converter showing separation of neutrons and γ-rays.

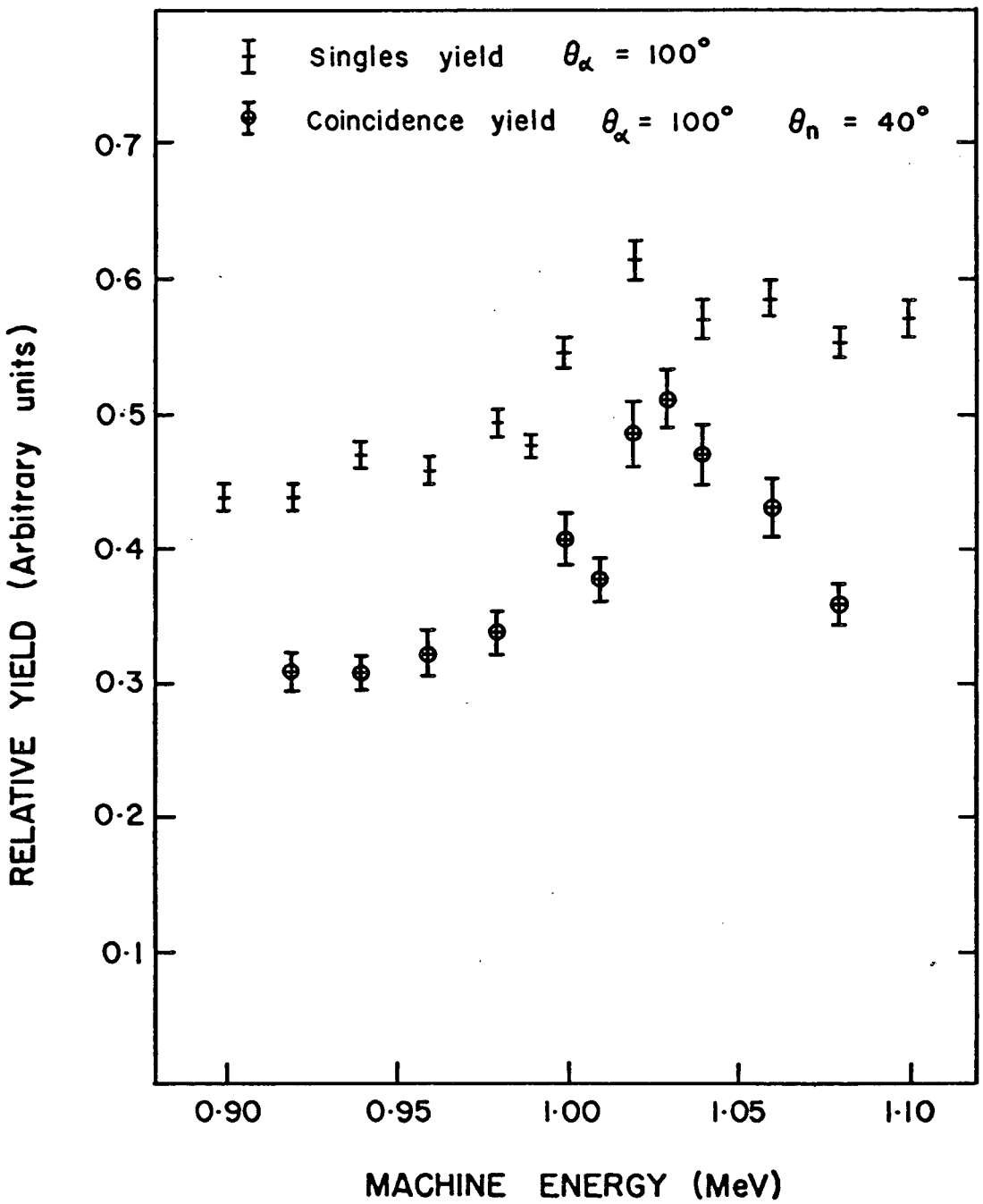

Fig 4.4 Relative Yield as a function of machine energy.

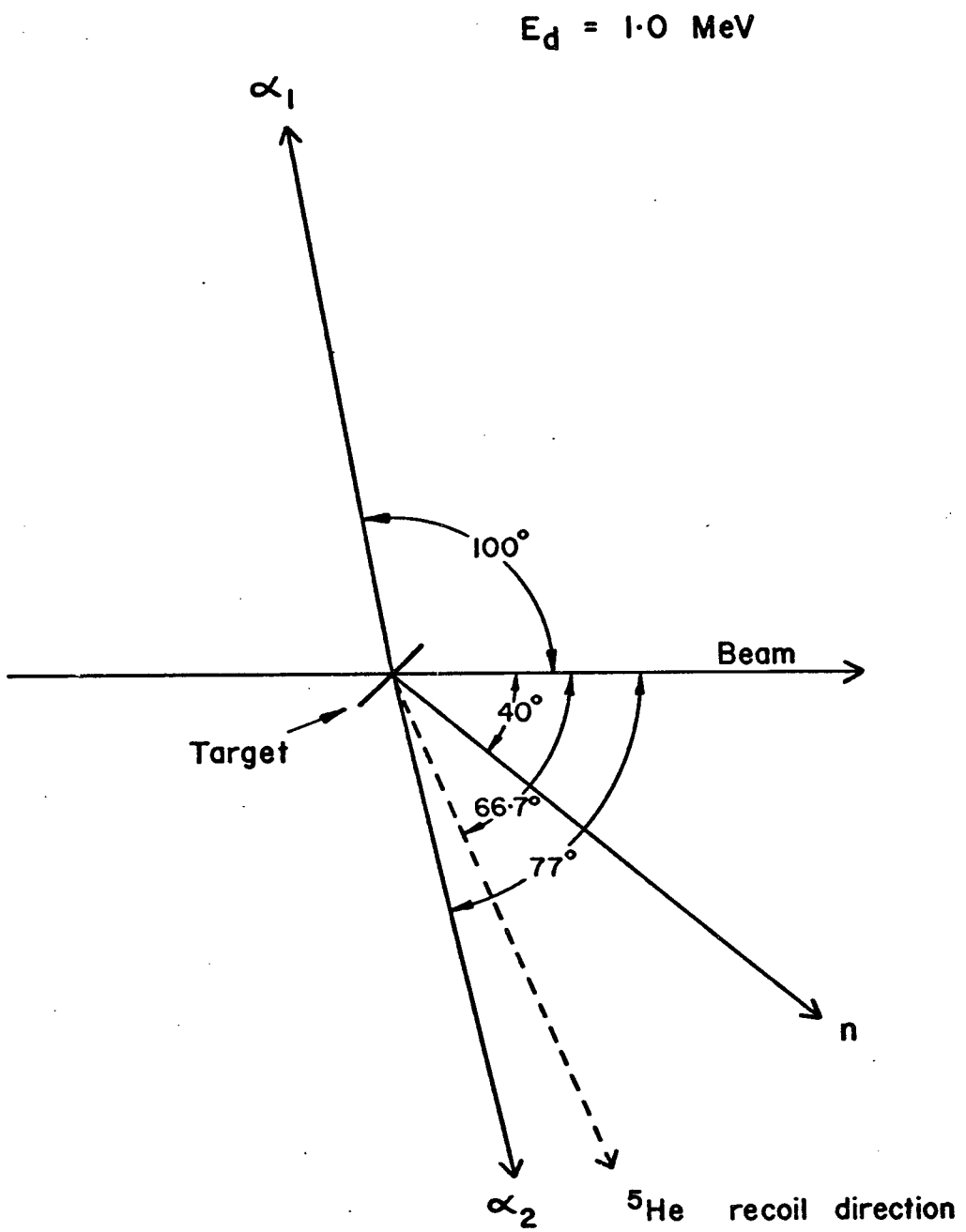

Fig 4.5 Schematic diagram of typical detector locations for a triple coincidence measurement.

of 1.0 MeV there is some semblance of a bump or resonance. This resonance is considerably more pronounced if the excitation function is measured using the triple coincidence technique to isolate the ^{5}He state. A schematic diagram showing the detector angular settings used for these measurements is shown in Fig. 4.5. After correcting for solid angle variations with incident deuteron energy, the lower set of points in Fig. 4.4 is obtained. Now the resonance is responsible for as much as 40% of the total yield and is expected to result from compound nucleus formation through the $^{9}Be^{*}(17.48)$ level. This level is the subject of the bulk of the work undertaken in this thesis. All subsequent measurements were performed at an energy of 1.0 MeV (after correction for energy loss in the target) at which energy angular correlation measurements should yield information on possible spin assignments for this level.

§ 4.3 Coincidence Results

Examples of coincidence spectra are shown in Fig. 4.6, Fig. 4.7 and Fig. 4.8. The first two spectra were obtained with the α_1 detector at 65° and the neutron detector at 70°. The former spectrum, however, has been gated by the α_2 detector with a resulting decrease in background events throughout the plane. The solid curves represent the kinematically allowed contours along which events proceeding to a three body final state must lie. The single particle spectra, to the left and below each contour plot, are obtained by projecting the yield of events along the allowed contour onto the respective axes.

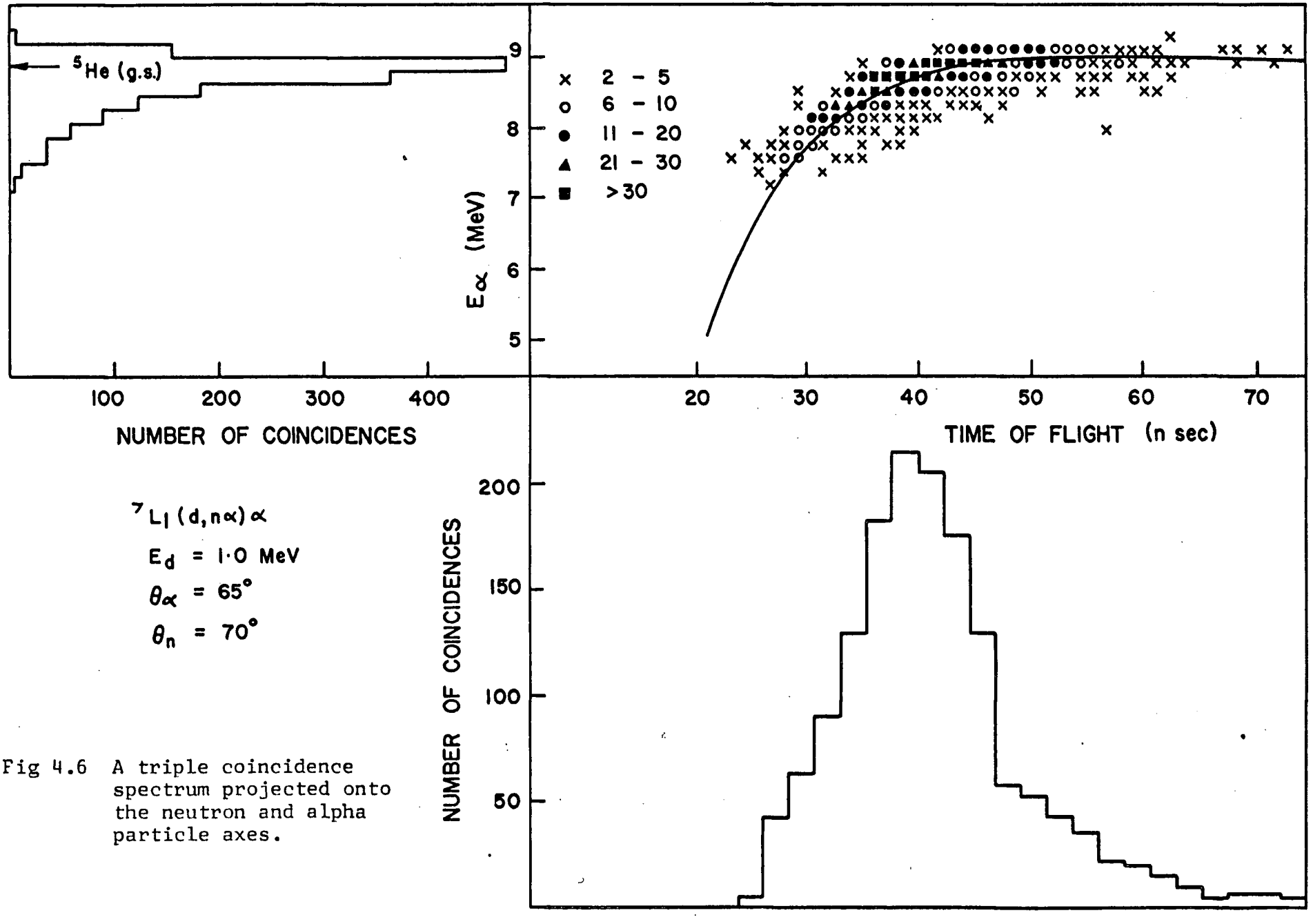

Fig 4.6 A triple coincidence spectrum projected onto the neutron and alpha particle axes.

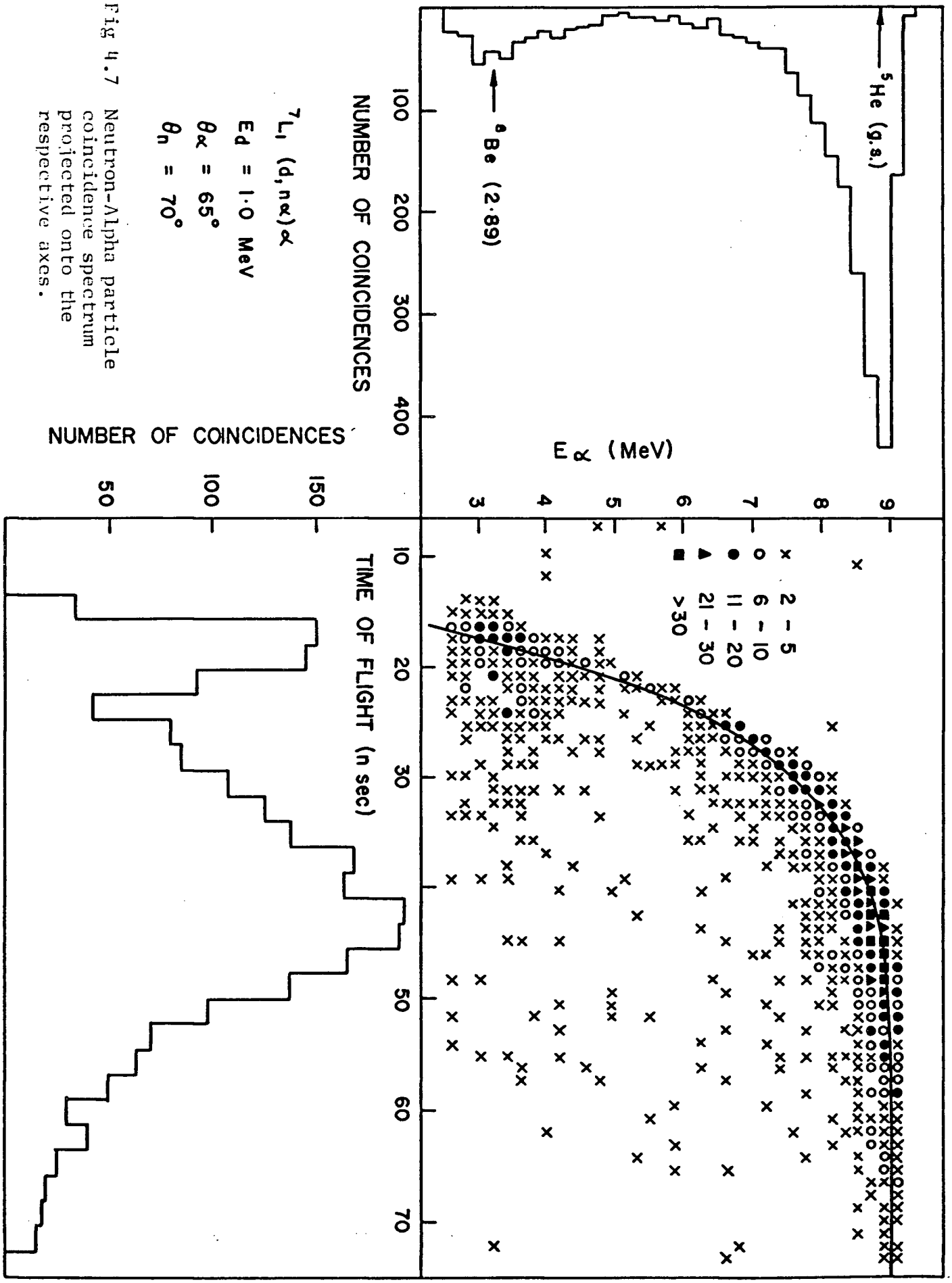

Fig 4.7 Neutron-Alpha particle coincidence spectrum projected onto the respective axes.

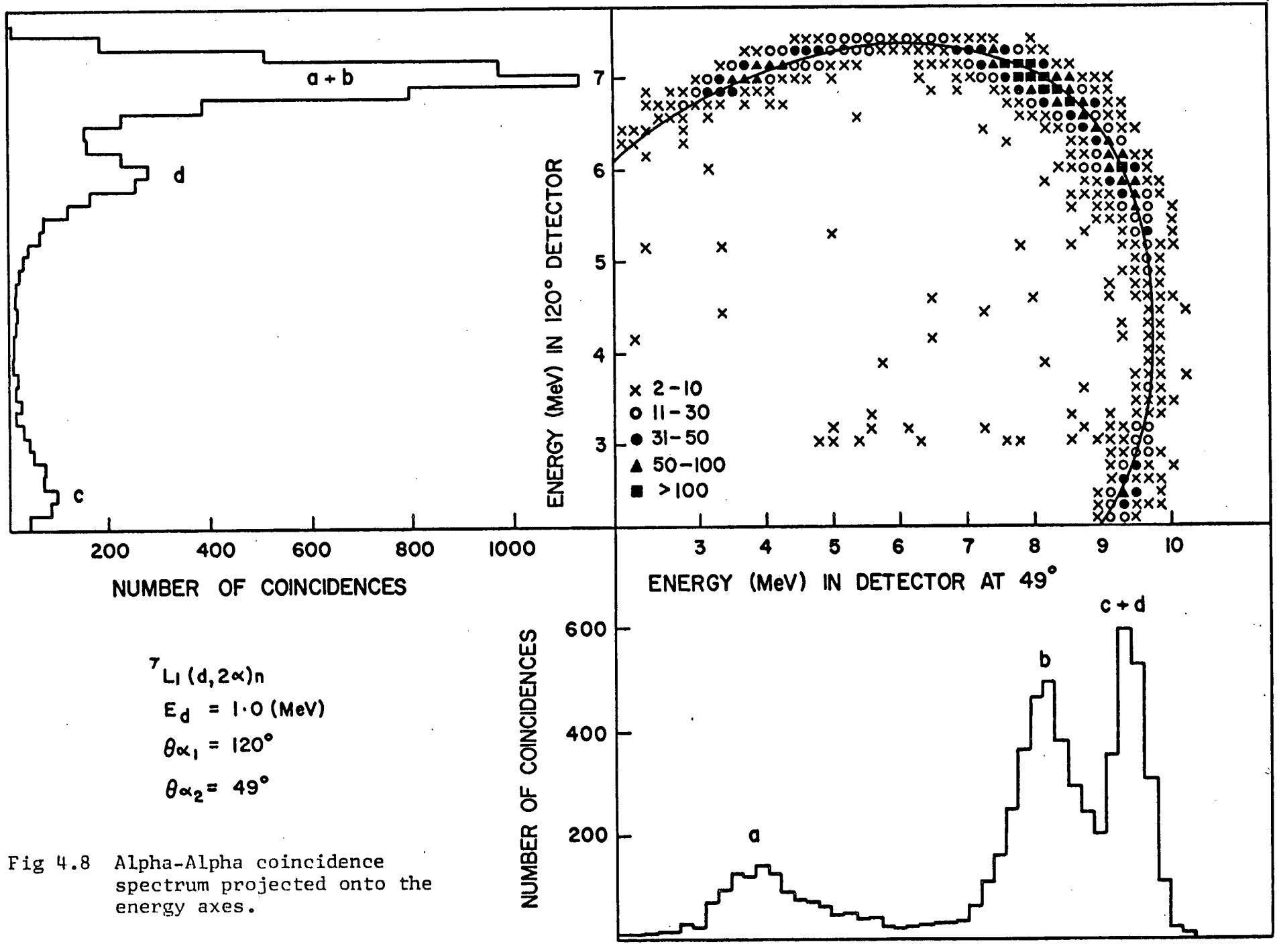

Fig 4.8 Alpha-Alpha coincidence spectrum projected onto the energy axes.

Sequential decay through the ground state of ^{5}He and the $^{8}Be^{*}$ (2.89) level are quite clearly evident in Fig. 4.7, but contributions from other states, if present, are certainly small. A comparison of Fig. 4.6 and Fig 4.7 does suggest that the introduction of the α_2 detector results in the loss of counts on the low energy side of the ^{5}He peak. Accordingly, the double coincidence results are expected to be more reliable for extracting angular correlation data. For the particular case of α_1 at 60^{o}, double coincidence results were not performed and the angular correlation data, obtained from triple coincidence measurements is likely to be subject to systematic error.

In the α-α coincidence spectrum of Fig. 4.8, events corresponding to sequential decay through the ^{5}He ground state appear in four distinct locations on the allowed contour. The peaks labelled "a" and "b" (see projected spectra) correspond to events in which the first emittedalpha particle is detected at 120^{o} and the ^{5}He breakup alphas are detected at 49^{o}. The groups "c" and "d" arise when the detector roles are interchanged.

The most convenient way of reproducing the experimental results is in the form of isometric contour plots (see Fig. 4.9, Fig. 4.10 and Fig. 4.11) in which, for a given α_1 angle, the coincidence yield is projected onto the alpha particle energy axis and plotted as a function of neutron angle. The various solid curves represent the theoretical positions at which enhancements from final state interactions should appear. In all cases only the ^{5}He ground state and the $^{8}Be^{*}$(2.89) level are at all strongly excited. The $^{5}He^{*}$ first excited state

Fig 4.9 Neutron-Alpha particle coincidence spectra projected onto the alpha particle axis as a function of neutron detector angle for $\alpha_1 = 65°$.

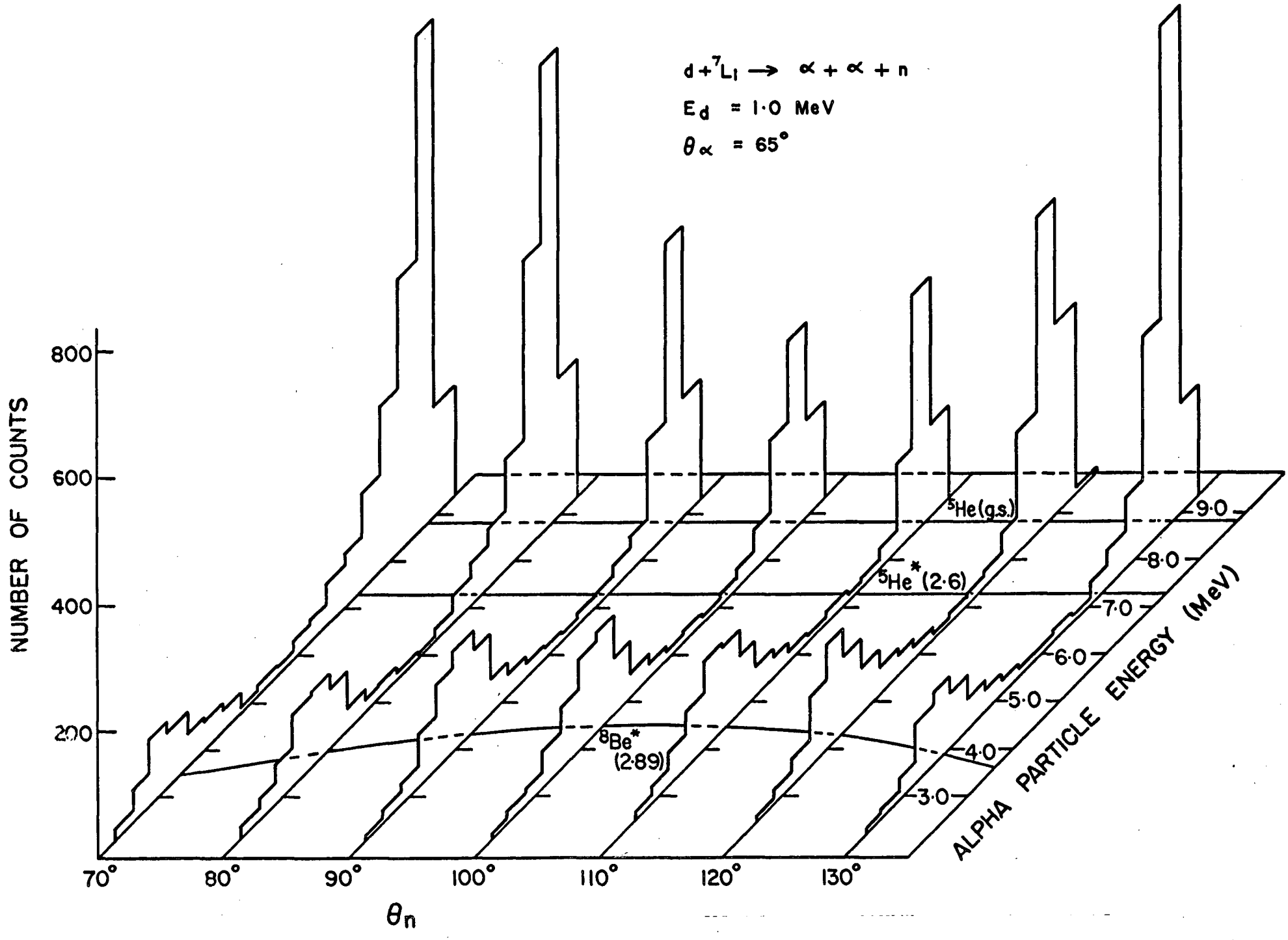

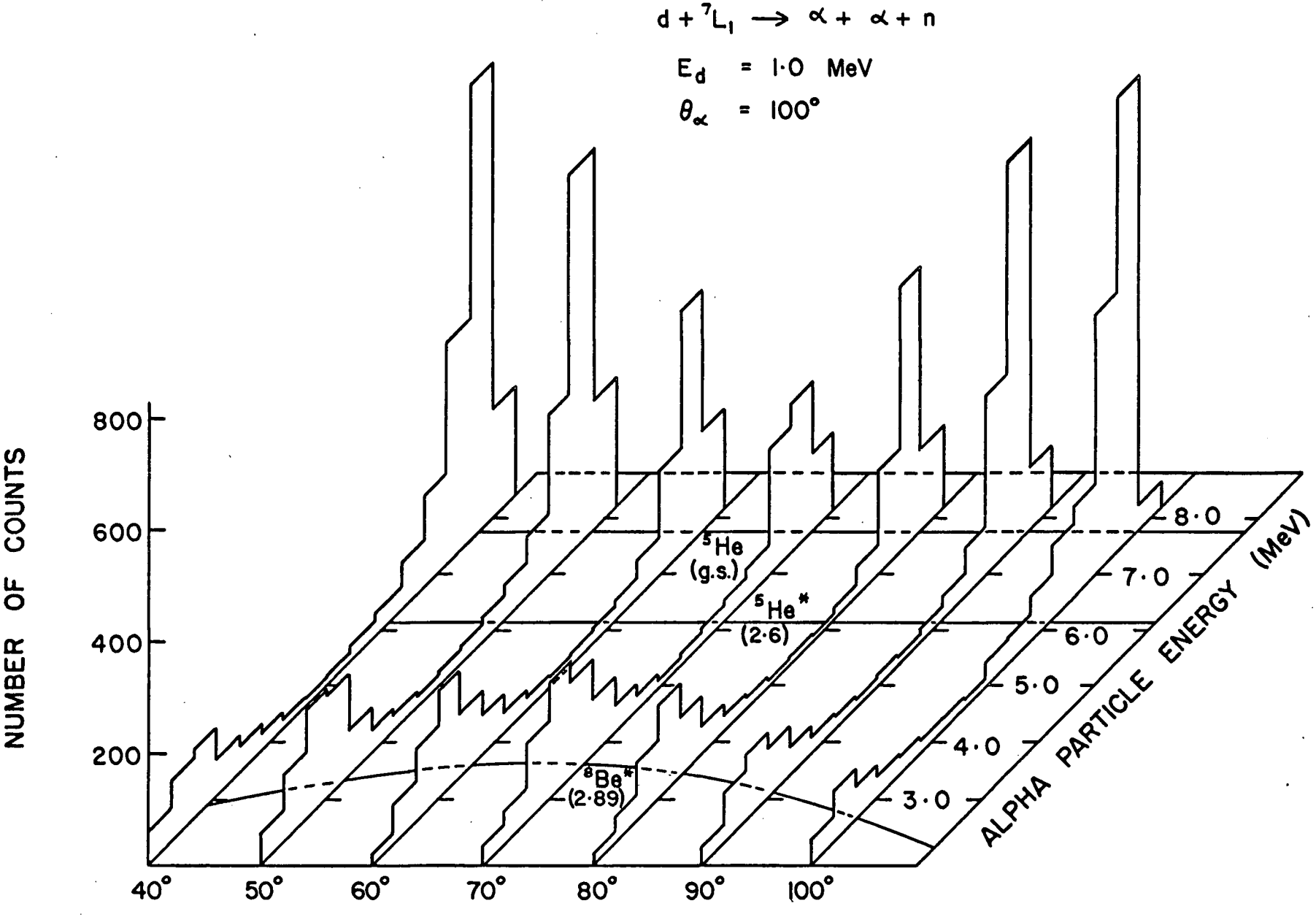

Fig 4.10 Neutron-alpha particle coincidence spectra projected onto the alpha particle axis as a function of neutron detector angle for $\alpha_1 = 100°$.

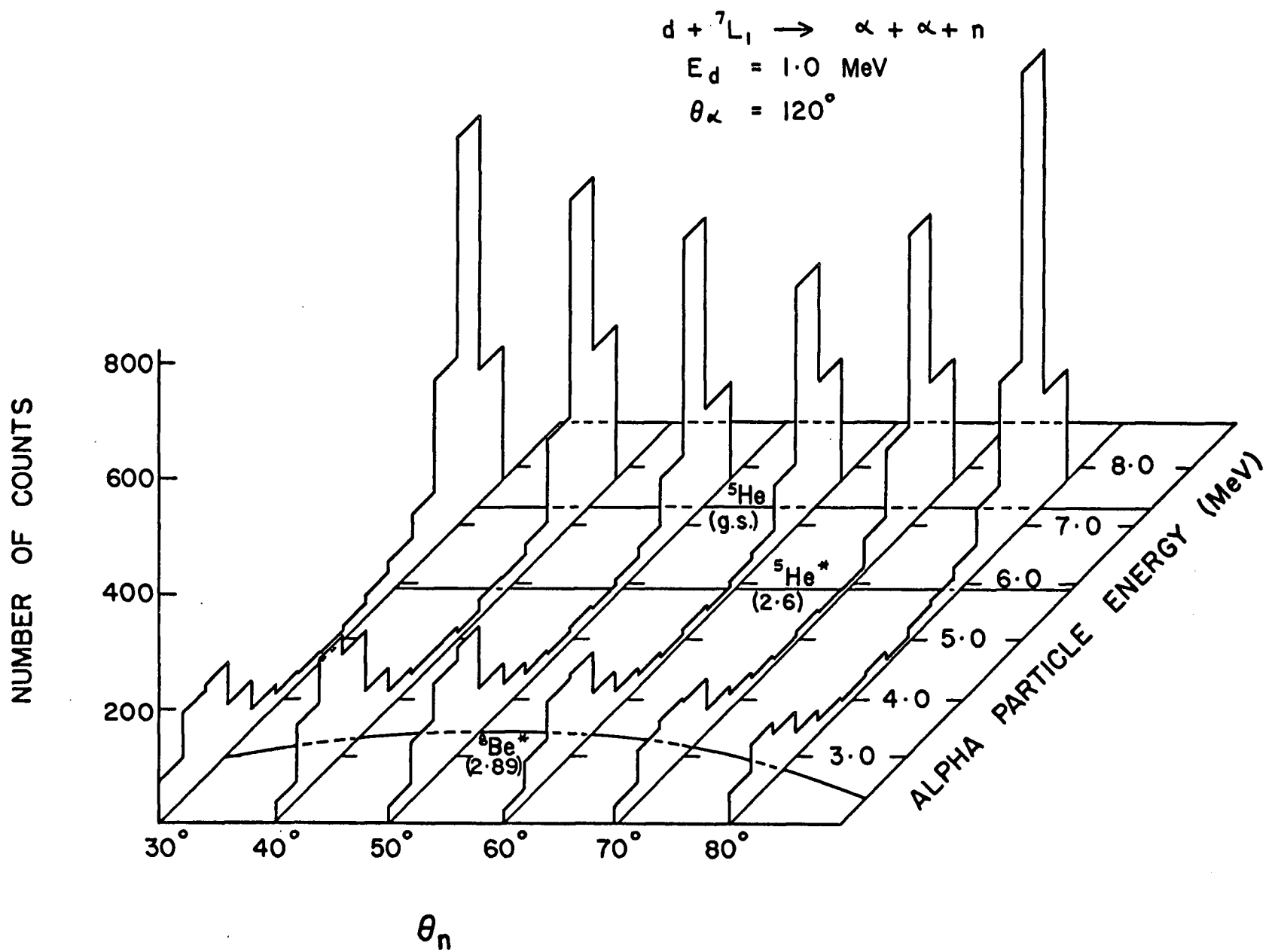

Fig 4.11 Neutron-alpha coincidences projected onto the alpha particle axis as a function of neutron detector angle for α_1 = 120°.

appears to be so weakly excited that its contribution to the yield can be neglected. All spectra are normalised with respect to 500,000 counts being registered in the single channel analyser used to monitor the α_1 yield.

The double differential cross section describing the formation and decay of ^{5}He is obtained by integrating the counts under the appropriate alpha particle peak and multiplying this number by the reciprocal of the neutron detector efficiency. The results are presented in Tables 4.1 to 4.4. The first two columns in these tables represent the angle of the neutron detector in the laboratory and ^{5}He recoil centre of mass (rcm) systems respectively with the incident beam direction defining the z-axis. The mean theoretical energy of the ^{5}He breakup neutron and the efficiency of the neutron detector at that energy are given in columns three and four. The efficiency has been obtained from Appendix 1 and has been assigned a rather arbitrary error of $\pm$ 0.02. The kinematic factors, given in column five, convert the laboratory cross sections to the corresponding centre of mass values on the assumption that ^{5}He is a narrow state of well defined energy. Columns six, seven and eight are largely self explanatory. The coincidence yield has been corrected for random coincidence events by noting the average density of events throughout the region of the energy-time of flight plane that is forbidden to three body final state events. The product of this areal density and the area of the plane in which the ^{5}He final state interaction is observed gives a crude measure of the random coincidence rate. Depending on the reaction yield, the background

Table 4.1

Angular Correlation Results for α_1 at 65°

A) Double Coincidence Measurements

θ_n (Lab)	Θ_n (rcm)	E_n (MeV)	Eff.	Conv. Fact.	α_1 Monitor	^{5}He Yield	$d^2\sigma$(rcm) mb.sr^{-2}
70	28	2.56	0.48	.204	500,050	1694±45	2.08±.13
80	52	3.27	0.44	.190	650,030	1536±42	1.49±.10
90	75	3.75	0.41	.181	500,023	740±31	0.95±.07
100	98	3.95	0.40	.178	525,896	576±29	0.71±.06
110	121	3.85	0.40	.179	750,097	864±34	0.74±.05
120	144	3.45	0.43	.186	500,287	926±33	1.17±.08
130	167	2.81	0.46	.199	500,022	1349±40	1.68±.11

B) Triple Coincidence Measurements

70	28	2.56	0.48	.204	250,049	759±28	1.87±.12
80	52	3.27	0.44	.190	360,049	748±27	1.31±.09
90	75	3.75	0.41	.181	550,019	713±26	0.83±.06
100	98	3.95	0.40	.178	663,045	355±19	0.37±.03
110	121	3.85	0.40	.179	500,071	456±21	0.59±.04
120	144	3.45	0.43	.186	500,070	903±30	1.14±.08
130	167	2.81	0.46	.199	500,094	1390±37	1.73±.10

Table 4.2

Angular Correlation Results for α_1 at 100°

A) Double Coincidence Measurements

θ_n (Lab)	Θ_n (rcm)	E_n (MeV)	Eff.	Conv. Fact.	α_1 Monitor	^{5}He Yield	$d^2\sigma$(rcm) mb.sr^{-2}
40	2	3.13	0.44	.201	500,023	1383±42	2.02±.14
50	27	3.85	0.40	.191	500,055	1065±34	1.63±.12
60	51	4.26	0.39	.185	750,031	1004±39	1.03±.08
70	75	4.32	0.39	.184	500,078	554 ±27	0.85±.07
80	99	4.02	0.40	.188	502,601	720±35	1.09±.09
90	122	3.39	0.43	.197	573,875	1224±40	1.58±.11
100	149	2.49	0.49	.209	500,029	1357±41	1.87±.13

B) Triple Coincidence Measurements

40	2	3.13	0.44	.201	500,025	1266±36	1.85±.13
50	27	3.85	0.40	.191	500,027	947±31	1.45±.11
60	51	4.26	0.39	.185	500,033	564±24	0.87±.07
70	75	4.32	0.39	.184	750,037	566±24	0.58±.04
80	99	4.02	0.40	.188	555,734	543±23	0.74±.06
90	122	3.39	0.43	.197	505,038	838±30	1.24±.09
100	149	2.49	0.49	.209	500,111	1250±35	1.72±.12

Table 4.3

Angular Correlation Results for α_1 at 120°

from Double Coincidence Measurements

θ_n (Lab)	$\textcircled{H}_n$ (rcm)	E_n (MeV)	Eff.	Conv. Fact.	α_1 Monitor	^{5}He Yield	$d^2\sigma$(rcm) mb.sr^{-2}
30	3	3.86	0.40	.198	500,076	1108±39	1.67±.13
40	27	4.38	0.38	.192	500,057	864±35	1.32±.10
50	45	4.53	0.38	.190	500,468	678±31	1.04±.09
60	76	4.28	0.39	.193	500,523	610±31	0.92±.08
70	101	3.67	0.41	.200	500,135	796±33	1.18±.09
80	128	2.74	0.47	.210	500,027	1200±39	1.65±.11

Table 4.4

Angular Correlation Results for α_1 at 60°

θ_n (Lab)	$\textcircled{H}_n$ (rcm)	E_n (MeV)	Eff.	Conv. Fact.	α_1 Monitor	^{5}He Yield	$d^2\sigma$(rcm) mb.sr^{-2}
72	26	2.27	0.49	.211	225,221	930±30	2.12±.15
77	38	2.66	0.48	.202	269,548	1187±34	2.23±.16
87	61	3.32	0.43	.188	250,844	880±30	1.82±.13
97	84	3.75	0.41	.180	553,924	1103±33	1.05±.08
107	107	3.90	0.40	.177	859,118	778±28	0.48±.03
117	129	3.76	0.41	.180	529,887	829±29	0.83±.06
127	153	3.33	0.43	.188	299,538	917±30	1.59±.11
137	176	2.67	0.48	.202	237,094	968±31	2.07±.15
142	8	2.28	0.49	.211	203,780	920±30	2.32±.16

subtraction amounted to between 10 and 20% of the total counts in the ^{5}He peak.

The errors quoted with the double differential cross section in the above tables include those arising in the measurement of solid angles but exclude any errors which arise from incorrect angle settings. In particular, the most difficult angle to set accurately is the neutron angle and an error of $\sim 1^\circ$ in this setting effectively introduces an angle error of $\sim 2^\circ$ in the rcm system. Thus, small angular shifts of the angular correlation symmetry axis from that theoretically predicted should not be taken too seriously (see next Chapter for further discussion on symmetry axes).

For comparison, the angular correlation results obtained from triple coincidence measurements are also given in the tables. With one exception, namely α_1 at 65° and n at 130°, the cross section results are lower, the discrepancy being particularly noticeable, as expected, whenever the scattered neutrons are attenuated by the α_2 detector and its mount.

Some comment on the procedure for obtaining the angular correlation results is necessary. To begin with, since the ^{5}He ground state has considerable width, the neutrons produced by the decay of this state are not monoenergetic. However, both the neutron detector efficiency and the kinematical factors are functions of this energy. Consequently, the simple multiplicative conversions used in the above tables are not strictly correct. A more correct procedure would be to apply the efficiency and kinematical corrections to each of several narrow energy bins

into which the alpha particle spectrum has been divided. Each of these bins is of course associated by energy and momentum conservation with a neutron energy bin. The resulting alpha particle spectrum would then be fitted using a final state interaction theory, such as the Watson-Migdal or PGB formulisms discussed in Chapter 1, and the double differential cross section for the formation and decay of ^{5}He extracted by integrating the counts under the theoretical curve. The computional difficulties are of course obvious, and are thought to be unnecessary in view of the crude background subtractions performed on the data. Moreover, the choice of a low bias (0.39 MeV) for the neutron detector implies that the efficiency curve is only slowly varying over a wide energy range (see Fig. A5) and the assumption of uniform efficiency for the neutron group of interest is reasonable.

CHAPTER 5

THEORETICAL ANALYSIS

§ 5.1 Reaction Mechanisms

In the previous chapters the experimental measurement of the double differential cross section for the sequential reaction

$$d + {}^{7}Li \rightarrow {}^{5}He(g.s) + \alpha_1$$
$$\hookrightarrow \alpha_2 + n$$

has been recorded. Evidence that the final state of two alpha particles and a neutron is indeed achieved predominantly via sequential decay through the $^{5}He(g.s)$ is presented in the previous chapter. Certainly, this conclusion is well supported by the literature (As 66, Va 67, Jo 65, Mi 66). In this chapter attention is focused on a theoretical explanation of these results.

During the formation of the ^{5}He ground state 14.164 MeV of energy is released, this energy appearing as kinetic energy shared between the alpha particle and the ^{5}He system. This energy is sufficient for a separation between these particles of the order of 39 fm. to be achieved in a time of 1.1×10^{-21} seconds, the approximate lifetime of the ^{5}He ground state. A large separation, on the nuclear scale, of this nature suggests that the ^{5}He decay products will not be influenced by the first emitted alpha particle and accordingly that the formation and decay of ^{5}He can be treated as independent processes. Such is the approach adopted here.

Three possible reaction mechanisms for the first stage are considered. A 1.0 MeV deuteron beam incident on a target of ^{7}Li represents an excitation energy of 17.47 MeV in the compound nucleus ^{9}Be. This is just slightly below a known level of positive parity but unknown spin at 17.48 MeV (see Fig. 5.1). Evidence for the existence of this level has been presented by Ford (Fo 64) and others (La 66). In addition the excitation function illustrated in Fig. 4.4, shows a resonance just above 1.0 MeV, amounting to as much as 40% of the total yield, which in all probability is attributable to this level in ^{9}Be. Compound nucleus formation through the tail of the broad ($\Gamma \sim 200$ keV) $5/2^{-}$ level at an excitation energy of 17.28 MeV is also expected to contribute significantly to the cross section.

Additional smaller contributions are to be expected from direct reactions in which two and three particles are transferred respectively. Schematic representations of these processes are illustrated in Fig. 5.2b and Fig. 5.2c respectively. They can, however, be distinguished experimentally. In the case of two particle pickup the ^{7}Li nucleus can be regarded as a "deuteron" moving around a ^{5}He core. The interaction responsible for the reaction is then that existing between the two deuterons, with the ^{5}He core remaining largely as a spectator. The angular distribution of the alpha particle should show peaking in the forward direction as indicated by the arrows in Fig. 5.2b. How

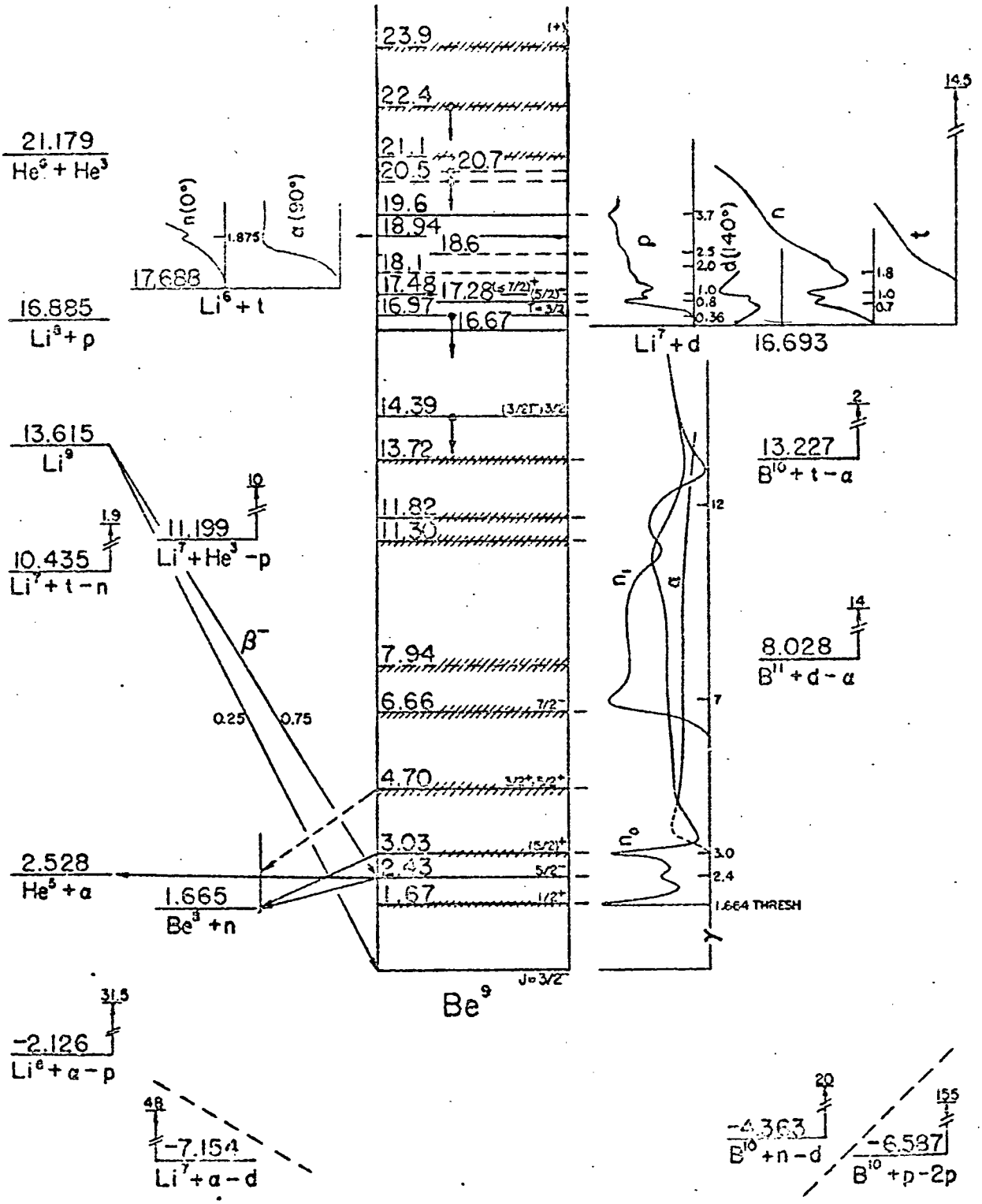

Fig 5.1 Level scheme for ^{9}Be (La 66).

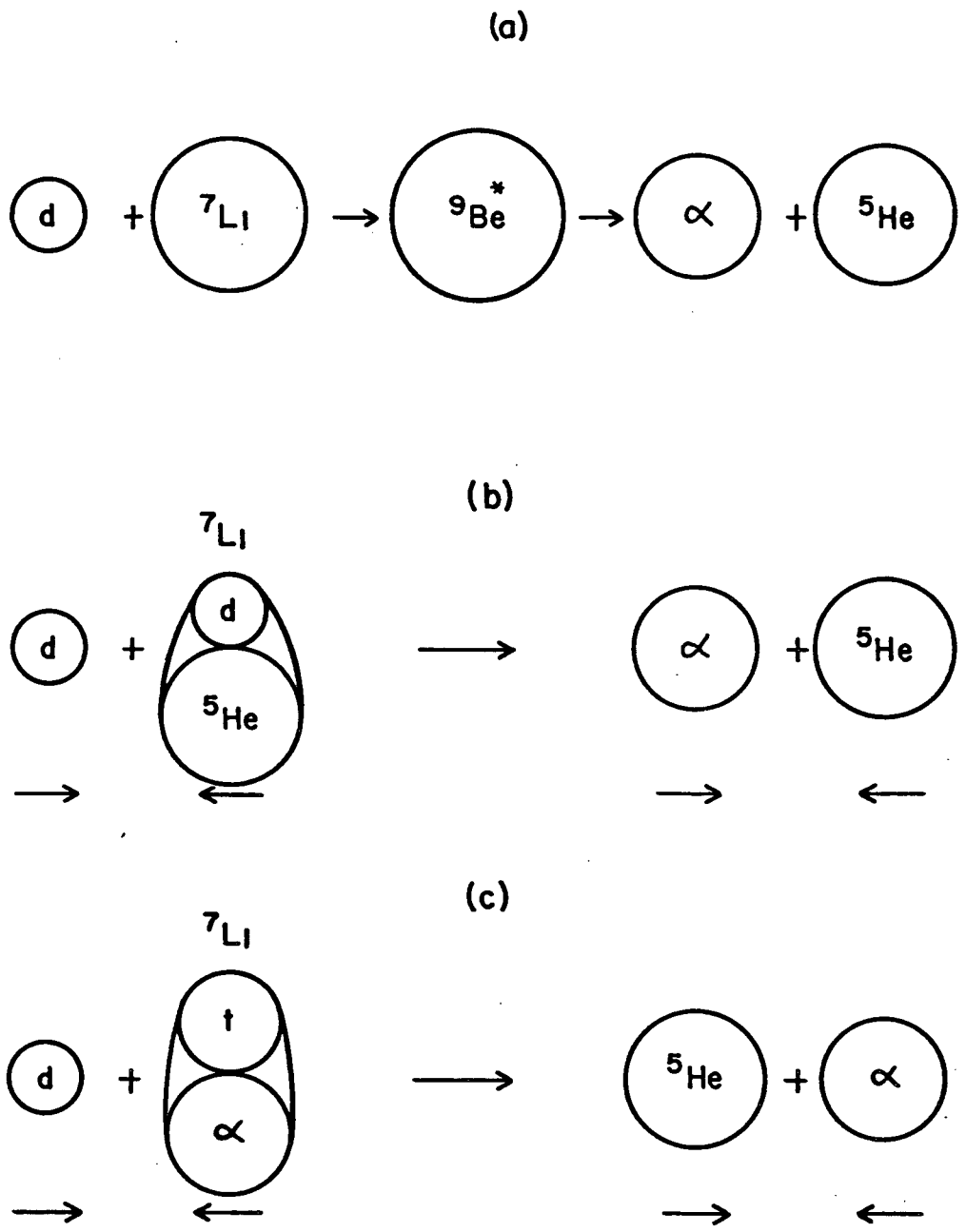

Fig 5.2 Schematic diagram of Possible Reaction Mechanisms.
(a) Compound Nucleus Formation
(b) Two Particle Pickup
(c) Three Particle Transfer.

readily this reaction proceeds is then largely determined by the overlap integral of the ^{7}Li wave function with the deuteron-^{5}He product wave function. A detailed calculation, within the framework of the Distorted-Wave-Born-Apprximation (DWBA) has been carried out and the results of this calculation can be found in Appendix 3. A comparison of Fig. A7 and Fig. 5.5 shows that the theoretical predictions for the angular correlation are quite the wrong shape. Attempts to obtain the correct shape by varying the optical model parameters used in the calculation proved negative. While the validity of doing DWBA calculations with such light nuclei is questionable, one can still reasonably conclude that the two particle pickup process is not the prime reaction mechanism. Further discussion of these calculations is deferred to Appendix 3.

In the alternative direct process the ^{7}Li is regarded as a triton cluster moving around an alpha particle core. The interaction causing the reaction is that existing between the incident deuteron and the triton. The emitted alpha particle is now the spectator and should show a preference for scattering in the backward direction. The assumption of an alpha particle-triton cluster model for the ^{7}Li ground state is well founded (To 61). However, if the reaction is to proceed readily the overlap integral of the ^{5}He ground state wave function with the triton-deuteron wave function should also be significantly different from zero. There is no evidence to support this and in fact the ^{5}He ground state wave function is well described by a single $p^{3/2}$ neutron orbiting about an alpha particle core

(Ph 60). In view of this fact, it seems unlikely that the three particle transfer process is significantly important when in competition with compound nucleus formation and no attempt is made to estimate it. The remainder of this chapter will be devoted to compound nucleus formation as the prime mechanism responsible for the reaction.

§ 5.2 Compound Nucleus Formation

§ 5.21 The Triple Correlation Function

The theory of angular correlations has long been understood. However, the often quoted definitive work on the subject by Biedenharn and Rose (Bi 53) is both long and difficult to read. More recently, several excellent review articles on the subject have been published (Go 59,Fe 65). In the present work the notation used follows closely that of Ferguson. A summary of definitions employed for the reduced matrix elements and other relevant quantities is contained in Appendix 2 where the general triple correlation is derived for a sequential reaction proceeding through the compound nucleus.

Schematically the reaction can be written $s_1 + a \rightarrow b$, $b \rightarrow s_2 + c$, $c \rightarrow s_3 + d$ where s_1, s_2 and s_3 are the spins of the three particle radiations and a,b,c and d are the spins of the target, compound nucleus, intermediate state and final product respectively. If the channel spin representation is adopted for the initial stage and the L-representation for the subsequent transitions the following angular momentum equations hold:

$$\underline{s} + \underline{l}_1 = \underline{b} \qquad \underline{s} = \underline{s}_1 + \underline{a}$$

$$\underline{b} = \underline{j}_2 + \underline{c} \qquad \underline{j}_2 = \underline{l}_2 + \underline{s}_2$$
$$\underline{c} = \underline{j}_3 + \underline{d} \qquad \underline{j}_3 = \underline{l}_3 + \underline{s}_3$$

where $\underline{l}_1$, $\underline{l}_2$ and $\underline{l}_3$ represent the orbital angular momentum carried by the three radiations. The triple correlation function is then given by equations (23) and (25) of Appendix 2 as

$$W(\theta_1\phi_1\theta_2\phi_2\theta_3\phi_3)=\sum(4\pi)^{-3}(-)^{\sigma}(\hat{a}\hat{s}_1)^2\hat{l}_1\hat{l}_1'\hat{l}_2\hat{l}_2'\hat{l}_3\hat{l}_3'\hat{j}_2\hat{j}_2'\hat{j}_3\hat{j}_3'(\hat{b}\hat{b}')^2$$

$$\times\ \hat{c}\hat{c}'\hat{k}_2\hat{k}_3\langle k_1 0|l_1 l_1' 00\rangle\langle k_2 0|l_2 l_2' 00\rangle\langle k_3 0|l_3 l_3' 00\rangle W(bl_1 b' l_1'; sk_1)$$

$$\times\ W(l_2 l_2' j_2 j_2'; k_2 s_2) W(l_3 l_3' j_3 j_3'; k_3 s_3) W(j_3 j_3' cc'; k_3 d)\langle k_1 q_1|k_2 k_3 q_2 q_3\rangle$$

$$\times \begin{Bmatrix} j_2 & c & b \\ j_2' & c' & b' \\ k_2 & k_3 & k_1 \end{Bmatrix} \langle b\|l_1|s\rangle\langle b'\|l_1'|s\rangle^*\langle c|j_2\|b\rangle\langle c'|j_2'\|b'\rangle^*\langle d|j_3\|c\rangle$$

$$\times\ \langle d|j_3'\|c'\rangle^* C^*_{k_1 q_1}(\theta_1\phi_1) C_{k_2 q_2}(\theta_2\phi_2) C_{k_3 q_3}(\theta_3\phi_3) \qquad (1)$$

with $\sigma = s_2+s_3+s+l_1-l_1'-j_3-j_3'-b'-c+d+k_1+k_2-j_2$ and the summation extending over $l_1 l_1' l_2 l_2' l_3 l_3' j_2 j_2' j_3 j_3' s_1 s_2 s_3 s a b b' c c' d$ $k_1 k_2 k_3 q_1 q_2 q_3$. Here $\langle a\alpha|bc\beta\gamma\rangle$ is a Clebsch-Gordan coefficient, W(abcd;ef) a Racah coefficient and the expression in curly brackets a 9-j symbol. The factors $\langle b\|l|s\rangle$ and $\langle c|j\|b\rangle$ are reduced matrix elements for absorption and emission respectively while $C_{kq}(\theta\phi)$ is a renormalised spherical harmonic.

As it stands, equation (1) is completely general, the only assumption made being that the incident radiation and target are unpolarised. There are, however, a number of obvious simplifications that can be made.

(1) The particles 1,2,3 and the nuclei a,c,d are states of definite parity and spin. Accordingly the sums over $s_1 s_2 s_3$ acc' and d disappear. Further, the Clebsch-Gordon coefficient $\langle k_3 0 | l_3 l_3' 00 \rangle$ vanishes unless $k_3 + l_3 + l_3'$ is even.

(2) As yet no choice of laboratory coordinate system has been made. If the direction of the incident radiation is taken as the z-axis, the renormalised spherical harmonic $C_{k_1 q_1}(\theta_1 \phi_1)$ reduces to $\delta_{q_1 0}$ and the sum over q_1 disappears. If the y-axis is taken in a direction perpendicular to the reaction plane the spherical harmonics are real.

Additional simplifications arise in the application of equation (1) to the reaction

$$d + {}^7Li \longrightarrow {}^9Be^* \longrightarrow \alpha_1 + {}^5He \longrightarrow n + \alpha_2 .$$

(3) Since an alpha particle has no spin, $s_2=0$ and the Racah coefficient $W(l_2 l_2' j_2 j_2'; k_2 s_2) = \delta_{l_2 j_2} \delta_{l_2' j_2'} (\hat{l}_2 \hat{l}_2')^{-1}$ causes the sum over j_2 and j_2' to disappear.

(4) The residual nucleus, d, is also an alpha particle and combined with the neutron spin of $\frac{1}{2}$, spin and parity conservation give $j_3 = j_3' = 3/2$ and $l_3 = l_3' = 1$ for the decay of the $3/2^-$ ^{5}He ground state. Also, k_3 must be 0 or 2. The product of the reduced matrix elements, $\langle d | j_3 \| c \rangle \langle d | j_3 \| c \rangle^*$, can now be factored out and regarded as a simple constant of proportionality.

(5) If the reaction proceeds through a compound nucleus state of definite spin and parity then the sum over b and b' disappears and parity conservation restricts both k_1 and k_2 to

even values. In the present case, the reaction yield is expected to be dominated by compound nucleus formation through two levels of opposite parity and only if interference effects between these two levels are neglected, are k_1 and k_2 restricted to even values. There is no sound basis for neglecting such interference effects but failure to do so leads to tremendous computational difficulties. Experimentally, one could determine their importance by measuring the angular distribution of α_1 and looking for departures from symmetry about 90^o. The characteristics of each state appear through the reduced matrix elements given by (Fe 65)

$$\langle b\|l_1|s\rangle\langle c|j_2\|b\rangle \propto 2i\left\{\left[\Gamma(sl_1)\Gamma(cj_2)\right]^{\frac{1}{2}}/\Gamma\right\}\sin\beta\exp i(\beta+\xi_1) \qquad (2)$$

where $\Gamma(sl_1)$ is a partial width for the incoming particle and $\Gamma(cj_2)$ is the partial width for the emitted radiation. The total width of the level is Γ and β is a resonance phase shift given by

$$\tan\beta = \Gamma/2(E_o-E).$$

The phase shift ξ_1 is associated with the incoming particle and is a sum of the usual Coulomb phase shift and a hard sphere phase shift.

(6) At 1.0 MeV bombarding energy the reaction can be regarded as proceeding predominantly through s and p-waves. If higher partial waves than p-waves are neglected, then assumption (5) above implies that there can be no interference between different l_1 values and the selection rule k_1=0 or 2 results.

With the above simplifications, the contribution to the correlation function from a single value of b becomes

$$W(\theta_2\phi_2\theta_3\phi_3)\propto\sum(-)^{\sigma_1}\hat{l}_1^2\hat{l}_2\hat{l}_2'\hat{b}^4\hat{k}_2\hat{k}_3\langle k_1 0|l_1 l_1 00\rangle\langle k_2 0|l_2 l_2' 00\rangle$$

$$\times\begin{Bmatrix} l_2 & 3/2 & b \\ l_2' & 3/2 & b \\ k_2 & k_3 & k_1 \end{Bmatrix} W(l_1 b l_1 b; s k_1)\langle k_1 0|k_2 k_3 q_2 -q_2\rangle|\langle b\|l_1|s\rangle|^2\langle c|l_2\|b\rangle$$

$$\times\langle c|l_2'\|b\rangle^* C_{k_2 q_2}(\theta_2\phi_2) C_{k_3 -q_2}(\theta_3\phi_3) \qquad (3)$$

with $\sigma_1 = s - b + k_3/2 - l_2$ and the summation extending over $l_2 l_2' s k_1 k_2 k_3 q_2$.

(7) As it stands equation (3) still contains interference terms between different l_2 values. For ease of calculation these terms will be neglected. As will be seen in the subsequent analysis this loss of generality will not affect the final conclusions.

Writing

$$f(\theta_2\phi_2\theta_3\phi_3, s, l_2) = a_1 + a_2 C_{20}(\Theta) + a_3 C_{20}(\theta_2) + a_4 C_{20}(\theta_3)$$
$$+ a_5\sum_q \langle 22q\text{-}q|20\rangle C_{2q}(\theta_2\phi_2) C_{2-q}(\theta_3\phi_3)$$
$$+ a_6\sum_q \langle 42q\text{-}q|20\rangle C_{4q}(\theta_2\phi_2) C_{2-q}(\theta_3\phi_3) \qquad (4)$$

where $\Theta = \theta_2 + \theta_3$ and the coefficients a_i are defined by

$$a_1 = \hat{b}^2/2 ,$$

$$a_2 = (-)^{b-\frac{1}{2}}\hat{l}_2^2\hat{b}^2\langle l_2 l_2 00|20\rangle W(3/2 l_2 3/2 l_2; b2) ,$$

$$a_3 = 3\sqrt{5}\,(-)^{s-b-1}\langle 1100|20\rangle W(1b1b; s2)\hat{l}_2^2\hat{b}^4\langle l_2 l_2 00|20\rangle \begin{Bmatrix} 3/2 & l_2 & b \\ 3/2 & l_2 & b \\ 0 & 2 & 2 \end{Bmatrix} ,$$

$$a_4 = 3\sqrt{5}(-)^{s-b}\langle 1100|20\rangle W(1b1b;s2)\hat{1}_2^2\hat{b}^4\langle l_2 l_2 00|00\rangle \begin{Bmatrix} 3/2 & l_2 & b \\ 3/2 & l_2 & b \\ 2 & 0 & 2 \end{Bmatrix},$$

$$a_5 = 15(-)^{s-b}\langle 1100|20\rangle W(1b1b;s2)\hat{1}_2^2\hat{b}^4\langle l_2 l_2 00|20\rangle \begin{Bmatrix} 3/2 & l_2 & b \\ 3/2 & l_2 & b \\ 2 & 2 & 2 \end{Bmatrix},$$

$$a_6 = 9\sqrt{5}(-)^{s-b}\langle 1100|20\rangle W(1b1b;s2)\hat{1}_2^2\hat{b}^4\langle l_2 l_2 00|40\rangle \begin{Bmatrix} 3/2 & l_2 & b \\ 3/2 & l_2 & b \\ 2 & 4 & 2 \end{Bmatrix},$$

the angular correlation function can be rewritten as

$$W(\theta_2\phi_2\theta_3\phi_3) \propto \sum_{sl_2} c(s,l_2) f(\theta_2\phi_2\theta_3\phi_3, s, l_2). \qquad (5)$$

The coefficient $c(s,l_2)$ is a product of reduced matrix elements and explicitly is defined by

$$c(s,l_2) = |\langle b\|l_1|s\rangle\langle c|l_2\|b\rangle|^2 \propto \frac{\Gamma(sl_1)\,\Gamma(cl_2)}{(E_o-E)^2+\Gamma^2/4}. \qquad (6)$$

The coefficients, a_i, are tabulated in Table 5.1 and 5.2 for all allowed values of l_1, l_2, b and s.

§5.22 The Maximum Likelihood Technique for Curve Fitting

In testing the validity of any theory with respect to experiment it is usual to adopt some form of fitting procedure. In the present instance, the technique of Maximum Likelihood was employed(Or 58, Or 68). Briefly the procedure is as follows.

Consider the case when the experimental points, $y_i(x_i)$, are Gaussian distributed with standard deviation,

Table 5.1

Values of the coefficients a_i for incident s-waves

Set Number	$b\pi$	l_2	a_1	a_2	Shape*
1	1/2-	2	1.0	1.0	$1-k\sin^2\theta$
2	3/2-	0	2.0	0.0	1
3		2	2.0	0.0	1
4	5/2-	2	3.0	-2.14	$1+k\sin^2\theta$
5		4	3.0	2.14	$1-k\sin^2\theta$

* k is a positive number.

Table 5.2

Values of the coefficients a_i for incident p-waves

Set Number	$b\pi$	s	l_2	a_1	a_2	a_3	a_4	a_5	a_6
6	1/2+	1/2	1	1.0	1.0	-	-	-	-
7		3/2	1	1.0	1.0	-	-	-	-
8	3/2+	1/2	1	2.0	-1.6	-1.6	0.4	-2.99	-
9			3	2.0	1.6	1.6	0.4	0.85	3.85
10		3/2	1	2.0	-1.6	1.28	-0.32	2.39	-
11			3	2.0	1.6	-1.28	-0.32	-0.68	-3.08
12		5/2	1	2.0	-1.6	-0.32	0.08	-0.60	-
13			3	2.0	1.6	0.32	0.08	0.17	0.77
14	5/2+	3/2	1	3.0	0.6	1.68	1.68	0.90	-
15			3	3.0	-0.6	1.32	-1.32	-1.86	1.73
16		5/2	1	3.0	0.6	-1.92	-1.92	-1.03	-
17			3	3.0	-0.6	-1.51	1.51	2.13	-1.98
18	7/2+	5/2	3	4.0	-2.67	1.90	-0.57	-2.03	-2.75
19			5	4.0	2.67	2.67	0.80	1.42	3.85

σ_i, about the expected value, $\bar{y}_i(x_i)$. Then, the Likelihood function is defined by (Or 58)

$$L = \prod_1^n \frac{1}{\sqrt{2\pi}\,\sigma_i} \exp\left[-(y_i-\bar{y}_i)^2/2\sigma_i^2\right]. \qquad (7)$$

If the $\bar{y}_i$ are obtained from a theory involving a number of parameters, c_j, then those values of the parameters which yield a maximum in L are the best values consistent with the theory. In terms of logarithmic probabilities,

$$W = \ln L = -\tfrac{1}{2}M - \sum_{i=1}^{n} \ln\sqrt{2\pi}\sigma_i \qquad (8)$$

where

$$M = \sum_{i=1}^{n} (y_i-\bar{y}_i)^2/\sigma_i^2 \qquad (9)$$

then maximising L is equivalent to minimising M, which, from its definition, is seen to be the usual expression for χ^2. Thus, for Gaussian distributed points the Maximum Likelihood Technique and that of the usual Least Squares procedure are identical.

§5.23 Application of the Maximum Likelihood Technique.

For a given value of compound nucleus spin and parity, equation (5) gives the expected contribution to the yield from resonant compound nucleus formation. Naturally, it is anticipated that not all possible channel spins and orbital angular momentum values, l_2, will contribute equally since this would imply that the partial widths and hence the nuclear phase shifts are independent of these quantities. Accordingly, in the fitting procedure described below, each possible set of quantum numbers,

characterised by b,s and l_2 is initially tested in turn to determine which sets can fit the results. Once these sets have been obtained, only then are channel spin and orbital angular momentum mixing introduced. In this manner it is hoped that a unique spin can be assigned to the positive parity level at an excitation energy of 17.48 MeV in ^{9}Be.

As noted in §5.1 contributions to the yield will also be expected from the broad level of spin and parity $5/2^-$, which exists at an excitation energy of 17.28 MeV in ^{9}Be. As Table 5.1 indicates, any contribution to the reaction from this level should then show symmetry about the system centre of mass (s.c.m.) recoil direction. Further, Milone's results (Mi 66), performed at a deuteron energy of 800 keV, a little above this resonance, show that the angular correlation is of the form $1 + k \sin^2(\Theta)$, with $k = 3.\pm0.3$. This would suggest that the quantum numbers of set #4 must be largely responsible for the reaction yield.

At an incident deuteron energy of 1.0 MeV, the high energy tail of this state should still be important. Certainly, the shape of the measured correlations, characterised by a mimimum near the s.c.m. recoil direction, is consistent with this interpretation. It is appropriate, then to use a fitting function of the form

$$Y = c_0(\theta_2\phi_2) + c_1(3.-2.14C_{20}(\Theta)) + c_2 f(\theta_2\phi_2\theta_3\phi_3,s,l_2) \qquad (10)$$

and at the same time demand that all three varied parameters, c_0, c_1 and c_2 be positive to be physically acceptable.

While it is not reasonable to expect that the $5/2^-$ resonance decays entirely by d-waves, as the second term of

equation (10) suggests, any orbital angular momentum mixing will be accounted for by c_o. The larger the g-wave component the larger c_o must be. The parameter, c_o, will also partially account for any direct contribution to the reaction yield. The dependence of c_o on θ_2 and ϕ_2 has been shown explicitly but in fact it may also depend on θ_3 and ϕ_3 as well. This latter dependence would manifest itself as a shift of the axis of symmetry from that predicted by compound nucleus formation. However, since the direct processes are expected to be relatively insignificant for reasons outlined in §5.1, this dependence will be ignored.

One further point should be made with regard to the application of equation (10). Complicated as the angular dependence of the equation appears to be, in the recoil centre of mass frame it can always be reduced to the form

$$Y = k_1 + k_2 \sin^2 (\theta_3 - \theta_o)$$

where k_1 , k_2 and θ_o are parameters to be determined by the fitting procedure. Accordingly, in testing the validity of a given spin assignment for the positive parity resonance, a small χ^2 will <u>not</u> necessarily imply that this spin assignment is consistent with the results. All it will establish is that the earlier assumptions that the reaction proceeds <u>sequentially</u> through a $3/2^-$ state of ^{5}He, is well founded. Table 5.3 lists the values of χ^2 and the corresponding confidence levels for the four experimentally measured angular correlations. All four measurements establish that the assumption is well founded.

Turning now to the experimental measurements, it is

Table 5.3

Values of χ^2 and Confidence Levels for the Measured Angular Correlations.

Angle α_1	χ^2	Probability
60	6.4	0.27
65	2.2	0.71
100	2.2	0.70
120	0.12	0.98

immediately apparent that the angular correlation for $\alpha_1=120^o$ stands apart from the others in that it exhibits a marked shift in the symmetry axis from the s.c.m. recoil direction. Such a shift can only arise if the reaction proceeds in part through a positive parity level of the $^9Be^*$ compound nucleus. It is to be expected, then, that the fit obtained with equation (10) will be most sensitive to the spin assignment given to the level and also to the quantum numbers appropriate to the incoming and outgoing channels. Accordingly, the fitting procedure is first carried out for this correlation alone. Table 5.4 lists the values of c_0 , c_1 and c_2 which give rise to the best fit, the latter shown drawn as a dashed curve in Figure 5.6. It is immediately obvious from Table 5.4 that only sets #14 and #17 satisfy the necessary requirement that the fitted parameters be positive.

The question of consistency must now be considered. Can either or both of these quantum number sets give physically acceptable fits in all cases? As Table 5.5 indicates this question can be answered in the affirmative. Even the $\alpha_1=60^o$ results, illustrated in Figure 5.3, which are subject to systematic error because they have been obtained from triple coincidence measurements, can be fitted. It should be noted, however, that the point marked "X" in Figure 5.3 has not been considered in the fitting process, since the geometrical arrangement used in this measurement had the α_2 detector located between the target and the neutron detector, resulting in a considerable attenuation of the scattered neutrons.

Table 5.4

Best Fit Parameters for the $\alpha_1 = 120^\circ$ Results.

Set #	c_0	c_1	c_2
8	0.95±0.10	-0.35±0.15	0.76±0.20
9	4.83±1.05	-0.49±0.19	-0.96±0.25
10	0.53±0.11	0.94±0.19	-0.96±0.25
11	-2.50±0.84	0.80±0.15	0.77±0.20
12	1.68±0.25	-2.65±0.74	3.85±0.99
13	-15.5±4.2	3.10±0.75	3.80±0.90
14	0.05±0.20	0.27±0.04	0.18±0.05
15	1.26±0.16	0.29±0.04	-0.23±0.06
16	1.37±0.18	0.18±0.05	-0.16±0.04
17	0.32±0.14	0.16±0.04	0.20±0.05
18	0.90±0.10	0.89±0.17	-0.54±0.14
19	-2.22±0.77	0.70±0.13	0.38±0.10

Table 5.5

Best Fit Parameters for the α_1=60°,65° and 100° Results.

Angle	Set #	c_0	c_1	c_2
60°	14	0.00±0.18	0.49±0.04	0.10±0.05
	17	0.07±0.14	0.42±0.05	0.12±0.06
65°	14	0.02±0.14	0.38±0.04	0.12±0.05
	17	0.06±0.12	0.31±0.05	0.14±0.06
100°	14	0.47±0.18	0.37±0.05	0.03±0.08
	17	0.48±0.17	0.35±0.09	0.04±0.09

Table 5.6

Best Fit Parameters obtained by fitting the α_1=65°, 100° and 120° results simultaneously.

Parameter	Set #14	Set #17
c_0(65)	0.02±0.09	0.06±0.08
c_0(100)	0.21±0.09	0.23±0.09
c_0(120)	0.03±0.11	0.26±0.07
c_1	0.33±0.02	0.24±0.03
c_2	0.16±0.03	0.17±0.03

There does appear to be some dispersion in the values of the fitted parameters, when the results for the four correlations are compared. For example, if one considers set #14 say, the value of c_2 ranges from a minimum of 0.03 ± 0.08 when $\alpha_1 = 100^\circ$ to a maximum of 0.18 ± 0.05 when $\alpha_1 = 120^\circ$. However, the large errors indicate that the parameters are strongly correlated with each other, and accordingly, the quality of the fit is not expected to deteriorate seriously for parameter changes of the order of the standard deviations. In particular, if the parameters for $\alpha_1 = 100^\circ$ are changed from those in Table 5.5 to $c_o = 0.25$, $c_1 = 0.35$ and $c_2 = 0.12$ the value of χ^2 changes from 2.2 to 3.7, a not unacceptable increase. This suggests that it may be possible to obtain an adequate fit to the experimental measurements by simultaneously fitting all four angular correlations, allowing only c_o to vary from correlation to correlation. This is, of course, the final test of consistency.

In the present instance, the $\alpha_1 = 60^\circ$ correlation is not considered since it is felt that the systematic errors associated with its measurement would impose false restrictions on the fitted parameters. Table 5.6 lists the parameters which give rise to the best fit drawn as a solid curve in Figures 5.4 5.5 and 5.6. (The solid curve shown in Figure 5.3 is obtained by using the best fit parameters of Table 5.5, $\alpha_1 = 60^\circ$). The value of χ^2 for the simultaneous fit is 11.8 which corresponds to a confidence level of 0.69 for 15 degrees of freedom (20 points fitted with 5 parameters). As Table 5.6 indicates, both

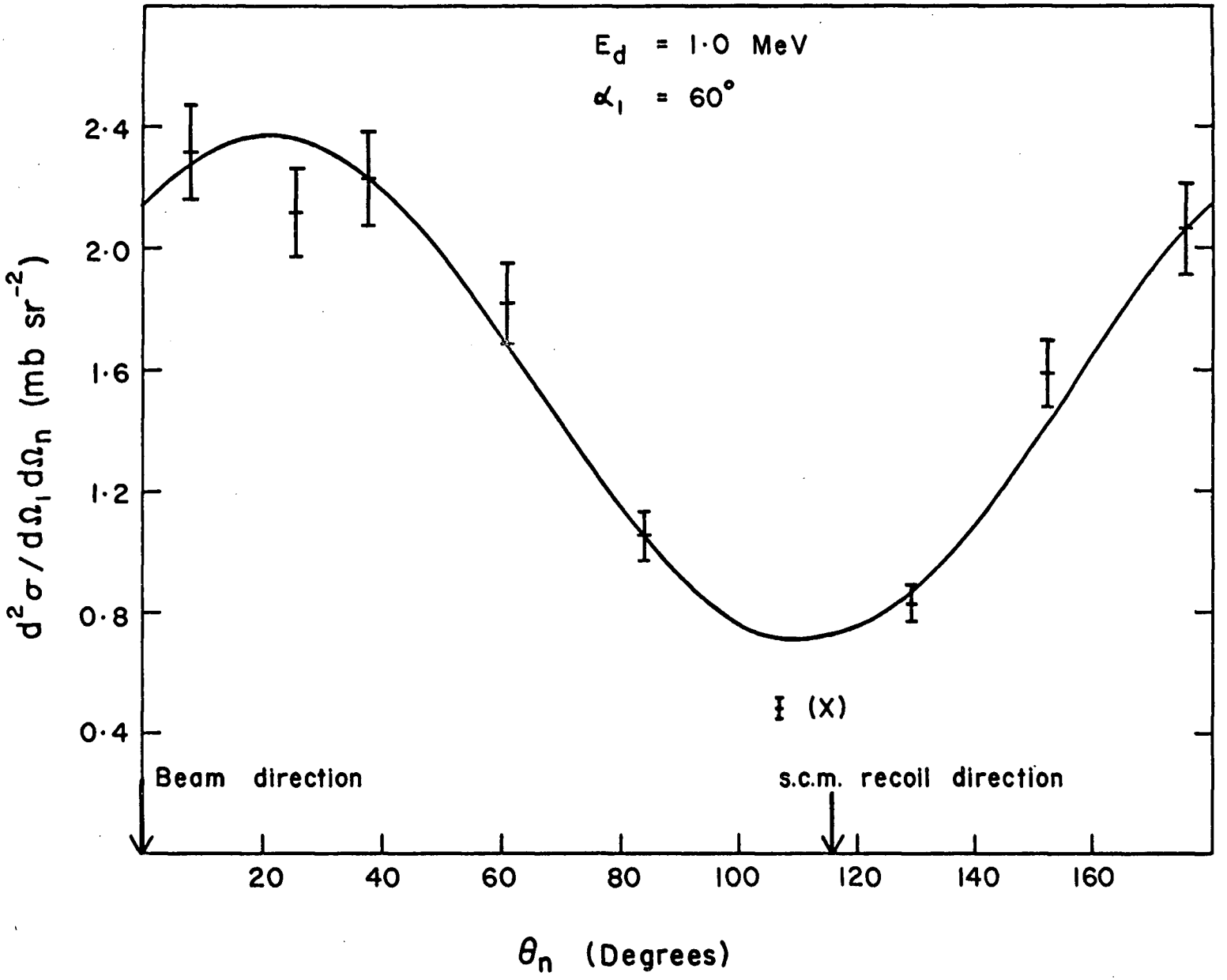

Fig 5.3 The Double Differential Cross Section plotted as a function of neutron angle in the recoil centre of mass frame for $\alpha_1 = 60^o$. The curve is the best fit obtained as described in text.

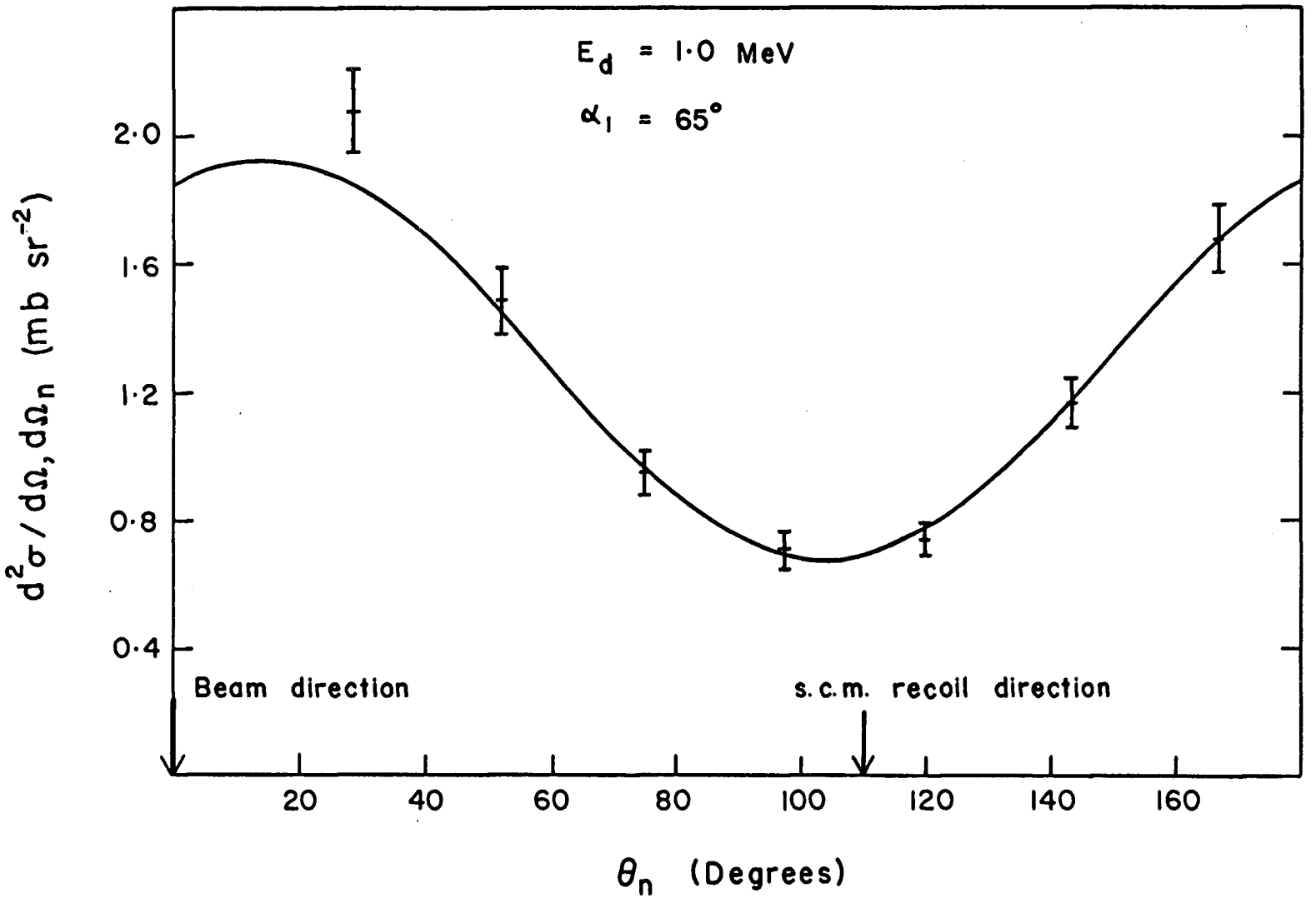

Fig 5.4 The Double Differential Cross Section plotted as a function of neutron angle in the recoil centre of mass frame for α_1 =65°. The curve is the best fit obtained when the data for α_1 =65°, 100° and 120° are fitted simultaneously.

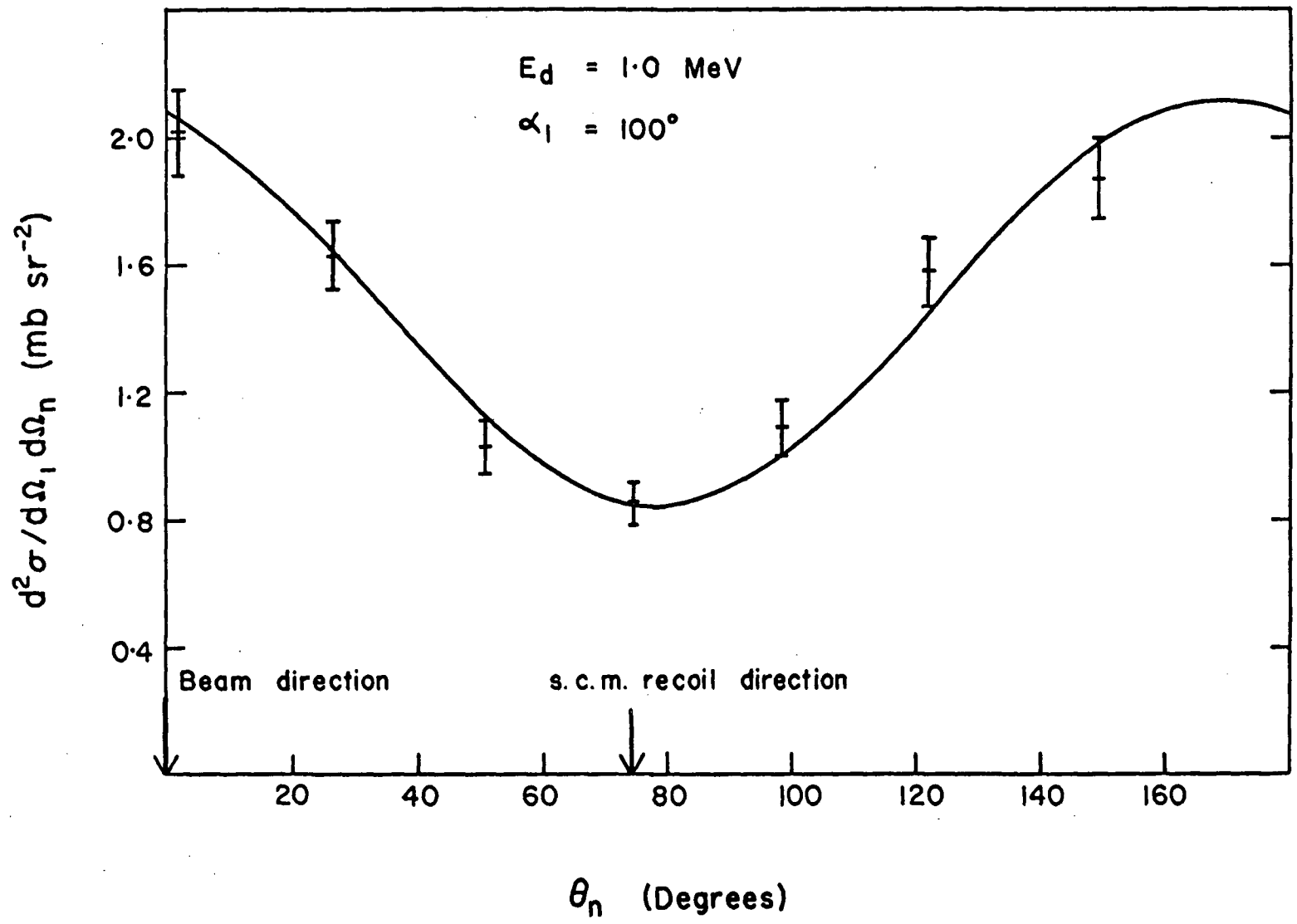

Fig 5.5 The Double Differential Cross Section plotted as a function of neutron angle in the recoil centre of mass frame for $\alpha_1 = 100^o$. The curve is the best fit obtained when the data for $\alpha_1 = 65^o$, 100^o and 120^o are fitted simultaneously.

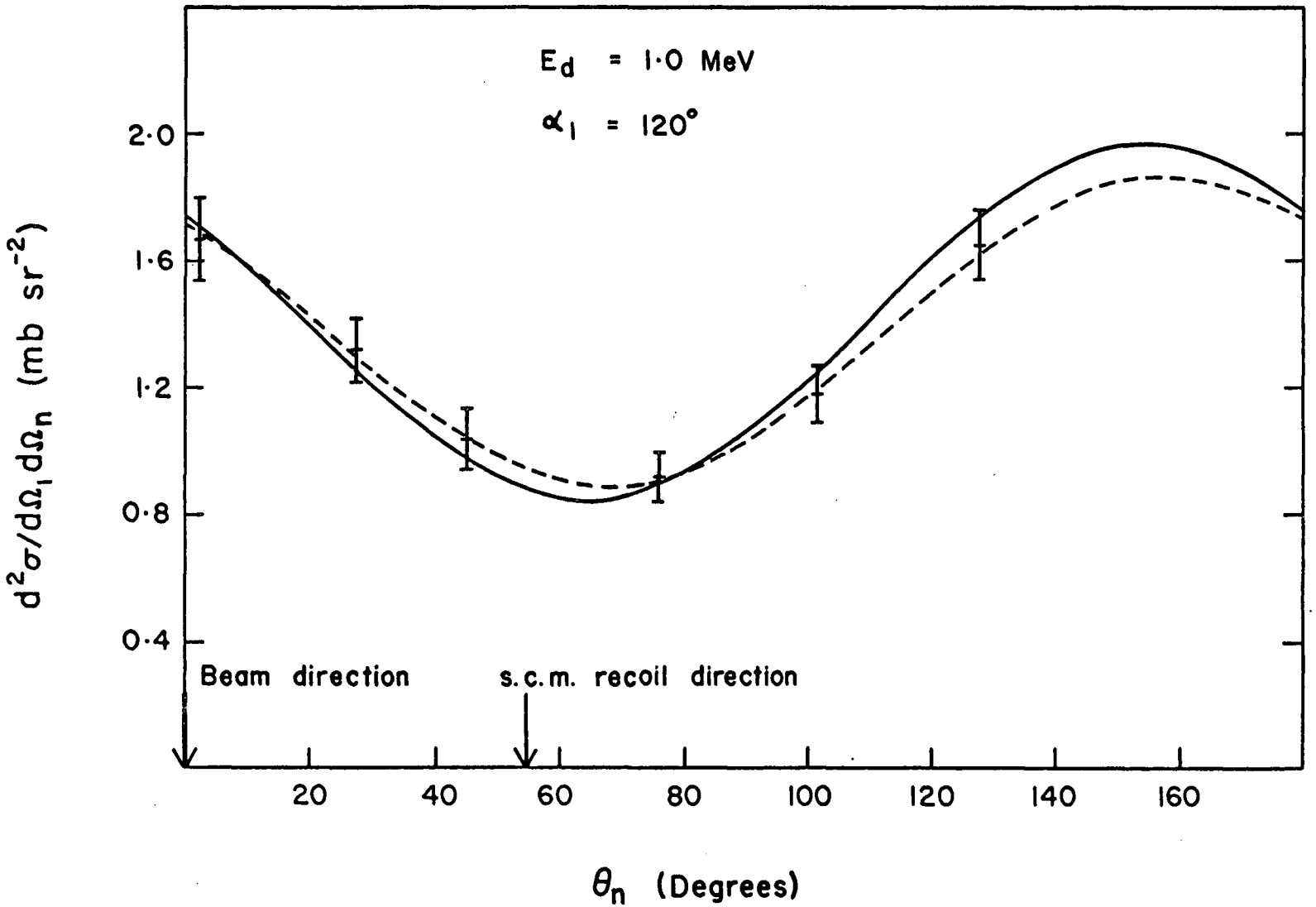

Fig 5.6 The Double Differential Cross Section plotted as a function of neutron angle in the recoil centre of mass frame for $\alpha_1 = 120^o$. The dashed curve is obtained by fitting the $\alpha_1 = 120^o$ data by itself while the solid curve is the fit obtained when the results for $\alpha_1 = 65^o$, 100^o and 120^o are fitted simultaneously.

quantum number sets give physically acceptable solutions.

One might now ask, what effect do the inclusion of channel spin and orbital angular momentum mixing have on the fitted parameters? As a general rule, it is found that small amounts (<10 %) of mixing are acceptable but if larger quantities are included, one or more of the fitted parameters becomes negative. Whilst small negative excursions of the parameters should not be interpretated too seriously, in view of the latter's large standard deviations, such a result supports the conclusion that the reaction yield through the ^{9}Be level at an excitation energy of 17.48 MeV is dominated by a single set of quantum numbers, either set #14 or set #17, with mixing effects being of secondary importance. Both of these sets predict a spin and parity of $5/2^{+}$ for this level but differ in their assignment of the resonance quantum numbers for the incoming and outgoing channels, viz:

Set #14; $s = 3/2$, $l_2 = 1$,

Set #17; $s = 5/2$, $l_2 = 3$.

In conclusion, it appears that the experimental measurements discussed in this thesis cannot distinguish between these two sets of quantum numbers. On the other hand, from a theoretical point of view, if one takes the radius of the interaction in the ^{5}He -α channel to be 3.3 fm., the ratio of the α - particle penetrabilities for p- and f-waves is 1.6:1 at the appropriate energy. This suggests that set #14 should be mildly favoured over set #17.

§ 5.3 Conclusion

From the analysis undertaken here, one can conclude that in the neighbourhood of 1.0 MeV deuteron bombarding energy, the first stage of the sequential reaction

$$d + {}^{7}Li \rightarrow \alpha_1 + {}^{5}He(\tfrac{3}{2}^-) \hookrightarrow n + \alpha_2$$

proceeds predominantly through compound nucleus formation in the ${}^{9}Be^{*}$ system. The observed asymmetry of the reaction products about the ${}^{5}He$ recoil direction can be explained on the basis of angular correlation arguments. In particular, evidence is presented that the level at an excitation energy of 17.48 MeV in ${}^{9}Be$ can be assigned spin and parity of $5/2^+$, whilst the resonance quantum numbers for the incoming and outgoing channels are either

$$l_1 = 1 , \quad s = 3/2 , \quad l_2 = 1 ;$$

or

$$l_1 = 1 , \quad s = 5/2 , \quad l_2 = 3 .$$

No attempt has been made to extract values for the total width, Γ, or the partial widths, $\Gamma(sl_1)$ and $\Gamma(l_2)$. Information on the magnitudes of these widths could be obtained if angular correlation measurements were performed at several energies both on this resonance and on the competing $5/2^-$ resonance some 200 keV lower in energy. The latter measurements would determine the partial widths for the 17.28 MeV level of ${}^{9}Be$. In any subsequent analysis of data obtained at higher energies, the yield through this level is now well defined and there is no need to parametrise it in the manner of the previous section. It may then be possible to determine which of the two possible

sets of quantum numbers, listed above , is responsible for the formation and decay of the ^{9}Be level at 17.48 MeV excitation. Such an experiment is very time consuming and is planned for a future date.

Further support for our conclusions, is witnessed by the failure of the direct two particle transfer mechanism to fit the results. There is, of course, some doubt as to the validity of doing DWBA calculations with such light nuclei at low energy.

APPENDIX 1

NEUTRON DETECTOR EFFICIENCY

§A1.1 Introduction

One of the disadvantages of measurements involving the use of neutron detectors is that before any comparison of theory with experiment can be made, account must be taken of the variation of neutron detector efficiency with energy. This is particularly important in the present work where Legendre polynomial fits are made to the experimental data. Accordingly we have computed the theoretical efficiency of the neutron detector, and in addition, used the $d(d,n)^3He$ reaction to determine expermentally the detector efficiency over a limited energy range.

§A1.2 Theoretical Calculation

The computer program used in the calculation was obtained from the University of Alberta (Gr 67). The program considers as possibilities both single and double scattering of neutrons from protons and single scattering of neutrons from carbon. To simplify the calculation, the scintillator is assumed to have infinite area. Accordingly, one would anticipate that efficiencies calculated with the program would be larger than true efficiences. However, the discrepancy is not as serious as might be expected for the following two reasons:

1) The laboratory differential cross section for (n,p) scattering is proportional to the cosine of the neutron scattering angle which ensures predominantly forward scattering.

2) The energy of neutrons scattered from protons is proportional to the square of the cosine of the scattering angle which implies that the few neutrons scattered through large angles are slow and consequently have a greatly reduced mean free path in the scintillator because of the rapidly rising (n,p) cross section with neutron energy.

Naturally, the calculated efficiency depends on the electronic discrimination level used and it is important to have a reliable means of reproducing this bias level. This is done most readily by looking at a ^{22}Na recoil spectrum (Sc 66). The two thirds amplitude points on the Compton edges of the ^{22}Na recoil spectrum correspond to energies of 0.341 and 1.066 MeV respectively (see Fig. A 1). The low level discrimination level was obtained immediately in terms of electron energy. To transform from electron energy to proton energy the following equations due to Batchelor (Ba 61) were used:

$$E_e = \begin{cases} 0.215\ Ep + 0.028\ Ep^2 & 0<Ep<8\ \text{MeV} \\ 0.60\ Ep - 1.28 \end{cases}$$

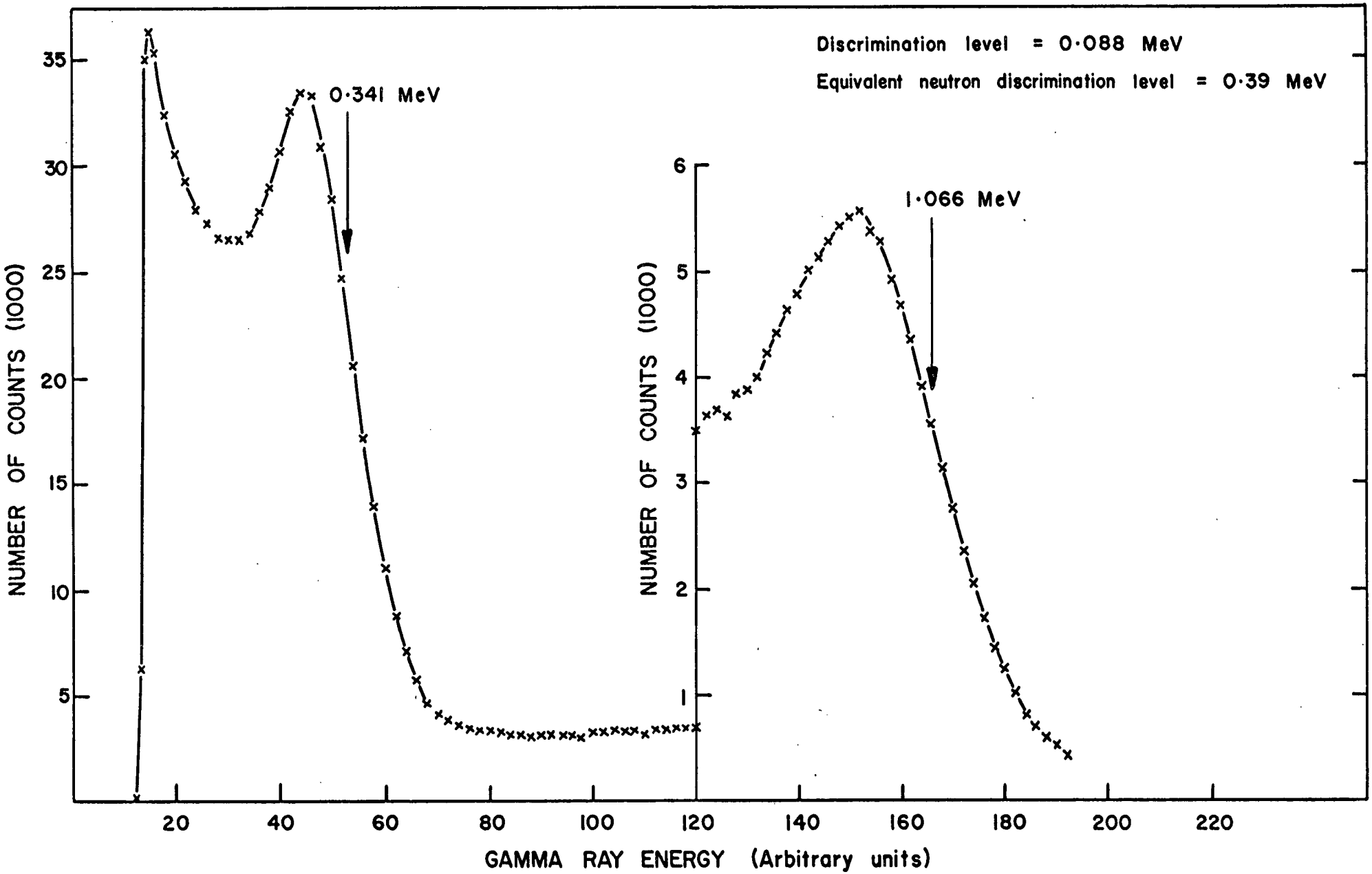

Fig A 1 Energy spectrum of ^{22}Na source in the neutron detector (NE 218).

The discrimination level was then found to correspond to a proton recoil energy of 0.39 MeV. Figure A5 shows the plot of theoretical efficiency versus energy for a 5" x 3" right cylinder of NE 218 with the lower cut-off taken to be 0.39 MeV.

§ A1.3 Experimental Measurement of Efficiency:

The $d(d,n)^3He$ reaction

A deuteron beam of 0.2μA was obtained from the UBC 3 MeV Van de Graaff accelerator and allowed to bombard a self supporting target of deuterated polyethylene (40μgm/cm^2) on a carbon backing (10μgm/cm^2), the targets being prepared in a similar manner to that described by Tripard et al (Tr 67). At a bombarding energy of 0.5 MeV the recoiling ^{3}He particles were resolved from the elastically scattered deuterons by using a high resolution surface barrier detector. The ^{3}He detector then defines a direction for the neutron. In order to reproduce as closely as possible the experimental conditions encountered in the $Li^7(d,n)\ 2\alpha$ reaction, care was taken to ensure that the neutrons associated with the detected ^{3}He particles were distributed over the entire area of the neutron detector rather than confined to the central region. With the neutron flight path held constant at 1.0 metre, this was achieved by adjusting the distance of the ^{3}He detector from the target such that the neutron and ^{3}He detector solid angles in the centre of mass frame were the same. The required distance was readily calculated for each angular position of the neutron detector from kinematical

considerations. The neutron detector efficiency is then a simple ratio of the number of neutron-^{3}He coincidences to the number of detected ^{3}He particles.

The electronics used incorporated the usual fast-slow coincidence typical of time of flight measurements (see Figure A2). The start pulse for the time of flight measurement was derived from the ^{3}He signal. The latter was first amplified with a charge sensitive preamplifier, further amplified and shaped with a Timing Filter Amplifier and then fed into a Constant Fraction Timing Discriminator (CFTD). The CFTD is a new timing device for use with solid state detectors, incorporating the advantages of both leading edge timing (low jitter) and cross-over timing (low walk). The fast negative output of the CFTD, after a suitable delay, was used as a start pulse for the Time to Amplitude Convertor (TAC). On the neutron side a fast signal was taken from the anode of the photomultiplier, regenerated as a positive pulse by the Time Pickoff Control (TPOC) and delayed with the Gate and Delay Generator. The fast negative output of the Gate and Delay Generator provided the stop pulse for the TAC which was operated on the 100nsec range. The delayed output of the TAC was presented to one analogue input of the ND 160 dual parameter analyser, the other input being provided by a suitably shaped, amplified and delayed pulse from the ^{3}He Linear Amplifier.

The slow coincidence was in essence the same as that described in Chapter 3 where the operation of an alpha particle -neutron coincidence was discussed. Briefly, the two prompt

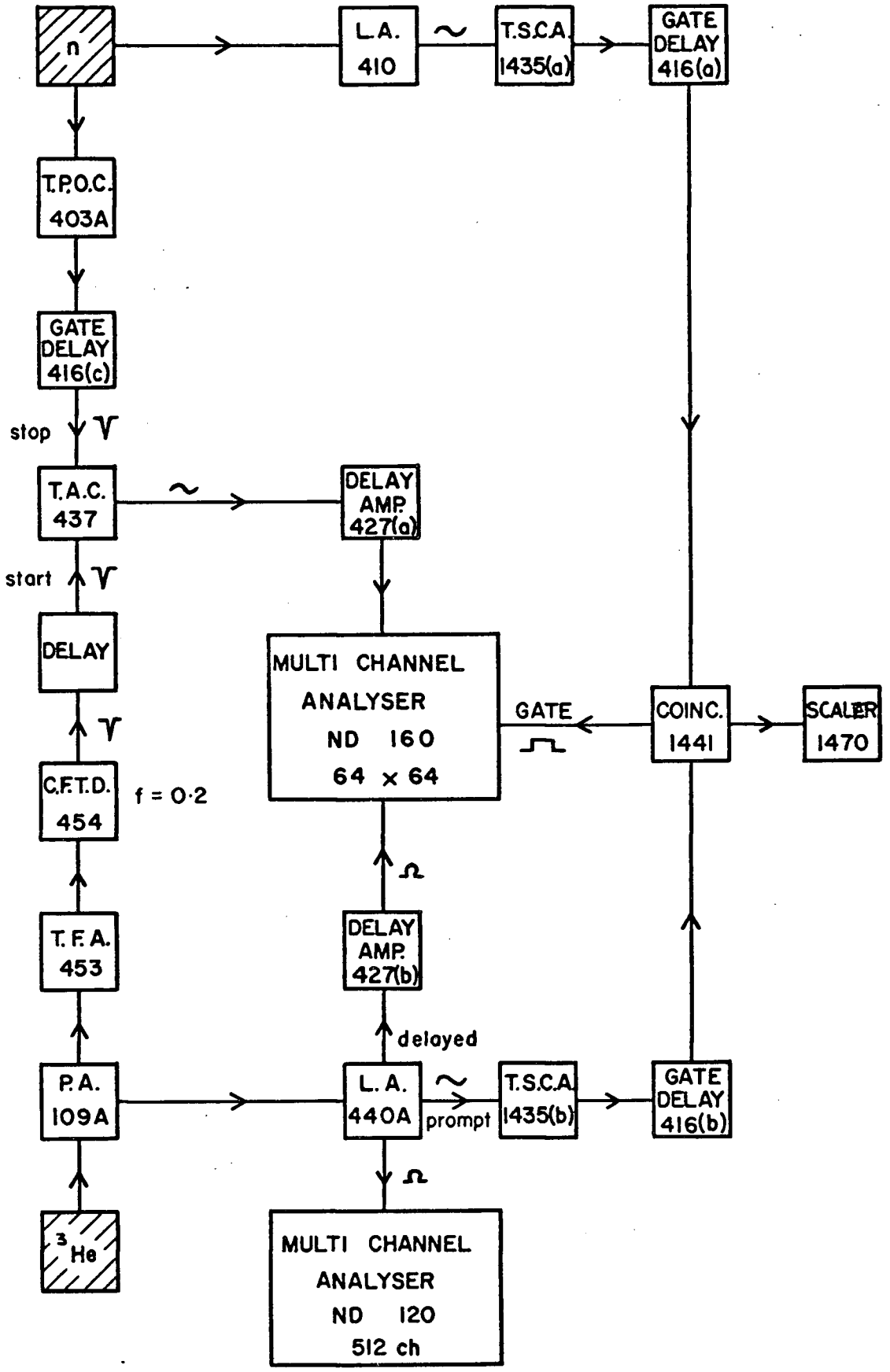

Fig A2 Electronics used in determining the neutron detector efficiency.

Table A1

Electronics used in Efficiency Measurement

Number	Device	Manufacturer
109A	Low Noise Preamplifier	Oak Ridge
403A	Time Pickoff Control Unit	Technical Enterprises
410	Multimode Linear Amplifier	Corporation
416	Gate and Delay Generator	Oak Ridge,
427	Delay Amplifier	Tennessee.
437	Time to Amplitude Converter	
440A	Active Filter Amplifier	
453	Timing Filter Amplifier	
454	Constant Fraction Timing Discriminator	
1435	Timing Single Channel Analyser	Canberra Industries,
1441	Fast Coincidence	Meriden,
1470	Scaler	Connecticut.
ND 120	512 Channel Analyser	Nuclear Data Inc.,
ND 160	Dual Parameter Analyser	Palatine, Illinois.

bipolar outputs of the linear amplifiers generate Timing Single Channel Analyser (TSCA) outputs which are suitably delayed with Gate and Delay Generators for coincidence operation (2τ=200nsec). The coincidence output was used directly to gate the ND 160.

An additional output from the ^{3}He Linear Amplifier was processed by an ND 120 multi-channel analyser, in this way simultaneously enabling us to make singles and coincidence measurements.

One point should be made with regard to the neutron TSCA. Since it is the lower level discriminator of this TSCA which determines the bias, it is vital that the discrimination level on the fast timing side (controlled by the TPOC) be well below that of the TSCA. This was most readily checked by gating a recoil proton energy spectrum by the TPOC and TSCA in turn and observing the respective discrimination levels.

Figure A3 illustrates a typical charged particle spectrum, in this instance taken at an angle of 30 degrees. The ^{3}He peak is clearly resolved from the elastically scattered deuterons and from the triton group from the reaction d(d,T)p. Also clearly shown are two proton groups, one from the $^{12}C(d,p)^{13}C$ reaction and the other from the d(d,p)T reaction. Figure A4 is the corresponding two dimensional coincidence spectrum and illustrates the very good timing obtained with the use of the CFTD.

The measured efficiencies are listed in Table A2 and are plotted as a function of energy along with the theoretical

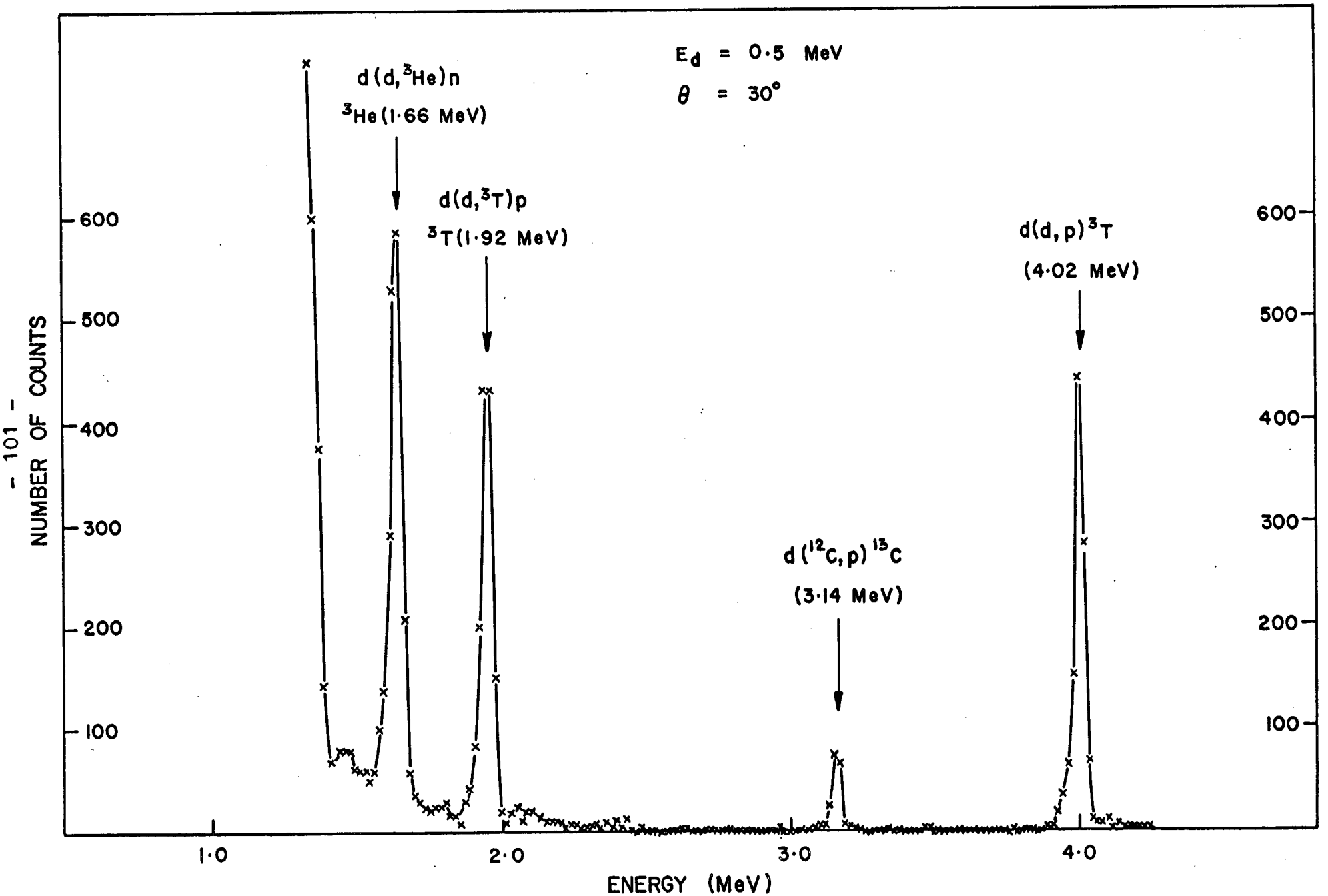

Fig A3 A typical spectrum resulting from the bombardment of deuterated polyethylene with 0.5 MeV deuterons.

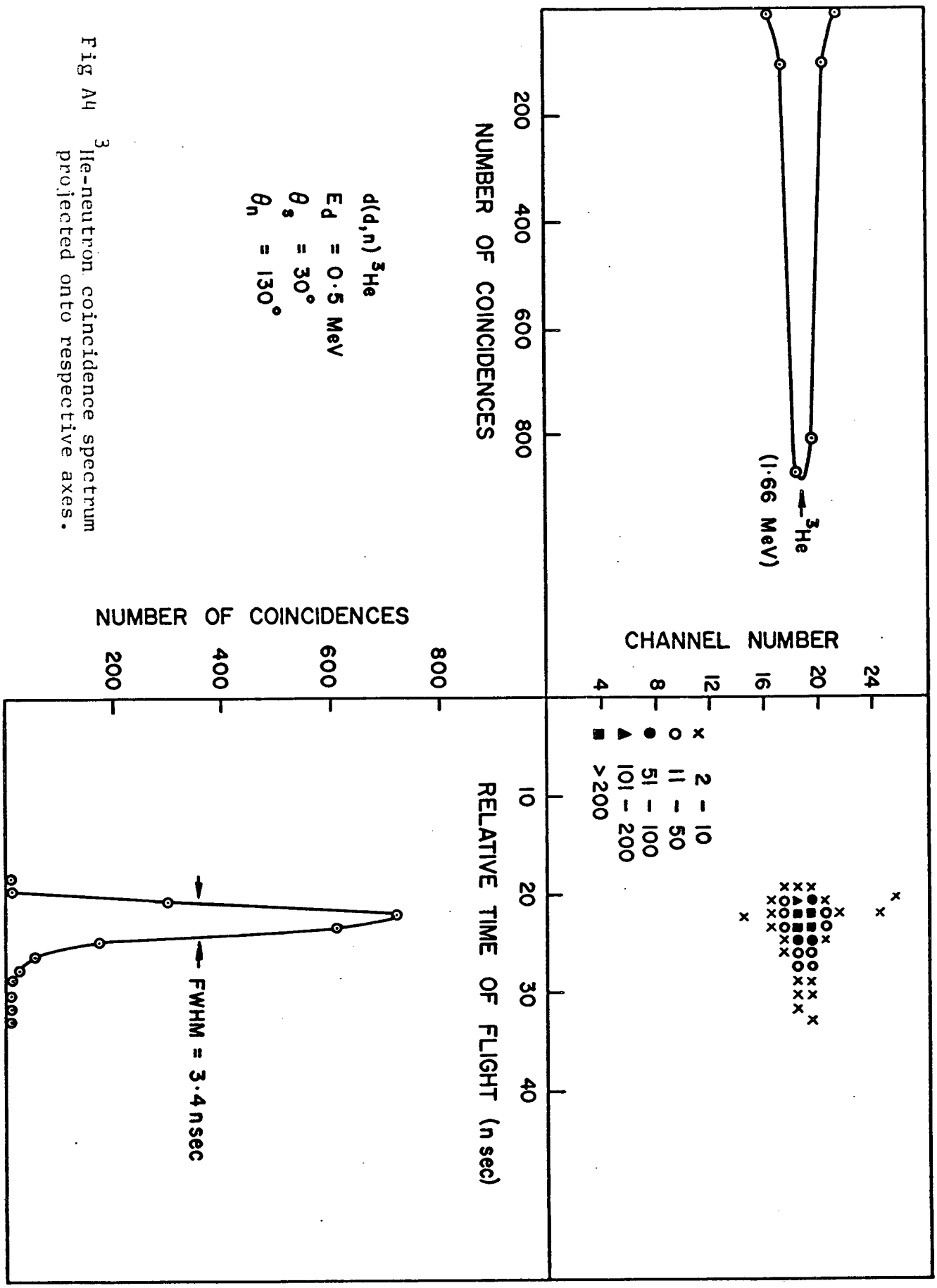

Fig A4 ^{3}He-neutron coincidence spectrum projected onto respective axes.

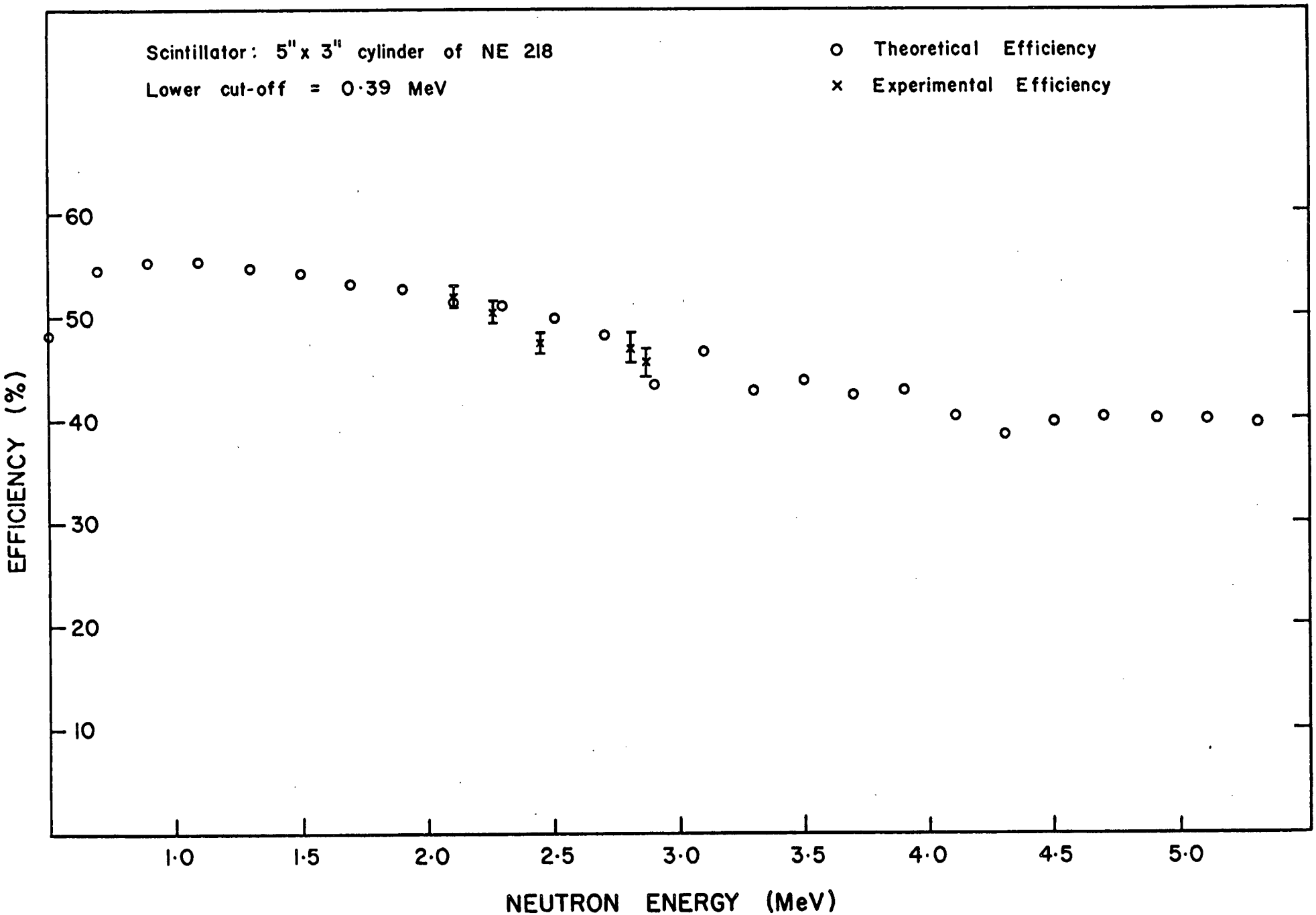

Fig A5 Neutron detector efficiency as a function of neutron energy.

efficiencies in Figure A5. As can be readily seen, the agreement between the two is excellent indicating,as expected, that the approximations made in the theoretical calculations are valid. Accordingly, it was decided to accept the validity of the theoretical curve over the entire neutron energy range encountered in the work reported in this thesis.

Table A2

Measured Neutron Detector Efficiency

Energy (MeV)	Efficiency %
2.1	51.9 ± 1.2
2.26	50.6 ± 1.0
2.44	47.5 ± 0.9
2.79	47.1 ± 1.3
2.86	45.7 ± 1.4

APPENDIX 2

THE GENERAL TRIPLE CORRELATION FUNCTION

§A 2.1 Introduction

In this appendix the triple correlation function is derived for the process represented by

$$j_1 + a \rightarrow b \rightarrow j_2 + c \qquad\qquad c \rightarrow j_3 + d \,.$$

Physically such a process corresponds to the formation of a compound nucleus, b, from an incident particle radiation, j_1, and a target, a. The nucleus, b, then decays with the emission of radiation j_2, leaving an unstable residual nucleus, c, which in turn decays with the emission of radiation j_3. The final product of the reaction is the stable product d.

Throughout, the terminology of statistical and efficiency tensors is employed. Definitions and relevant properties of these tensors have been included for completeness, the notation used being essentially the same as employed by Ferguson (Fe 65).

§A2.2 The Density Matrix and Statistical Tensors

If a system is in pure state $|P\rangle = \sum_i a_i |i\rangle$, the density matrix for the system is $\rho = |P\rangle\langle P|$ and the matrix elements of ρ are

$$\rho_{ij} = \langle i \,|\, P\rangle \langle P | j\rangle = a_i a_j^{*} .$$

Then, the expectation value of an observable, F, of the system is

$$\langle F\rangle = \sum_{ij} \langle P|j\rangle \langle j|F|i\rangle \langle i|P\rangle$$

$$\text{ie } \langle F \rangle = \mathrm{Tr}(\rho F). \tag{1}$$

Usually, it is more convenient to work with the related statistical tensors. These tensors, defined by

$$\rho_{kq}(\alpha j, \alpha' j') = \sum_{mm'} \langle kq | jj' m-m' \rangle \langle \alpha jm | \rho | \alpha' j' m' \rangle (-1)^{j'-m'} \tag{2}$$

then form a " contragredient standard tensorial set " (Fa 59) and transform under elements of the rotational matrices according to

$$\rho'_{kq'} = \sum_{q} D^{k*}_{qq'}(R) \rho_{kq} \tag{3}$$

where $R \equiv (\alpha, \beta, \gamma)$ is the rotation carrying the original coordinate system into the primed system, α, β, γ being the Euler angles. The definition of the rotational matrix elements employed in (3) is that of Messiah (Me 65).

§A2.3 Decomposition Formula for Statistical Tensors

Now suppose that ρ describes a composite system with ρ_1 being the density matrix for part one of the system ($\alpha_1 j_1 m_1$ represent the quantum numbers) and ρ_2 being the density matrix of part two ($\alpha_2 j_2 m_2$ quantum numbers). The statistical tensor describing the total system, ρ_{kq}, in terms of the statistical tensors $\rho_{k_1 q_1}$ and $\rho_{k_2 q_2}$ describing parts one and two is obtained as

$$\rho_{kq}(\alpha_1\alpha_2(j_1 j_2) j, \alpha'_1\alpha'_2(j'_1 j'_2) j') = \sum_{k_1 q_1 k_2 q_2} \langle kq | k_1 k_2 q_1 q_2 \rangle \hat{k}_1 \hat{k}_2 \hat{j}' \hat{j}$$

$$\times \begin{Bmatrix} j_1 & j_2 & j \\ j'_1 & j'_2 & j' \\ k_1 & k_2 & k \end{Bmatrix} \rho_{k_1 q_1}(\alpha_1 j_1, \alpha'_1 j'_1) \rho_{k_2 q_2}(\alpha_2 j_2, \alpha'_2 j'_2) \tag{4}$$

where $\langle kq|k_1k_2q_1q_2\rangle$ is a Clebsch-Gordon coefficient, the expression in curly brakets is a 9-j symbol and $\hat{x}$ is a shorthand notation for $(2x+1)^{\frac{1}{2}}$. The above formula is called the decomposition formula for statistical tensors and together with its inverse

$$\rho_{k_1q_1}\rho_{k_2q_2} = \sum_{kqjj'} \rho_{kq}(\alpha_1\alpha_2(j_1j_2)j, \alpha_1'\alpha_2'(j_1'j_2')j') \langle kq|k_1k_2q_1q_2\rangle \times \hat{k}_1\hat{k}_2\hat{j}\hat{j}' \begin{Bmatrix} j_1 & j_2 & j \\ j_1' & j_2' & j' \\ k_1 & k_2 & k \end{Bmatrix} \tag{5}$$

proves most useful in the development of angular correlation theory.

§A2.4 The Efficiency Matrix and Efficiency Tensors

The response of a radiation detector is a physically observable quantity. To it may be assigned a linear Hermitian operator, ε, which is defined so that its expectation value $\langle P|\varepsilon|P\rangle$ is the probability for detecting radiation in a state $|P\rangle$. In analogy to the statistical tensor, an efficiency tensor can be defined, viz.

$$\varepsilon_{kq}(\alpha j, \alpha' j') = \sum_{mm'} \langle kq|jj'm-m'\rangle (-1)^{j'-m'} \langle \alpha jm|\varepsilon|\alpha' j'm'\rangle \tag{6}$$

which will transform according to (3) and which will satisfy the decomposition formula, (4). In terms of the efficiency and statistical tensors the relation (1) yields

$$W = \langle\varepsilon\rangle = \sum_{kqjj'} \varepsilon^*_{kq}\rho_{kq} \tag{7}$$

as the response of a detector to a given radiation.

§A2.5 The Wigner-Eckart Theorem

Consider a state which undergoes a dynamical change by the emission of a particle or photon. The initial state can be described by $|jm\rangle$ and the final state by $|j_1 j_2 m_1 m_2\rangle$ where $\underline{j} = \underline{j}_1 + \underline{j}_2$. If V is the interaction responsible for the transition then the Wigner-Eckart theorem can be expressed in the form (Fe 65)

$$\langle j_1 j_2 m_1 m_2 | V | jm \rangle = \langle j_1 j_2 m_1 m_2 | jm \rangle \langle j_1 | j_2 \| j \rangle \qquad (8)$$

where $\langle j_1 | j_2 \| j \rangle$ is a reduced matrix element and is independent of the magnetic quantum numbers. In essence, the original matrix element has been factored into two parts, one containing the angular momentum coupling (the Clebsch-Gordon coefficent) and the other containing the nuclear information (the reduced matrix element). The notation used here, which distinguishes between absorption and emission was first introduced by Goldfarb (Go 60). If the state formed by coupling angular momenta $\underline{j}_1$ and $\underline{j}_2$ to total angular momentum $\underline{j}$ is written as $|jm(j_1 j_2)\rangle$ then it can readily be shown by using the result (8) that

$$\langle jm(j_1 j_2)| = \langle j_1 | j_2 \| j \rangle \langle jm| . \qquad (9)$$

An application of this equation will be seen below.

§A2.6 Radiation Parameters

An important class of statistical tensors arises in the description of plane wave states. First introduced by Racah (Ra 51), these tensors, whether describing particles, with or without spin, or photons, are called radiation parameters.

The case of particles with spin is most easily treated by combining the radiation parameters of spinless particles with the statistical tensors describing the particle's spin according to the decomposition formula.

Consider a beam of spinless particles travelling along the z-axis. Writing $|\Omega_o\rangle \equiv |\theta = 0, \phi\rangle$ then the density matrix for the beam in the momentum representation is

$$\rho = |\Omega_o\rangle\langle\Omega_o| \,.$$

Changing to the orbital angular momentum representation, which is physically the same as decomposing the plane wave into spherical waves, one has

$$\begin{aligned}\langle l\lambda|\rho|l'\lambda'\rangle &= \sum_{\Omega\Omega'}\langle l\lambda|\Omega\rangle\langle\Omega|\rho|\Omega'\rangle\langle\Omega'|l'\lambda'\rangle \\ &= \sum_{\Omega\Omega'} Y_l^{\lambda*}(\Omega)Y_{l'}^{\lambda'}(\Omega')\langle\Omega|\Omega_o\rangle\langle\Omega_o|\Omega'\rangle \\ &= Y_l^{\lambda*}(0,\phi)Y_{l'}^{\lambda'}(0,\phi) \\ &= \frac{\hat{l}\hat{l}'}{4\pi}\,\delta_{\lambda o}\,\delta_{\lambda' o}\,.\end{aligned}$$

Thus the radiation parameters $C_{k_1q_1}$ for this state are given from (2) by

$$C_{k_1q_1}(ll') = \sum_{\lambda\lambda'}\langle k_1q_1|ll'\lambda-\lambda'\rangle\,(-1)^{l'-\lambda'}\frac{\hat{l}\hat{l}'}{4\pi}\,\delta_{\lambda o}\,\delta_{\lambda' o}$$

$$\text{ie}\quad C_{k_1q_1}(ll') = \frac{\hat{l}\hat{l}'}{4\pi}(-1)^{l'}\,\langle k_1 0|ll'00\rangle\,\delta_{q_1 o}\,. \qquad (10)$$

Now suppose that the particles have spin $\underline{s}$ coupled to the orbital angular momentum, $\underline{l}$, according to $\underline{j} = \underline{l} + \underline{s}$. Application of the decomposition formula, (4), together with (10) yields

$$C_{kq}(jj') = \sum_{k_1 k_s} \frac{\hat{1}\hat{1}'}{4\pi}(-1)^{1'} \langle k_1 0|11'00\rangle \langle kq|k_1 k_s 0q\rangle \hat{j}\hat{j}'\hat{k}_1\hat{k}_s$$

$$x \begin{Bmatrix} 1 & s & j \\ 1' & s' & j' \\ k_1 & k_s & k \end{Bmatrix} \rho_{k_s q}(ss') \,. \qquad (11)$$

Often the particle spin is unpolarised and for this case the density matrix is given by

$$\langle s\sigma|\rho_s|s'\sigma'\rangle = \delta_{ss'}\delta_{\sigma\sigma'}\hat{s}^{-2}.$$

Thus $\rho_{k_s q}(ss') = \delta_{q0}\delta_{k_s 0}\delta_{ss'}\hat{s}^{-1}$. (12)

Equation (11) then reduces to

$$C_{kq}(jj') = \left(\frac{-1}{4\pi}\right)^{s + k - j} \hat{1}\hat{1}'\hat{j}\hat{j}'\hat{s}^{-2} \langle k0|11'00\rangle W(11'jj';ks)\delta_{q0}\delta_{ss'} \qquad (13)$$

In a similar way the efficiency tensor for a beam of particles with spin $\underline{s}$ referred to the beam direction as z-axis can be obtained, viz.

$$\varepsilon^{o}_{kq}(jj') = \left(\frac{-1}{4\pi}\right)^{s + k - j} \hat{1}\hat{1}'\hat{j}\hat{j}' \langle k0|11'00\rangle W(11'jj';ks)\delta_{q0}\delta_{ss'} \qquad (14)$$

Equation (14) assumes that the detector is polarisation insensitive which in terms of the efficiency tensor for the spin means

$$\varepsilon_{k_s q_s}(ss') = \hat{s}\delta_{k_s 0}\delta_{q_s 0}\delta_{ss'} \qquad (15)$$

which differs only in the normalisation factor $\hat{s}^2$ from equation (12). This difference arises because (12) is an average over spin states whilst (15) is a sum over spin states.

§A2.7 The Angular Correlation Function For a Single Transition

In the previous sections the results needed in the derivation of angular correlation expressions have been derived. To begin with, the expression for a single transition will be derived with the extension to more difficult processes being made naturally in a subsequent section.

Consider the transition in which the initial and final states can be regarded as related by the vector addition formula

$$\underline{c} = \underline{j}_3 + \underline{d} = (\underline{l}_3 + \underline{s}_3) + \underline{d} \ .$$

The correlation function is then given by (7) as

$$W = \sum \mathcal{E}^*_{k_3 q_3}(j_3 j_3') \mathcal{E}^*_{k_d q_d}(dd') \rho_{k_3 q_3}(j_3 j_3') \rho_{k_d q_d}(dd') \qquad (16)$$

where the summation extends over $k_3 q_3 k_d q_d j_3 j_3' dd' l_3 l_3' s_3 s_3'$. Using first the inverse of the decomposition formula, (5), and subsequently equation (9), the two statistical tensors can be combined to give

$$\rho_{k_3 q_3}(j_3 j_3') \rho_{k_d q_d}(dd') = \sum_{k_c q_c cc'} \rho_{k_c q_c}(cc') \langle k_c q_c | k_3 k_d q_3 q_d \rangle \times \hat{k}_d \hat{k}_3 \hat{c}\hat{c}' \begin{Bmatrix} j_3 & d & c \\ j_3' & d' & c' \\ k_3 & k_d & k_c \end{Bmatrix} \langle d \| j_3 \| c \rangle \langle d' \| j_3' \| c' \rangle^* . \qquad (17)$$

The dependence of W on the angular position of the detector of the outgoing radiation can be made explicit by means of equation (3), viz.

$$\mathcal{E}^*_{k_3 q_3}(j_3 j_3') = \sum_{q_3'} D^{k_3}_{q_3 q_3'}(R_3) \mathcal{E}^{o*}_{k_3 q_3'}(j_3 j_3') .$$

Here $R_3 \equiv R(0, -\theta_3, -\phi_3)$ is the rotation taking the detector centred coordinate system into the laboratory system and

$\varepsilon^{o}_{k_3q_3'}(j_3j_3')$ is given by equation (14). Thus

$$\varepsilon^{*}_{k_3q_3}(j_3j_3') = \frac{(-)^{s_3+k_3-j_3}}{4\pi}\hat{l}_3\hat{l}_3'\hat{j}_3\hat{j}_3'\langle k_3 0|l_3 l_3' 00\rangle\delta_{s_3s_3'}$$
$$\times W(l_3l_3'j_3j_3';k_3s_3)\ C_{k_3q_3}(\theta_3\phi_3) \qquad (18)$$

where $C_{k_3q_3}(\theta_3\phi_3)$ is a renormalised spherical harmonic (Br 62). In most cases, the recoiling nucleus is undetected and the efficiency tensor for it becomes quite straightforward, viz.

$$\varepsilon^{*}_{k_dq_d}(dd') = \hat{d}\delta_{k_d o}\delta_{q_d o}\delta_{dd'} \ . \qquad (19)$$

Combining the results (17),(18) and (19) in (16) yields

$$W(\theta_3\phi_3) = \sum \rho_{k_3q_3}(cc')\hat{c}\hat{c}'\hat{d}\hat{k}_3\hat{l}_3\hat{l}_3'\hat{j}_3\hat{j}_3'\frac{(-)^{s_3+k_3-j_3}}{4\pi}\langle k_3 0|l_3 l_3' 00\rangle$$
$$\times W(l_3l_3'j_3j_3';k_3s_3)\begin{Bmatrix} j_3 & d & c \\ j_3' & d & c' \\ k & 0 & k \end{Bmatrix}\langle d\|j_3\|c\rangle\langle d\|j_3'\|c'\rangle^{*}C_{k_3q_3}(\theta_3\phi_3)$$
$$= \sum \rho_{k_3q_3}(cc')\hat{c}\hat{c}'\hat{l}_3\hat{l}_3'\hat{j}_3\hat{j}_3'\frac{(-)^{s_3+d-c-j_3-j_3'}}{4\pi}\langle k_3 0|l_3 l_3' 00\rangle$$
$$\times W(l_3l_3'j_3j_3';k_3s_3)W(j_3j_3'cc';k_3d)\langle d\|j_3\|c\rangle\langle d\|j_3'\|c'\rangle^{*}C_{k_3q_3}(\theta_3\phi_3) \qquad (20)$$

where the summation is over $cc'dk_3q_3l_3l_3's_3j_3$ and j_3'. Further reductions result if it is assumed that the nuclei c and d are sharp, ie are states of definite angular momentum and parity. However , since the immediate concern is not with applications such assumptions are not made.

§A2.8 The Angular Correlation Function For a Cascade

Assume that the cascade proceeds from the state b through

c to d with the emission of successive radiations j_2 and j_3 as represented by the equations

$$\underline{b} = \underline{j_2} + \underline{c} \qquad \underline{c} = \underline{j_3} + \underline{d} \ .$$

Then, in analogy to the previous section, the correlation function will be

$$W = \sum \mathcal{E}^*_{k_2 q_2}(j_2 j_2')\mathcal{E}^*_{k_3 q_3}(j_3 j_3')\mathcal{E}^*_{k_d q_d}(dd')\rho_{k_2 q_2}(j_2 j_2')$$
$$\times \rho_{k_3 q_3}(j_3 j_3')\rho_{k_d q_d}(dd'). \qquad (21)$$

The statistical tensors must now be transformed back from the states d to b. A double application of the decomposition formula and the Wigner-Eckart theorem then results in

$$\rho_{k_2 q_2}(j_2 j_2')\rho_{k_3 q_3}(j_3 j_3')\rho_{k_d q_d}(dd') = \sum_{k_c k_b q_c q_b c c' b b'} \rho_{k_b q_b}(bb')$$
$$\times \langle k_b q_b | k_2 k_c q_2 q_c \rangle \hat{k}_2 \hat{k}_c \hat{b}\hat{b}' \begin{Bmatrix} j_2 & c & b \\ j_2' & c' & b' \\ k_2 & k_c & k_b \end{Bmatrix} \langle c | j_2 \| b \rangle \langle c' | j_2' \| b' \rangle^*$$
$$\times \langle k_c q_c | k_3 k_d q_3 q_d \rangle \hat{k}_3 \hat{k}_d \hat{c}\hat{c}' \begin{Bmatrix} j_3 & d & c \\ j_3' & d' & c' \\ k_3 & k_d & k_c \end{Bmatrix} \langle d | j_3 \| c \rangle \langle d' | j_3' \| c' \rangle^* . \qquad (22)$$

The expressions for the efficiency tensors $\mathcal{E}^*_{k_2 q_2}$ and $\mathcal{E}^*_{k_3 q_3}$ will be given by equation (18) with the appropriate changes being made in the former case, while $\mathcal{E}^*_{k_d q_d}$ is given by equation (19) as before. Using these expressions together with equation (22) yields for the correlation function of the cascade:

$$W(\theta_2\phi_2\theta_3\phi_3) = \sum \frac{(-)^{\sigma}}{(4\pi)} \hat{l}_2\hat{l}_2'\hat{l}_3\hat{l}_3'\hat{j}_2\hat{j}_2'\hat{j}_3\hat{j}_3'\hat{b}\hat{b}'\hat{c}\hat{c}'\hat{k}_2\hat{k}_3 \rho_{k_b q_b}(bb')$$

$$\times W(l_2 l_2' j_2 j_2'; k_2 s_2) W(l_3 l_3' j_3 j_3'; k_3 s_3) W(j_3 j_3' cc'; k_3 d) \langle k_2 0 | l_2 l_2' 00\rangle$$

$$\times \langle k_3 0 | l_3 l_3' 00\rangle \langle k_b q_b | k_2 k_3 q_2 q_3\rangle \langle c \| j_2 \| b\rangle \langle c' \| j_2' \| b'\rangle^* \langle d \| j_3 \| c\rangle$$

$$\times \langle d \| j_3' \| c'\rangle^* C_{k_2 q_2}(\theta_2\phi_2) C_{k_3 q_3}(\theta_3\phi_3) \begin{Bmatrix} j_2 & c & b \\ j_2' & c' & b' \\ k_2 & k_3 & k_b \end{Bmatrix} \qquad (23)$$

with $\sigma = s_2+s_3+k_2-j_3-j_3'-j_2+d-c$ and the summation extending over $bb'cc'dl_2l_2'l_3l_3'j_2j_2'j_3j_3'k_2k_3k_bq_2q_3q_bs_2s_3$. The angles $(\theta_2\phi_2)$ and $(\theta_3\phi_3)$ are the polar and azimuthal angles of the radiations j_2 and j_3 measured in the system centre of mass frame (scm) and recoil centre of mass frame of c (rcm) respectively. The statistical tensor describing the state b is as yet undetermined and will clearly depend on how b is formed. In the next section $\rho_{k_b q_b}$ is evaluated assuming that b is formed by a reaction.

§A2.9 The Triple Correlation Function

In the case of a reaction it is usual to work in the channel spin representation whenever the beam and target are unpolarised. In this representation the statistical tensors describing the orientation of the target and incident particle are very simple and the complexity of the problem is greatly reduced. The channel spin, s, is given by $\underline{s} = \underline{s}_1 + \underline{a}$ where $\underline{s}_1$ and $\underline{a}$ are the spins of the incident particles and target respectively. The transition is then represented by $\underline{s} + \underline{l}_1 = \underline{b}$. The tensors $\rho_{k_s q_s}(ss')$ are first determined by using the decomposition formula, viz.

$$\rho_{k_s q_s}(ss') = \delta_{k_s o}\delta_{q_s o}\delta_{ss'}\hat{s}(\hat{s}_1\hat{a})^{-2}. \tag{24}$$

The tensors $\rho_{k_{l_1} q_{l_1}}(l_1 l_1')$ representing the orbital motion of the particles are given by equations (10) and (3) as

$$\rho_{k_{l_1} q_{l_1}}(l_1 l_1') = D^{k_{l_1}*}_{o q_{l_1}}(R_1) C_{k_{l_1} o}(l_1 l_1')$$
$$= C^*_{k_{l_1} q_{l_1}}(\theta_1\phi_1)\hat{l}_1\hat{l}_1'(-)^{l_1'}\langle k_{l_1} 0 | l_1 l_1' 00\rangle \frac{}{4\pi}$$

where $R_1 = (-\phi_1, -\theta_1, 0)$ is the rotation that carries the coordinate axes from the direction of the beam to the laboratory frame. A second use of the decomposition formula together with the Wigner-Eckart theorem gives

$$\rho_{k_b q_b}(bb') = \sum \hat{s}(\hat{a}\hat{s}_1)^{-2}\hat{i}_1\hat{l}_1'\frac{(-)^{l_1'}}{4\pi}\langle k_b 0 | l_1 l_1' 00\rangle \hat{b}\hat{b}'\hat{k}_b$$

$$\times \begin{Bmatrix} s & l_1 & b \\ s & l_1' & b' \\ 0 & k_b & k_b \end{Bmatrix} \langle b \| l_1 | s\rangle \langle b' \| l_1' | s\rangle^* C^*_{k_b q_b}(\theta_1\phi_1)$$

$$= \frac{(-)^{l_1'-l_1+s+k_b-b'}}{4\pi}(\hat{a}\hat{s}_1)^{-2}\hat{l}_1\hat{l}_1'\hat{b}\hat{b}'\langle k_b 0 | l_1 l_1' 00\rangle$$

$$\times \langle b \| l_1 | s\rangle \langle b' \| l_1' | s\rangle^* C^*_{k_b q_b}(\theta_1\phi_1)\, W(b l_1 b' l_1'; s k_b) \tag{25}$$

with the summation extending over $l_1 l_1' s s_1 a$. Equations (23) and (25) now specify the desired triple correlation completely. Naturally, it is unusable in its present general form but in Chapter 5 one application is studied which allows considerable simplification.

APPENDIX 3

THE TWO NUCLEON TRANSFER PROCESS

§A3.1 Introduction

A considerable number of investigations into nuclear spectroscopy from two nucleon transfer processes have been concerned with examining the effects of a pairing force model (Yo 62, Li 66, Br 68). More recently Frahn and Sharp (Fr 69) have been able to obtain a closed expression for the differential cross section using the so called "Strong Absorption" model. However, this model has limited applicability since it demands that the nuclear interior give no significant contribution to the direct process. A more generally applicable model of two nucleon transfer processes is that originally developed by Glendenning (Gl 63, Gl 65) and more recently refined by Towner and Hardy (To 69). It provides a sensitive test of shell model wave functions within the framework of the Distorted-Wave-Born Approximation (DWBA) and will be employed in the present work. No attempt is made to present a mathematically complete formulation of the theory although most of the basic steps and all assumptions made in the development are outlined. For a more detailed discussion the reader is referred to the work of Towner and Hardy.

§A3.2 The Transition Amplitude in DWBA

The DWBA theory of direct nuclear reactions has been successfully developed in recent years by Tobocman (To 61a)

Satchler (Sa 64) and others. Three basic assumptions are made:

(1) Particle transfers occur directly between the incident and outgoing channels;

(2) The relative motion of the pair of nuclei before and after the event is described by distorted waves, which take account of elastic scattering. These distorted waves are calculated in an optical model approximation and are assumed to be correct throughout all relevant regions of configuration space;

(3) The transfer process is sufficiently weak that a perturbation treatment can be used.

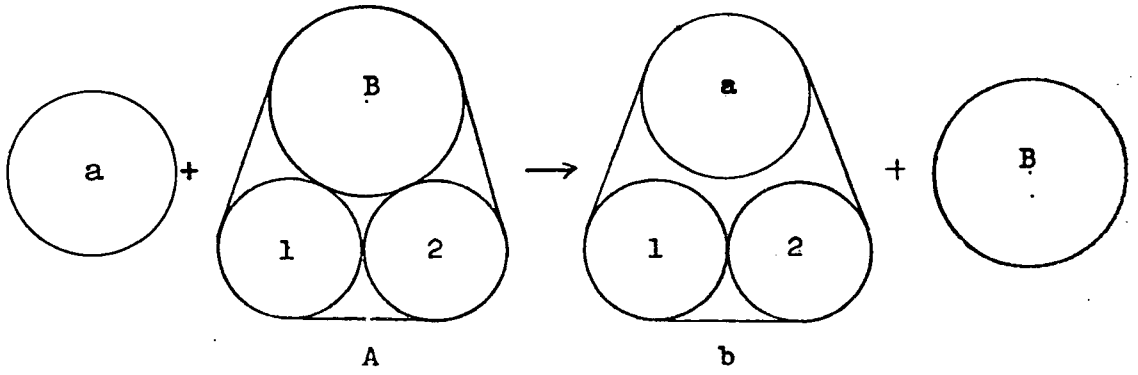

Figure A.6 Schematic Diagram of a 2-nucleon pickup process.

For the reaction A(a,b)B, illustrated as a pickup reaction in Figure A.6, these assumptions lead directly to the transition amplitude

$$T_{m_a M_A, m_b M_B}(\underline{k}_a, \underline{k}_b) = J \sum_{m'_a m'_b} \int \phi^{(-)*}_{m'_b, m_b}(\underline{k}_b, \underline{r}_{bB}) \langle \psi_{b',B} | V_{aA} - \bar{U}_{aA} | \psi_{a',A} \rangle$$

$$\times \phi^{(+)}_{m'_a, m_a}(\underline{k}_a, \underline{r}_{aA})\, d\underline{r}_{aA}\, d\underline{r}_{bB} \qquad (1)$$

where J is the Jacobian of the transformation to the relative coordinates $\underline{r}_{aA}$ and $\underline{r}_{bB}$. The wave functions $\phi^{(-)}_{m'_b,m_b}(\underline{k}_b,\underline{r}_{bB})$ and $\phi^{(+)}_{m'_a,m_a}(\underline{k}_a, \underline{r}_{aA})$ are distorted waves satisfying the equations:

$$(-\nabla^2_{aA} + \frac{2\mu_a \bar{U}_{aA}}{\hbar^2})\phi^{(+)}_{m'_a,m_a}(\underline{k}_a,\underline{r}_{aA}) = k_a^2 \phi^{(+)}_{m'_a,m_a}(\underline{k}_a,\underline{r}_{aA}) \qquad (2a)$$

$$(-\nabla^2_{bB} + \frac{2\mu_b \bar{U}_{bB}}{\hbar^2})\phi^{(-)}_{m'_b,m_b}(\underline{k}_b,\underline{r}_{bB}) = k_b^2 \phi^{(-)}_{m'_b,m_b}(\underline{k}_b,\underline{r}_{bB}) \qquad (2b)$$

where $\mu_a(\mu_b)$, $\hbar\underline{k}_a(\hbar\underline{k}_b)$ and $\bar{U}_{aA}(\bar{U}_{bB})$ are the reduced mass, the relative momentum and the optical potential describing elastic scattering in the initial (final) channel. The z-component of the spin of particle a(b) is denoted by m_a (m_b). The remaining factor in equation (1) is the matrix element of the interaction causing the inelastic event taken between the internal states of the colliding pairs. V_{aA} is the sum of all two-body interactions between each nucleon in the projectile,a, and those in the target nucleus,A. Within this matrix element is contained all the details of the actual interaction, while the dynamics of the reaction, characterised by the distorted waves, may be determined with a knowledge of only the most general properties of the matrix element itself.

Three additional assumptions are usually made in order to simplify the evaluation of the transition amplitude:

(4) All exchange terms such as knockout are unimportant;

(5) The final state,B, does not contain components corresponding to core excitations and

(6) The relative motion of each pair of nucleons in

the light particles, a and b, is a pure s-state.

Strobel and Scott (St 65) have demonstrated in a study of the reaction $^{10}B(d,p)^{11}B^*(2.14\ MeV)$ that assumption (4) has some basis. The spin of ^{10}B is 3 whilst that of $^{11}B^*(2.14\ MeV)$ is $\frac{1}{2}-$. Consequently, the transfer of a p-wave nucleon to ^{10}B is then angular momentum forbidden and the observed cross section, found to be very small, is then a measure of the exchange terms.

Levin (Le 66) has shown that whenever a core-independent transition is allowed, it will dominate over the mechanism that first excites and then de-excites the core nucleus,B. Assumption (5) would thus appear to have some validity in most circumstances.

The restriction (6) is expected to be good for projectiles with mass number less than four. Johnson and Santos (Jo 68) have carried out detailed calculations with the inclusion of a deuteron D-state in single nucleon transfer reactions. Their findings indicate that the effect is never large but does increase as the transferred angular momentum increases. In any case the inclusion of such terms in two nucleon transfer processes makes the calculation prohibitively difficult and in light of other approximations is probably not justified.

In evaluating the transition amplitude of equation (1), it is convenient to adopt the following conventions. The spins of the target and final nucleus (A and B) are written as upper case letters (J_A and J_B) and those of the light particles as lower case letters. The quantum numbers of the transferred pair are denoted by L,S,J,T. The single particle orbitals of

the transferred pair (the Shell Model is assumed throughout), which are characterised by the quantum numbers n,l, and j are written as $[nlj]$.

Carrying out the various spin integrations and making the usual partial wave expansions for the distorted waves (Sa 64) yields for the DWBA amplitude:

$$T_{m_a M_A, m_b M_B}(\underline{k}_a,\underline{k}_b) = 4\pi\binom{a+2}{2}^{\frac{1}{2}}\binom{A}{2}^{\frac{1}{2}}\sum\frac{(-)^{b+1}}{\sqrt{2}}\delta_{S+T,1}\langle J_B J M_B M | J_A M_A\rangle$$

$$x\langle T_B T N_B N | T_A N_A\rangle\langle s_a S m'_a m_s | s_b m'_b\rangle\langle t_b T n_b N | t_b n_b\rangle\langle L S m_l m_s | J M\rangle$$

$$x\langle l_a l_b \lambda'_a \lambda'_b | L - m_l\rangle\langle l_a s_a \lambda_a m_a | j_a \mu_a\rangle\langle l_a s_a\, \lambda m'_a | j_a \mu_a\rangle\langle l_b s_b \lambda_b - m_b | j_b \mu_b\rangle$$

$$x\langle l_b s_b \lambda'_b - m'_b | j_b \mu_b\rangle \begin{Bmatrix} l_1 & l_2 & L \\ \frac{1}{2} & \frac{1}{2} & S \\ j_1 & j_2 & J \end{Bmatrix} Y^*_{l_a \lambda_a}(\underline{k}_a) Y^*_{l_b \lambda_b}(\underline{k}_b) i^{l_b - l_a - L}$$

$$x\,(-)^{m_b - m'_b - m_l}\, I_{AB}(\,[n_1 l_1 j_1]\,[n_2 l_2 j_2]\,; J T) I^{l_1 l_2 L l_a j_a l_b j_b S T} \qquad (3)$$

where

$$I^{l_1 l_2 L l_a j_a l_b j_b S T} = \frac{4\pi}{k_a k_b} J \int u_{l_b j_b}(k_b, r_{bB}) F^{l_1 l_2 L l_a l_b S T}(r_{aA}, r_{bB})$$

$$x\; u_{l_a j_a}(k_a, r_{aA}) r_{aA} r_{bB} dr_{aA} dr_{bB} \qquad (4)$$

with the summation extending over $[n_1 l_1 j_1]\,[n_2 l_2 j_2] L S J T m_l m_s M N m'_a$ $m'_b \lambda_a \lambda'_a \mu_a \lambda_b \lambda'_b \mu_b$. The $u_{l_a j_a}(k_a, r_{aA})$ $\left\{u_{l_b j_b}(k_b, r_{bB})\right\}$ are the radial solutions of the Schrödinger equation for the incoming $\left\{\text{outgoing}\right\}$ channels and $F^{l_1 l_2 L l_a l_b S T}(r_{aA}, r_{bB})$ is the so called "Form Factor". The specific evaluation of these form factors is deferred to the next section.

The expansion coefficients I_{AB} represent the overlap of the target nucleus wavefunction $\psi_A(\xi_B, \underline{r}_1, \underline{r}_2)$ with the

wavefunction obtained by vector coupling the core wavefunction $\psi_B(\xi_B)$ to the wavefunction of the transferred pair, $\psi(\underline{r}_1,\underline{r}_2)$. Explicitly they are defined by :

$$I_{AB}(JT) = \int \left[\psi^{*J_B}_{M_B}(\xi_B)\psi^{*j_1 j_2 JT}_{MN}(\underline{r}_1,\underline{r}_2)\right]^{J_A T_A}_{M_A N_A} \times \psi^{J_A T_A}_{M_A N_A}(\xi_B,\underline{r}_1,\underline{r}_2)\, d\xi_B\, d\underline{r}_1\, d\underline{r}_2 \quad . \tag{5}$$

The LS-jj transformation bracket in equation (3) is related to the 9-j symbol (Br 62) by

$$\begin{bmatrix} l_1 & l_2 & L \\ \frac{1}{2} & \frac{1}{2} & S \\ j_1 & j_2 & J \end{bmatrix} = \hat{L}\hat{S}\hat{j}_1\hat{j}_2 \begin{Bmatrix} l_1 & l_2 & L \\ \frac{1}{2} & \frac{1}{2} & S \\ j_1 & j_2 & J \end{Bmatrix}$$

where $\hat{x}$ is a shorthand notation for $\sqrt{2x+1}$.

Considerable simplification of equation (3) results by making a suitable choice for the orientation of the coordinate system. Choosing the z-axis to be in the direction of $\underline{k}_a$, the y-axis along $\underline{k}_a \times \underline{k}_b$ and letting θ be the scattering angle, one obtains

$$T_{m_a M_A, m_b M_B}(\underline{k}_a,\underline{k}_b) = \sum_{MN}^{LSJT} \hat{s}_b \hat{J} \langle J_B J M_B M | J_A J\rangle \langle T_B T N_B N | T_A N_A\rangle \times B^{LSJT}_{m_a m_b MN}(\underline{k}_a,\underline{k}_b) \quad . \tag{6}$$

The reduced amplitude $B^{LSJT}_{m_a m_b MN}(\underline{k}_a,\underline{k}_b)$ is defined by

$$B^{LSJT}_{m_a m_b MN}(\underline{k}_a,\underline{k}_b) = i^{l_b - l_a - L}(-)^{m_a - s_a + L - J + S} \hat{l}_a \hat{J}^{-1} \sqrt{4\pi}\, Y_{l_b\, b}(\theta,0) \times S^{\frac{1}{2}}_{AB}(\left[n_1 l_1 j_1\right]\left[n_2 l_2 j_2\right]; JT) \langle l_a s_a 0 m_a | j_a m_a\rangle \langle l_b s_b \lambda_b - m_b | j_b \lambda_b - m_b\rangle\, b_{ST} \times \langle j_a j_b m_a \lambda_b - m_b | J - M\rangle \begin{bmatrix} l_1 & l_2 & L \\ \frac{1}{2} & \frac{1}{2} & S \\ j_1 & j_2 & J \end{bmatrix} \begin{bmatrix} l_a & l_b & L \\ s_a & s_b & S \\ j_a & j_b & J \end{bmatrix} I^{l_1 l_2 L l_a j_a l_b j_b ST} \tag{7}$$

where $\lambda_b = m_b - m_a - M$ and the summation is over $[n_1 l_1 j_1]\,[n_2 l_2 j_2]\, l_a l_b j_a j_b$. The "spectroscopic amplitude" $S^{\frac{1}{2}}_{AB}$ is analogous to that used in single particle stripping theory (Fr 60), viz.

$$S^{\frac{1}{2}}_{AB}([n_1 l_1 j_1]\,[n_2 l_2 j_2];JT) = \binom{A}{2}^{\frac{1}{2}} I_{AB}([n_1 l_1 j_1]\,[n_2 l_2 j_2];JT) \quad (8)$$

whilst

$$b_{ST} = (-)^{b+1}\binom{a+2}{2}^{\frac{1}{2}}(\sqrt{2}\hat{s})^{-1}\langle t_a T n_a N \,|\, t_b n_b\rangle \delta_{S+T,1} \quad (9)$$

is evidently a spectroscopic amplitude for the light particles. For the particular case of a (d,α) reaction it has the value $-\delta_{S,1}\delta_{T0}$ giving rise to the selection rules $S = 1$, $T = 0$.

§A3.3 Form Factors

In the previous section the form factors $F^{l_1 l_2 L l_a l_b S T}(r_{aA}, r_{bB})$ were introduced. It is in the evaluation of these quantities that the various DWBA treatments of 2-nucleon transfer processes differ. Most treatments, because of the complexity of the problem, approximate the interaction potential by a δ-function. Finite range corrections may be applied subsequently.

If one follows the procedure suggested by Glendenning (Gl 65) and first implemented by Drisko and Rybicki (Dr 66), the transferred particles are described by Saxon-Wood single particle functions having different radial arguments:

$$\phi^{[n_i l_i j_i]}_{\lambda_i}(r_i) = \frac{1}{r_i} u_{n_i l_i j_i}(r_i) i^{l_i} Y_{l_i \lambda_i}(\theta_i, \phi_i). \quad (10)$$

These radial functions are then expanded in terms of oscillator wavefunctions

$$\frac{u_{n_i l_i j_i}(r_i)}{r_i} = \sum_{p_i} a_{p_i} R_{p_i l_i}(\nu r_i^2) \qquad (11)$$

where ν is the oscillator parameter and the oscillator radial function is defined as

$$R_{pl}(\nu r^2) = \left[\frac{2(p-1)!\,\nu^{\frac{3}{2}}}{\Gamma(p+l+\frac{1}{2})}\right]^{\frac{1}{2}} (\nu r^2)^{\frac{1}{2}}\ e^{-\nu r^2/2} L_{p-1}^{l+\frac{1}{2}}(\nu r^2) \qquad (12)$$

with

$$L_{p-1}^{l+\frac{1}{2}}(\nu r^2) = \sum_{k=0}^{p-1} \binom{p+l-\frac{1}{2}}{p-k-1} \frac{(-\nu r^2)^k}{k!}\ ; \qquad \nu = m\omega/\hbar. \qquad (13)$$

The product of the two functions u_1 and u_2 can then be separated by a Moshinsky Transformation (Br 67) into components describing the relative (r_{12}) and centre of mass motions (r_{bB}).

$$\phi_{\lambda_1}^{[n_1 l_1 j_1]}(r_1)\phi_{\lambda_2}^{[n_2 l_2 j_2]}(r_2) = \sum_{p_1 p_2} a_{p_1} a_{p_2} \sum_{nN} \langle p_1 l_1, p_2 l_2; L | n0, NL; L\rangle$$

$$\times\ R_{no}(\tfrac{1}{2}\nu r_{12}^2) R_{NL}(2\nu r_{bB}^2) Y_{L\Lambda}(\theta,\phi) i^{l_1+l_2-L}/(4\pi)^{\frac{1}{2}} \qquad (14)$$

where n and N are the principal quantum numbers of the relative and centre of mass motions respectively and can take on all values such that

$$n + N = p_1 + p_2 + \tfrac{1}{2}(l_1 + l_2 - L). \qquad (15)$$

The appearance of a zero coefficient in the Moshinsky bracket is a consequence of the earlier assumption of pure relative s-states for the light particles.

The foregoing treatment of the transferred particle wavefunctions is expected to be more exact than the earlier Glendenning theory (Gl 62) and that of Rook and Mitra (Ro 64).

In the Glendenning theory the two particles were described by pure oscillator functions of different radial arguments. While correctly describing the bound state wavefunction in the nuclear interior, the theory suffers from the disadvantage that the asymptotic form of the bound state wavefunction does not reflect the correct binding energy of the transferred nucleons. On the other hand, in the Rook-Mitra theory, the particles are described by Saxon-Wood wavefunctions of the same radial argument. This implies that the relative motion of the two particles is ignored. Clearly, neither of the earlier theories is expected to give as good a bound state wavefunction as that described by equation (14).

If a Gaussian form is chosen for the interaction potentials and for the wavefunction of the nucleide, b, viz;

$$V_{jk}(r_{jk}) \propto \exp(-\beta^2 r_{jk})$$

and

$$\phi_o^{l_b=o}(\xi_b) \propto \exp(-\eta^2 \sum_{jk} r_{jk}^2)$$

with β^{-1} being the range of the potential and η a size parameter for the wavefunction, then application of the zero range approximation enables the integrations, implicit in the form factors, to be carried out. The final result is given by Towner and Hardy (To 69) and Nelson (Ne 69) as

$$F^{l_1 l_2 L l_a l_b}(r_{aA}, r_{bB}) = J^{-1} \left(\frac{A}{B r_{bB}}\right)^2 \hat{l}_a \hat{l}_b \frac{1}{(4\pi)^{\frac{3}{2}} \hat{L}} \langle l_a l_b 00 | L0 \rangle$$

$$\times \delta(r_{aA} - B/A r_{bB})\, F_o^{l_1 l_2 L}(r_{bB}) \qquad (16)$$

with

$$F_o^{l_1 l_2 L}(r_{bB}) = i^{l_1+l_2-L}\, g\, C_o \sum_{p_1 p_2} a_{p_1} a_{p_2}$$

$$\times \sum_{Nn} \Omega_n \langle p_1 l_1, p_2 l_2; L | n0, NL; L\rangle\, R_{NL}(2\nu r_{bB}^2) \quad . \qquad (17)$$

The factor g has the values

$$g = 1 \quad \text{if} \quad n_1 l_1 j_1 \equiv n_2 l_2 j_2$$
$$= \sqrt{2} \ \text{otherwise}$$

and Ω_n, which is the overlap of the relative motion wavefunction of the transferred nucleons on the Gaussian wavefunction of the heavy particle, is given by

$$\Omega_n = \frac{\left[(2n-1)!\right]^{\frac{1}{2}}}{2^{n-1}(n-1)!}\,(xy)^{\frac{3}{2}}\,(1-x)^{n-1} \qquad (18)$$

with $x = 2\nu/(2b\eta^2 + \nu + \beta^2)$, $y = \eta(2b/\nu)^{\frac{1}{2}}$.

This expression differs from that defined by Glendenning in that it takes into account the range of the interaction potential, through the factor β^2, before the zero range approximation is made (Ch 70). The overall effect is to reduce the magnitude of the cross section by an order of magnitude for normal values of the interaction range. In this manner, some account of finite range effects is made. Other more detailed calculations of finite range effects have been made by Chant and Mangelson (Ch 70) and others (Be 66, Sm 67).

The remaining factor, C_o, in equation (17), is a measure of the strength of the interaction between the picked up particles and the incident projectile. Attempts have been made to evaluate C_o (Gl 66) but it is more convenient to regard it

as a simple scaling factor for normalising experiment with theory.

§A3.4 Non-Local Corrections

The wavefunctions used in distorted wave calculations should be the eigenfunctions of non-local potentials. Since local potentials are used it is necessary to make appropriate corrections. The standard method is to adopt the local-energy approximation of Perey and Saxon (Pe 64). Briefly this amounts to multiplying the local wavefunctions by a damping factor

$$F(r) = C\left(1 - \frac{\mu\beta^2}{2\hbar^2}V(r)\right)^{\frac{1}{2}} \qquad (19)$$

where $V(r)$ is the nuclear part of the real central potential, μ is the particle reduced mass and β is the range of the non-locality. The constant C is unity unless the correction is applied to the bound state wavefunctions in which case it is chosen to give a correctly normalised non-local wavefunction. Typical values used for β are 0.85 for nucleons, 0.54 for deuterons and 0.22 for ^{4}He.

§A3.5 The Statistical Tensor for the Residual Nucleus

As the next step in the problem of deriving an expression for the double differential cross section for the sequential process A(a,b)B$\rightarrow$c + C it is necessary to relate the statistical tensor of the residual nucleus,B, to the reduced amplitudes of §A3.2.

To begin with the density matrix for the final state

(b + B) can be written

$$\rho_f = H\rho_i H^\dagger$$

where H is the interaction responsible for the transition A(a,b)B and ρ_i is the density matrix describing the initial system (a + A). Invoking completeness arguments, one obtains

$$\rho_f = \sum |s_b J_B m_b M_B\rangle\langle s_b J_B m_b M_B|H|s_a J_A m_a M_A\rangle$$

$$\times\langle s_a J_A m_a M_A|\rho_i|s_a J_A m'_a M'_A\rangle\langle s_a J_A m'_a M'_A|H^\dagger|s_b J_B m'_b M'_B\rangle\langle s_b J_B m'_b M'_B|$$

$$= \sum |s_b J_B m_b M_B\rangle T_{m_a M_A, m_b M_B}\langle s_a J_A m_a M_A|\rho_i|s_a J_A m'_a M'_A\rangle$$

$$\times T^*_{m'_a M'_A, m'_b M'_B}\langle s_b J_B m'_b M'_B|$$

where the summation is over $M_B M'_B M_A M'_A m_a m'_a m_b m'_b$. Since both a and A are unpolarised

$$\langle s_a J_A m_a M_A|\rho_i|s_a J_A m'_a M'_A\rangle = (\hat{J}_A \hat{s}_a)^{-2}\delta_{m_a m'_a}\delta_{M_A M'_A} .$$

Thus

$$\rho_f = \sum_{M_A M_B M'_B}^{m_a m_b m'_b} (\hat{J}_A \hat{s}_a)^{-2} T_{m_a M_A, m_b M_B} T^*_{m_a M_A, m'_b M'_B} |s_b J_B m_b M_B\rangle\langle s_b J_B m'_b M'_B| .$$

Taking matrix elements of ρ_f between states $\langle s_b J_B m_b M_B|$ and $|s_b J_B m_b M'_B\rangle$ yields

$$\langle s_b J_B m_b M_B|\rho_f|s_b J_B m_b M'_B\rangle = \sum_{M_A m_a} T_{m_a M_A, m_b M_B} T^*_{m_a M_A, m_b M'_B} (\hat{J}_A \hat{s}_a)^{-2}$$

ie. $\langle s_b m_b|\rho_f(s_b)|s_b m_b\rangle\langle J_B M_B|\rho_f(J_B)|J_B M'_B\rangle$

$$= \sum_{M_A m_a} (\hat{J}_A \hat{s}_a)^{-2} T_{m_a M_A, m_b M_B} T^*_{m_a M_A, m_b M'_B} .$$

Summing over m_b and noting that $\mathrm{tr}(\rho) = 1$ gives

$$\langle J_B M_B | \rho_f(J_B) | J_B M_B' \rangle = (\hat{J}_A \hat{s}_a)^{-2} \sum_{M_A m_a m_b} T_{m_a M_A, m_b M_B} T^*_{m_a M_A, m_b M_B'} \quad (20)$$

In terms of the reduced amplitudes of equation (7),

$$\langle J_B M_B | \rho_f(J_B) | J_B M_B' \rangle = \left(\frac{\hat{s}_b}{\hat{J}_A \hat{s}_a}\right)^2 \sum_{M_A M M' m_b m_a}^{LL'JJ'} \hat{J}\hat{J}' \langle J_B J M_B M | J_A M_A \rangle \times \langle J_B J' M_B' M' | J_A M_A \rangle B^{LJ}_{m_a m_b M} B^{L'J'*}_{m_a m_b M'} \quad (21)$$

where the dependence of the reduced amplitudes on S and T has been dropped in view of the spin-isospin selection rule which applies in the case of (d,α) reactions. Finally from the definition of the statistical tensor (see Appendix 2) one obtains

$$\rho_{kq}(J_B) = \left(\frac{\hat{s}_b}{\hat{J}_A \hat{s}_a}\right)^2 \sum (-)^{J_B - M_B'} \hat{J}\hat{J}' \langle kq | J_B J_B M_B - M_B' \rangle \times \langle J_B J M_B M | J_A M_A \rangle \langle J_B J' M_B' M' | J_A M_A \rangle B^{LJ}_{m_a m_b M} B^{L'J'*}_{m_a m_b M'} \quad (22)$$

with the summation extending over $LL'JJ'MM'M_A M_B M_B' m_a m_b$. The reduction of equation (22) to a more usable form is straightforward but time consuming. A great deal of Racah algebra yields

$$\rho_{kq}(J_B) = \left(\frac{\hat{s}_b}{\hat{s}_a}\right)^2 \sum^{LL'JJ'} \hat{J}', \hat{J}\, W(JJ' J_B J_B; k J_A)\, (-)^{J_A - J_B - J} \times \tilde{\rho}_{kq}(L'J', LJ) \quad (23)$$

where

$$\tilde{\rho}_{kq}(L'J', LJ) = \sum_{m_a m_b M M'} \langle kq | J' J M' - M \rangle (-)^{J-M} B^{LJ}_{m_a m_b M} B^{L'J'*}_{m_a m_b M'}. \quad (24)$$

§A3.6 The Angular Correlation

For the sequential reaction A(a,b)B$\rightarrow$c + C the angular correlation function for detecting c and b in coincidence,

measured in the recoil frame of reference of B, is given by (see Appendix 2, equation (20))

$$W(\theta_b\phi_b\theta_c\phi_c) = \sum_{ll'jj'kq} (-)^{J_C-J_B+s_c-2}\hat{j}\hat{j}'\hat{J}_B^2\langle k0|ll'00\rangle W(ll'jj';ks_c)$$

$$\times W(J_BJ_Bjj';kJ_C)\langle J_C|j\|J_B\rangle\langle J_C|j'\|J_B\rangle^* \rho_{kq}(J_B)\, C_{kq}(\theta_c\phi_c) \qquad (25)$$

where $W(abcd;ef)$ is a Racah coefficient, $C_{kq}(\theta\phi)$ is a renormalised spherical harmonic, and $\langle J_C|j\|J_B\rangle$ is a reduced matrix element. The angles θ_b and ϕ_b define the direction of emission of the radiation b in the system centre of mass, the dependence of the correlation on these angles appearing through the statistical tensor $\rho_{kq}(J_B)$. The nuclei B,C and c have been assumed to be states of definite spin and parity. The summation over l,l',j and j' takes on all values allowed by the angular momentum selection rules

$$|J_B - J_C| \leq j(j') \leq |J_B + J_C|$$

and

$$|j - s_c| \leq l(l') \leq |j + s_c| .$$

If in addition, the initial reaction A(a,b)B proceeds via 2-nucleon transfer then $\rho_{kq}(J_B)$ is given by equations (23) and (24) and the angular correlation function is uniquely determined.

§A3.7 Time Reversal

The DWBA code used to calculate the reduced amplitudes was obtained from Dr. J.M. Nelson at the University of Manitoba (Ne 69). Unfortunately, the program suffers from the disadvantage that it calculates the reduced amplitudes for the stripping

process and not those for the pickup process. To obtain the correct amplitudes for the latter process one can invoke time reversal principles.

Under normal conditions, the wavefunctions transform under time reversal invariance according to

$$K_t \psi^J_M = (-)^{J-M} \psi^J_{-M}. \tag{26}$$

Applied to the definition of the transition amplitude given by equation (1), one soon obtains

$$T_{m_a M_A, m_b M_B}(\underline{k}_a, \underline{k}_b) = (-)^{\sigma} T_{-m_b -M_B, -m_a -M_A}(-\underline{k}_b, -\underline{k}_a) \tag{27}$$

with $\sigma = J_B - M_B - J_A + M_A + s_b - m_b + s_a - m_a$ which relates the transition amplitude for the pickup process, A(a,b)B, $\underline{k}_a \rightarrow \underline{k}_b$, to that for the stripping reaction B(b,a)A, $-\underline{k}_b \rightarrow -\underline{k}_a$, with reversed spins but with the same quantization axes used to define the z-components in both amplitudes. In terms of the reduced amplitudes, equation (27) yields

$$\hat{s}_b \hat{J}_A B^{LJ}_{m_a m_b M}(\underline{k}_a, \underline{k}_b) = (-)^{\sigma + J - M_A + M_B} \hat{s}_a \hat{J}_B B^{LJ}_{-m_b -m_a M}(-\underline{k}_b, -\underline{k}_a) \tag{28}$$

which in turn implies that the statistical tensor describing the orientation of the residual nucleus, B, is given by

$$\rho_{kq}(J_B) = \left(\frac{\hat{J}_B}{\hat{J}_A}\right)^2 \sum_{LL'JJ'} \hat{J}\hat{J}' W(JJ' J_B J_B; k J_A) (-)^{J_A - J_B - J'} \tilde{\rho}_{kq}(L'J', LJ) \tag{29}$$

with

$$\tilde{\rho}_{kq}(L'J', LJ) = \sum_{m_a m_b M M'} \langle kq | J'JM' - M \rangle (-)^{J-M} B^{LJ}_{m_b m_a M}(-\underline{k}_b, -\underline{k}_a) \times B^{L'J'*}_{m_b m_a M'}(-\underline{k}_b, -\underline{k}_a) . \tag{30}$$

The $\rho_{kq}(J_B)$ of equation (29) are of course defined with respect to the same coordinate axes used to define the reduced amplitudes for the stripping process, viz; z-axis in the direction of $-\underline{k}_b$ and the y-axis in the direction of $\underline{k}_b \times \underline{k}_a$. To obtain the ρ_{kq} with respect to a more meaningful coordinate system one can take advantage of their rotational properties. In particular, the most commonly used coordinate system is the one with the z-axis defined by the direction of $\underline{k}_a$ and the y-axis in the direction of $\underline{k}_a \times \underline{k}_b$. Denoting this system by primed quantities, the statistical tensors are given by (see equation (3), Appendix 2)

$$\rho'_{kq'}(J_B) = \sum_q D^{k*}_{qq'}(R)\, \rho_{kq}(J_B) \qquad (31)$$

where $R \equiv (\pi, \pi-\theta_b, 0)$ is the rotation carrying the original coordinate system into the primed system. Here, θ_b is the system centre of mass scattering angle defined with respect to the incident beam direction.

The required angular correlation function is now given by equations (25), (29), (30) and (31). Nelson's DWBA code was modified to calculate the angular correlation function for the particular case of the $^7Li(d,\alpha)^5He \rightarrow n + \alpha$ reaction. The results are given in the next section.

§A3.8 Application to the reaction $^7Li(d,\alpha)^5He \rightarrow n + \alpha$

§A3.81 Selection Rules and Spectroscopic Amplitudes

Earlier, in §A3.2, mention was made of selection rules for the quantum numbers S,T of the transferred pair. In

particular in a (d,α) reaction the spin and isospin quantum numbers are restricted to but one value each, namely S=1, T=0. Other general rules for J and L also apply:

$$\underline{J}=\underline{j}_1 + \underline{j}_2 \ , \ \underline{L}=\underline{l}_1 + \underline{l}_2 ,$$

$$\underline{J}_A - \underline{J}_B = \underline{J} = \underline{L} + \underline{S} \ ,$$

$$\pi_{A\,B} = (-1)^{l_1 + l_2} = (-1)^{L} .$$

Whenever the two transferred nucleons originate from the same shell, the additional rule J + L + S = even also applies (Gl 63). Since S = 1 and L must be even in order to satisfy parity considerations, this rule implies that J be restricted to odd values.

If one adopts the extreme j - j coupling scheme, ^{7}Li(^{5}He) can be regarded as three (one) $p^{\frac{3}{2}}$ nucleons orbiting around an alpha particle core. The transferred pair will then both originate from the same shell and the above selection rules apply giving

$$S = 1 \quad T = 0 \quad J = 1 \quad L = 0,2 \qquad (32)$$
$$J = 3 \quad L = 2 .$$

Writing the ^{7}Li wavefunction as $|j^3(J_A T_A)\rangle$, an expansion into products of two particle wavefunctions and "core" wavefunctions can be obtained:

$$|j^3(J_A T_A)\rangle = \sum_{J_B' T_B' J' T'} \langle j(J_B' T_B') \ ; \ j^2(J' T') \,|\}\, j^3(J_A T_A)\rangle \, |J_B' T_B' \times J' T'\rangle$$

where $\langle|\}\rangle$ is a coefficient of fractional parentage. For two particle transfers in the 1 - p shell they have been tabulated

by Towner and Hardy (To 69). The overlap integral or spectroscopic amplitude is then given by equations (5) and (8) as

$$S_{AB}^{\frac{1}{2}}(\left[n_1 l_1 j_1\right]\left[n_2 l_2 j_2\right];JT) = \binom{3}{2}^{\frac{1}{2}} \langle j(J_B T_B); j^2(JT) \} j^3(J_A T_A)\rangle \ .$$

In view of the selection rules (32) one obtains the relevant spectroscopic amplitudes as

$$S_{AB}^{\frac{1}{2}}(10) = 0.67 \ , S_{AB}^{\frac{1}{2}}(30) = 1.02 \ .$$

These values for the spectroscopic amplitudes are expected to serve only as guides to the true values in view of the assumption of a pure j - j coupling scheme.

SA3.82 Reduction of the Angular Correlation

Since the alpha-particle has zero spin, the angular correlation of equation (25) becomes particularly simple when applied to the present case, viz

$$W(\theta_b,\phi_b,\theta_c,\phi_c) = \frac{-3}{\pi} \sum_{kq} |\langle 0 \| \tfrac{3}{2} \| \tfrac{3}{2} \rangle|^2 \langle k0|1100\rangle W(11\tfrac{3}{2}\tfrac{3}{2};k\tfrac{1}{2}) \rho_{kq}(J_B) C_{kq}(\theta_c,\phi_c)$$

where the Clebsch-Gordon coefficient ensures that the sum over k is restricted to even values. Evaluating the various angular momentum coupling coefficients and regarding the square of the reduced matrix element as a constant of proportionality one obtains

$$W(\theta_b,\phi_b,\theta_c,\phi_c) \propto \left[\rho_{oo}(J_B) - \sum_q \rho_{2q}(J_B) C_{2q}(\theta_c,\phi_c)\right]. \qquad (33)$$

§A3.83 Optical Model Potentials

The distorted waves , $u_{lj}(r)$, which appear in the expression for the reduced amplitude are generated from optical model potentials defined by

$$V = V_c(r_c) - Vf(r_o,a_o) - iWf(r_w,a_w) + 4iW_d\frac{df}{dr}(r_{wd},a_{wd}) + \left(\frac{\hbar}{m_\pi c}\right)^2 V_{so}\frac{1}{r}\frac{df}{dr}(r_{so},a_{so})\,\underline{l}\cdot\underline{\sigma} \qquad (34)$$

where $f(r_i,a_i) = \left[1 + \exp(r-r_iA^{\frac{1}{3}}/a_i)\right]^{-1}$ and

V_c is the Coulomb potential due to a uniformly charged sphere of radius $r_cA^{\frac{1}{3}}$, V is the real central potential strength, W is the volume absorption strength, W_d is the surface absorption strength and V_{so} is the spin-orbit potential strength.

The normal procedure is to use those parameters which give the best fit to known elastic scattering and polarisation data at the appropriate energies. For the d + ^{7}Li channel there is a dearth of elastic scattering data available and what little there is (Fo 64) can be equally well fitted with widely different potentials. An examination of the literature reveals several attempts to find optical model parameters for deuterons incident on 1p-shell nuclei. Table A3 lists several parameter sets which were used to generate distorted waves.

The situation for the alpha-^{5}He channel is even worse because ^{5}He is unstable and obviously no scattering data exists. An appropriate potential might be one that reflects some of the characteristics of both alpha-alpha scattering and alpha-neutron scattering. Darriulat et al (Da 65) have been able to describe alpha-alpha elastic scattering above 40 MeV using a shallow

Table A3

Optical Model Parameters used in the DWBA Calculation

	D + ^{7}Li							α + ^{5}He	B.S.
Set	D1	D2	D3	D4	D5	D6	D7	-	-
Ref.	Fi 67	Fi 67	Me 70	Me 70	Me 70	Me 70	Fo 71	-	-
V	78.0	118.0	128.0	120.0	106.4	100.7	86.3	50.0	65.0*
r_o	.967	.869	.920	1.44	1.06	1.6	1.105	1.75	1.2
a_o	1.04	1.01	.83	.76	.82	.68	.938	.9	.9
W	10.0	-	-	-	-	-	-	5.0	-
r_w	1.07	-	-	-	-	-	-	1.75	-
a_w	.87	-	-	-	-	-	-	.9	-
W_d	-	6.87	3.9	9.6	4.2	22.2	9.9	-	-
r_{wd}	-	1.68	1.23	1.56	1.24	1.9	1.608	-	-
a_{wd}	-	.879	1.05	.69	1.06	.28	.598	-	-
V_{so}	6.05	6.0	5.0	5.0	5.0	5.0	5.0	-	10.0
r_{so}	.967	.869	1.07	1.30	.954	1.44	1.105	-	1.2
a_{so}	.964	1.01	.83	.76	.82	.68	.938	-	.9
r_c	1.3	1.3	1.3	1.3	1.3	1.3	1.3	1.3	1.3
β_{nl}	.54	.54	.54	.54	.54	.54	.54	.22	.85

* Adjusted by computer program to give correct asymptotic form.

attractive real potential plus a short range repulsive core. On the other hand nucleon-alpha scattering is typified by a real attractive potential of strength about 50 MeV. Potentials of both types were used to generate distorted waves. The parameters for the conventional well are shown in Table A3 while the repulsive core, when used, was taken to be of Saxon-Wood shape characterised by the parameters

$$V_{co} = 180 \ , \ r_{co} = 0.93 \quad \text{and} \quad a_{co} = 0.1 \ .$$

The bound state potential for each transferred particle was taken to be real and was defined by

$$V_{bs} = V_c(r_c) - Vf(r_o,a_o) + \left(\frac{\hbar}{m_\pi c}\right)^2 V_{so} \frac{1}{r} \frac{df}{dr}(r_{so},a_{so}) \ \underline{l}.\underline{\sigma}. \qquad (35)$$

The parameters r_o, a_o, r_{so}, a_{so} and V_{so} were input parameters (see Table A3) but V, the strength of the real central well, was adjusted by the computer program to obtain the correct asymptotic form for the bound state wavefunction. Other input parameters required in the calculation of the bound state wavefunction were:

(1) The oscillator parameter used in expansion (11). For 1p-shell nuclei an appropriate value is $\nu = 0.32$ (Tr 63);

(2) The size parameter for the alpha particle. The usual value used is $\eta = 0.233$ fm^{-1} (Gl 65);

(3) The interaction range parameter, $\beta = 1.62$ fm^{-1} (To 69).

§A3.84 Theoretical Results

Preliminary calculations indicated that for a given set of optical model parameters, the contribution from the J = 3

transfer predominated over the J = 1 transfer by more than an order of magnitude. Accordingly, only the results for J = 3 will be discussed further. The theoretical angular correlations obtained using the optical model parameters of Table A3 are shown in Figure A7 when the first emitted alpha particle comes off at 106.2° in the system centre of mass frame (s.c.m.). The labels D1, D2 etc. refer to the deuteron potential labels of Table A3. The curve labelled D1-RC represents the results for the case when a repulsive core is included in the alpha-^{5}He potential.

It is apparent that the shape of the correlation is largely independent of the choice of deuteron parameters used. On the other hand, the magnitude of the correlation is dependent on this choice. This is a reflection on the widely different strengths employed for the absorptive potential. However, a prediction of the absolute magnitude for the process is of secondary importance. Accordingly, this point will not be discussed further.

A comparison of Figure A7 and Figure 5.5 reveals that the predicted correlations are quite the wrong shape, having a maximum rather than a minimum near the s.c.m. recoil direction. Attempts to achieve the correct shape for the correlation by varying the optical model parameters for the transferred particles and for the alpha-^{5}He channel proved negative. While the choice of optical model parameters, used to generate the distorted waves, may be questionable, particularly in the alpha-^{5}He channel, it does seem unlikely that the DWBA calculation can reproduce

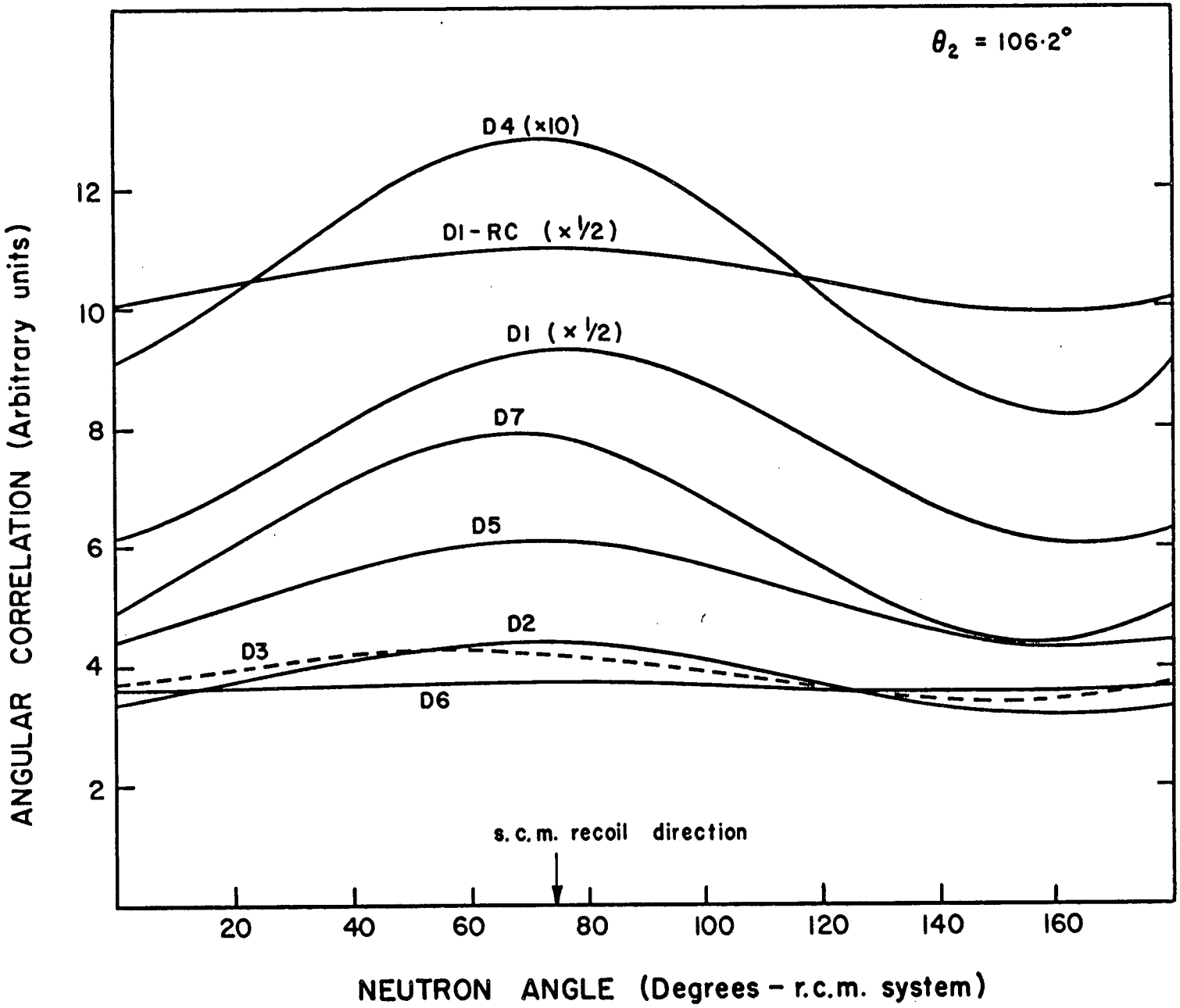

Fig A7 DWBA predictions for the Angular Correlation Function.

the correct shape for the angular correlation. This failure may be attributable to the non-validity of one or more of the earlier assumptions (§A3.2). Certainly, the basic assumptions underlying DWBA tend to breakdown for transfer reactions on light nuclei (Ma 69). On the other hand, at an energy of 1.0 MeV, the reaction would be expected to proceed predominantly through the compound nucleus, $^{9}Be^{*}$. That this is indeed the case, is supported by the arguments of Chapter 5. It is perhaps then not surprising that the DWBA calculations cannot fit the experimental results.

BIBLIOGRAPHY

Ai 65 I.J.R. Aitchison and C. Kacser, Revs. Mod. Phys. 37 (1965) 350

As 65 P.A. Assimakopoulos, N.H. Gangas and S. Kossionides, Phys. Lett. 19 (1965) 316

As 66 P.A. Assimakopoulos, N.H. Gangas and S. Kossionides, Nucl. Phys. 81 (1966) 305

Ba 52 L.M. Baggett and S.J. Bame, Phys. Lett. 85 (1952) 316

Ba 54 S. Baskkin, Phys. Lett. 95 (1954) 1012

Ba 61 R. Batchelor, W.B. Gilboy, J.B. Parker and J.H. Tonle Nucl. Inst. Meth. 13 (1961) 70

Ba 65 A.D. Bacher and T.A. Tombrello, Revs. Mod. Phys. 37 (1965) 433

Be 66 G.Y. Bencze and J. Zimanyi, Nucl. Phys. 81 (1966)76

Be 71 J.L. Beveridge and R.R. Johnson, Can. J. Phys. 49 (1971) 1374

Bi 53 L.C. Biedenharn and M.E. Rose, Revs. Mod. Phys. 25 (1953) 729

Bl 52 J.M. Blatt and V.F. Weiskoff, "Theoretical Nuclear Physics" Published by Wiley and Sons (1952)

Bl 68 E.W. Blackmore and J.B. Warren, Can. J. Phys. 46 (1968) 233

Br 62 D.M. Brink and G.R. Satchler, "Angular Momentum" Published by Clarendon Press,Oxford, 1962

Br 65 J.D. Bronson, W.D. Simpson, W.R. Jackson and G.C. Phillips, Nucl. Phys. 68 (1965) 241

Br 67 T.A. Brody and M. Moshinsky, "Tables of Transformation Brackets" 2nd edition published by Gordon and Breach (1967)

Br 68 R.A. Broglia, C. Riedel, B. Sorenson and T. Udagawa, Nucl. Phys. A115 (1968) 273

Ch 70 N.S. Chant, N.F. Mangelson, Nucl. Phys A140 (1970) 81

Da 65 P. Darriulat, G. Igo, H.G. Pugh and H.D. Holmgren, Phys. Rev. 137B (1965) 315

De 60 A. Dearnaley, Rev. Sc, Inst. 31 (1960) 197

Dr 66 R.M. Drisko and F. Rybicki, Phys. Rev. Lett. 16 (1966) 197

Fa 57 F.J.M. Farley and R.E. White, Nucl. Phys. 3 (1957) 561

Fa 59 U. Fano and A. Racah, "Irreducible Tensorial Sets" published by Academic Press (1959)

Fe 64 P. Fessenden and D.R. Maxson, Phys. Rev. 133B (1964) 71

Fe 65 A.J. Ferguson, "Angular Correlation Methods in Gamma-ray Spectroscopy" published by Academic Press (1965)

Fi 67 W. Fitz, R. Jahr and S. Santo, Nucl. Phys. A101 (1967) 449

Fo 64 J.L.C. Ford, Phys. Rev. 136B (1964) 956

Fo 71 H.T. Fortune, R. Middleton and J.D. Garret, Phys. Rev. 3C (1971) 1441

Fr 51 A.P. French and P.B. Treacy, Proc. Phys. Soc. (London) A64 (1951) 452

Fr 60 J.B. French, "Nuclear Spectroscopy" ed. by F. Ajzenberg-Selove and published by Academic Press, 1960. Part B p. 890

Fr 69 W.E. Frahn and M.A. Sharp, Nucl. Phys. A133 (1969) 543

Gl 63 N.K. Glendenning, Annual Rev. of Nucl. Sc. 13 (1963) 191

Gl 65 N.K. Glendenning Phys. Rev. 137B (1965) 102

Gl 66 R.N. Glover, A.D.W. Jones and J.R. Rook, Nucl.Phys. 81 (1966) 289

Go 59 L.J.B. Goldfarb, "Nuclear Reactions" ed. by P.M. Endt and M.Demeur and published by North Holland, 1959. Page 159

Go 60 L.J.B. Goldfarb and R.C. Johnson, Nucl. Phys. 18 (1960) 353

Gr 67 T.B. Grandy, Ph.D Thesis (1967) Univ. of Alberta

Gr 69 H. Grassler and R. Honecker, Nucl. Phys. A136 (1969) 446

Gu 71 H.M. Gutbrod, H. Yoshida and R. Bock, Nucl. Phys A165 (1971) 240

He 69 E.M. Henley, "Isospin in Nuclear Reactions" ed. by D.H. Wilkinson and published by North Holland,1969. Vol 15

Ho 69 G. Hofmann and D. Komke, Zeit. Phys. 224 (1969) 446

Jo 65 C.M. Jones, J.K. Blair, C.H. Johnson, H.B. Willard and M. Reeves, Revs. Mod. Phys. 37 (1965) 437

Jo 68 R.C. Johnson and F.D. Santos, "Proc. Int. Conf. on Nuclear Structure" Suppl. to J. Phys. Soc. (Japan) 24 (1968) 283

La 66 T.Lauritsen and F. Ajzenberg-Selove, Nucl. Phys. 78 (1966) 1

Le 66 F.S. Levin, Phys. Rev. 147B (1966) 715

Li 66 C.L. Lin, Prog. Th. Phys. 36 (1966) 251

Ma 64 M. Manalis and J.R. Henkel, Phys. Rev. 136B (1964) 1741

Ma 66 C. Maples, G.W. Goth and J. Cerny, Nuclear Data 2A (1966) 429

Ma 69 M.H. MacFarlane, "Proc. Int. Conf. on Properties of Nuclear States" Montreal (1969) Published by Les Presses De L'Universite de Montreal p385.

Me 65 A. Messiah, "Quantum Mechanics" Vol. 2 p1068 published by Wiley and Sons (1965)

Me 70 M.M. Meier, R.L. Walter, T.R. Donogue, R.G. Seyler and R.M. Drisko, Nucl. Phys. A159 (1970) 273

Mi 55 A.B. Migdal, Soviet Phys. JEPT 1 (1955) 2

Mi 66 C. Milone and R. Potenza, Nucl. Phys. 84 (1966) 25

Ne 69 J.M. Nelson and B.E.F. Macefield, Atlas Program Library Report No. 17, published by Oxford University Press (1969)

Ni 69 A. Niiler, C. Joseph, V. Valkovic, W. VanWitch and G.C. Phillips, Phys. Rev. 182 (1969) 1083

Or 58 J. ORear, Notes on Statistics for Physicists UCRL -8417 (1958)

Or 68 P.H.R. Orth, W.R. Falk and G. Jones, Nucl. Inst. Meth. 65 (1968) 301

Pa 63 P. Paul and D. Kohler, Phys. Rev. 129 (1963) 2698

Pe 64 F.G. Percy and D. Saxon, Phys. Lett.10 (1964) 107

Ph 60 G.C. Phillips and T.A. Tombrello, Nucl. Phys. 19 (1960) 555

Ph 60a G.C. Phillips, T.A. Griffy and L.C. Biedenharn, Nucl. Phys. 21 (1960) 327

Ph 64 G.C. Phillips, Revs. Mod. Phys. 36 (1964) 1085

Pr 62 M.A. Preston, "Physics of the Nucleus" Published by Addison - Wesley (1962)

Ra 51 G. Racah, Phys. Rev. 84 (1951) 910

Re 67 M.A. Reimann, P.W.Martin and E.W. Vogt, Phys. Rev. Lett. 18 (1967) 246

Re 68 M.A. Reimann, P.W. Martin and E.W. Vogt, Can. J. Phys. 46 (1968) 2241

Ri 56 A.C. Riviere, Nucl. Phys. 2 (1956,57) 81

Ri 57 A.C. Riviere and P.B. Treacy, Austr. J. Phys. 10 (1957) 209

Ro 64 J.R. Rook and D. Mitra, Nucl. Phys. 51 (1964) 96

Sa 64 G.R. Satchler, Nucl. Phys. 55 (1964) 1

Sc 66 S. Schwarz and H.O. Zetterstrom, Nucl. Instr. and Meth. 41 (1966) 820

Sl 67 R.J. Slobodrian, J.S.C. McKee, W.F. Tivol, D.J. Clark and T.A. Tombrello, Phys. Lett. 25B (1967) 19

Sl 68 R.J. Slobodrian, H.E. Conzett and F.G. Resmini, Phys. Lett. 27B (1968) 405

Sm 67 W.R. Smith, Nucl. Phys. A94 (1967) 550

St 65 G.L. Strobel and B.L. Scott, Phys. Rev. 140B (1965) 311

To 61 T.A. Tombrello and G.C. Phillips, Phys. Rev. 122 (1961) 224

To 61a W. Tobocman, "Theory of Direct Nuclear Reactions" Published by Clarendon Press, Oxford (1961)

To 69 I.S. Towner and J.C. Hardy, Advances in Physics 18 (1969) 401

Tr 63 W.W. True, Phys. Rev. 130 (1963) 1530

Tr 67 G.E. Tripard and B.L. White, Rev. Sc. Inst. 38 (1967) 435

Va 67 V.Valkovic, W.R. Jackson, Y.S. Chen, S.T. Emerson and G.C. Phillips, Nucl. Phys. A96 (1967) 241

Va 68 V. Valkovic, C. Joseph, A. Niiler and G.C. Phillips, Nucl. Phys. A116 (1968) 497

Wa 52 K.M. Watson, Phys. Rev. 88 (1952) 1163

We 58 G. Weber, Phys. Rev. 110 (1958) 529

Yo 62 S. Yoshida, Nucl. Phys. 33 (1962) 685

Yo 65 F.C. Young, K.S. Jayaraman, J.E. Etter, H.D. Holmgren and M.A. Waggoner, Revs. Mod. Phys. 37 (1965) 362

Ze 70 B. Zeitnitz, R. Maschun and P. Suhr, Nucl. Phys. 149A (1970) 449